

NAS8-38609 D.O.122

*FILE  
IN  
OUT  
0202149*

**AN ACOUSTIC EMISSION AND ACOUSTO-ULTRASONIC ANALYSIS  
OF IMPACT DAMAGED COMPOSITE PRESSURE VESSELS**

Prepared by

James L. Walker  
Center for Automation and Robotics  
University of Alabama in Huntsville  
Huntsville, AL 35899  
(205)-895-6578\*207

Principle Investigator

Gary L. Workman  
Center for Automation and Robotics  
University of Alabama in Huntsville  
Huntsville, AL 35899  
(205)-895-6578\*240

Submitted to

Samuel Russell  
EH13  
National Aeronautics and Space Administration  
Marshall Space Flight Center, AL 35812  
(205)-544-4411

January, 1996

## TABLE OF CONTENTS

<b>ABSTRACT .....</b>	<b>4</b>
<b>1.0 INTRODUCTION.....</b>	<b>5</b>
<b>2.0 ACOUSTIC EMISSION.....</b>	<b>7</b>
2.1 EXPERIMENTAL.....	8
2.1.1 Hydroburst Facility .....	8
2.1.2 Pressure Vessels.....	10
2.2 BACKPROPAGATION NEURAL NETWORKS .....	11
2.3 UN-FILLED 5.75 INCH DIAMETER GRAPHITE/EPOXY VESSELS .....	13
2.4 INERT FILLED GRAPHITE/EPOXY 5.75 INCH DIAMETER VESSELS .....	15
2.4.1 Test Summary .....	18
2.4.2 Neural Network Analysis .....	20
2.5 TALL GRAPHITE/EPOXY 5.75 INCH DIAMETER VESSELS .....	21
2.5.1 Test Summary .....	23
2.5.2 Neural Network Analysis .....	24
2.6 UN-FILLED KEVLAR/EPOXY 5.75 INCH DIAMETER VESSELS.....	25
2.6.1 Test Summary .....	26
2.6.2 Neural Network Analysis .....	27
2.7 INERT FILLED KEVLAR/EPOXY 5.75 INCH DIAMETER VESSELS .....	28
2.7.1 Test Summary .....	28
2.7.2 Neural Network Analysis .....	29
2.8 CONCLUSIONS (AE).....	29
2.9 RECOMMENDATIONS (AE) .....	30
<b>3.0 ACOUSTO-ULTRASONICS.....</b>	<b>31</b>
3.1 THEORY.....	31
3.2 AURES.....	31
3.3 INERT FILLED GRAPHITE/EPOXY 5.75 INCH DIAMETER VESSELS .....	35
3.3.1 Data Summary .....	37
3.3.2 Energy/Location Plots and Discussion.....	38
3.4 INERT FILLED KEVLAR/EPOXY 5.75 INCH DIAMETER VESSELS .....	47
3.4.1 Data Summary .....	47
3.4.2 Energy/Location Plots and Discussion.....	47
3.5 EMPTY KEVLAR/EPOXY 5.75 INCH DIAMETER VESSELS .....	52
3.5.1 Data Summary .....	52

3.5.2 Energy/Location Plots and Discussion.....	52
3.6 CONCLUSIONS (AU) .....	57
3.7 RECOMMENDATIONS (AU) .....	58
<b>4.0 CONCLUSIONS.....</b>	<b>58</b>
<b>5.0 REFERENCES.....</b>	<b>58</b>
<b>6.0 APPENDIX.....</b>	<b>60</b>
6.1 TRA2MLAB.BAS .....	60
6.2 ENGYDATA.M.....	60
6.3 OUTPUT.BAS.....	61
6.4 AEHITS.BAS .....	61
6.5 ROBOT OPERATIONS .....	65
6.6 CALIBRATION PROCEDURE FOR ROBOT LOAD CELL .....	65
6.7 LOAD CELL CIRCUIT.....	66
6.8 RBTBOT.M.....	66
6.9 DOWNRBT.EXE .....	68
6.10 UPRBT.EXE .....	68
6.11 SPINBT.EXE .....	69
6.12 PRESSURE VESSEL CRADLE.....	69
6.13 BROADBAND RECEIVER HOLDER.....	70
6.14 SENSOR ARM FOR AURES.....	70

## ABSTRACT

The research presented herein summarizes the development of acoustic emission (AE) and acousto-ultrasonic (AU) techniques for the nondestructive evaluation of filament wound composite pressure vessels. Vessels fabricated from both graphite and kevlar fibers with an epoxy matrix were examined prior to hydroburst using AU and during hydroburst using AE. A dead weight drop apparatus featuring both blunt and sharp impactor tips was utilized to produce a single known energy "damage" level in each of the vessels so that the degree to which the effects of impact damage could be measured. The damage levels ranged from barely visible to obvious fiber breakage and delamination.

Independent neural network burst pressure prediction models were developed from a sample of each fiber/resin material system. Here, the cumulative AE amplitude distribution data collected from low level proof test (25% of the expected burst for undamaged vessels) were used to measure the effects of the impact on the residual burst pressure of the vessels. The results of the AE/neural network model for the inert propellant filled graphite/epoxy vessels "IM7/3501-6, IM7/977-2 and IM7/8553-45" demonstrated that burst pressures can be predicted from low level AE proof test data, yielding an average error of 5.0 %. The trained network for the IM7/977-2 class vessels was also able to predict the expected burst pressure of taller vessels (three times longer hoop region length) constructed of the same material and using the same manufacturing technique, with an average error of 4.9 %. To a lesser extent, the burst pressure prediction models could also measure the effects of impact damage to the kevlar/epoxy "Kevlar 49/DPL862" vessels. Here though, due to the higher attenuation of the material, an insufficient amount of AE amplitude information was collected to generate robust network models. Although, the worst case trial errors were less than 6 %, when additional *blind* predictions were attempted, errors as high as 50 % were produced.

An acousto-ultrasonic robotic evaluation system (AURES) was developed for mapping the effects of damage on filament wound pressure vessels prior to hydroproof testing. The AURES injects a single broadband ultrasonic pulse into each vessel at preprogrammed positions and records the effects of the interaction of that pulse on the material volume with a broadband receiver. A stress wave factor in the form of the energy associated with the 750 to 1000 kHz and 1000 to 1250 kHz frequency bands were used to map the potential failure sites for each vessel. The energy map associated with the graphite/epoxy vessels was found to decrease in the region of the impact damage. The kevlar vessels showed the opposite trend, with the energy values increasing around the damage/failure sites.

## 1.0 INTRODUCTION

The technological improvements in many of today's aerospace structures are primarily due to advancements in materials and processes. As the performance requirements increase for these "advanced" materials, so does the need to accurately monitor the integrity of structural components fabricated from these material systems. Both nondestructive evaluation (NDE) and materials characterization are areas which continually need to be considered in the implementation of new materials into critical aerospace hardware. For these reasons, research efforts in NDE must keep pace with the development of new materials and processes.

Classically, NDE has been concerned with locating and identifying defects that could potentially hinder a structures ability to fulfill its mission. There are a number of NDE techniques which provide information about flaw size and location; including ultrasonics, eddy current, liquid penetrant and radiography to name a few, however, these techniques usually require a significant flaw size to exist in order for a minimum threshold of detection to be reached. Also, these techniques do not provide information as to the activation level of the flaw. In other words, will the flaw size increase with load, and if so, what effect will that have on the residual strength of the structure. Only one technique currently available actually does not depend upon flaw size, only that it is growing. This technique is acoustic emission (AE) testing.

Since AE does not depend upon size to characterize a flaw, only that it is growing , AE can be made extremely sensitive. Acoustic sensors and instrumentation available today can "hear" crack propagation events at such a minuscule level that the structure is not "appreciably" damaged. Thus acoustic emission testing has the potential to "proof-test" critical aerospace structures without impairing the ability of the structure to perform under normal operating conditions.

The sensitivity of AE NDE is primarily dependent upon the frequency range of the sensors used and the characteristics or physical properties of the test material. The strength "intensity" of the acoustic waves generated by a source are directly related to the energy released from flaw growth activity while ultrasonic wave propagation affects relate to the variations in time domain and waveform features of the received signal. Therefor, signal analysis requires an understanding of the complex interactions of the acoustic event with the material, the source mechanisms and the inherent nature of the instrumentation system. In general, AE signals have been characterized the same qualitative way for the last 15 years. Even with improvements in computing power, commercial instrumentation has not provided a noticeable improvement in acoustic emission signal analysis. Thus, this research is focused on providing some useful quantitative improvements in how acoustic emission signals are processed and interpreted.

The use of AE for monitoring composite structures during pressure testing has been accepted as a useful sensor technology. Characterization of the AE signals and interpretation of the structural properties contained in these signals as received during the test, still provides a challenge to the NDE research community. Recent developments in artificial neural networks though, have shown promise in sorting multidimensional data for distinguishing features that may in turn be used to

predict an outcome. This research will extend the use of these concepts by modeling the relationships between the AE signals recorded during the initial stages of loading and the ultimate failure of the structure.

In addition to AE, this study also provides an acousto-ultrasonics (AU) analysis of the regions in which the initiation of fracture is anticipated. Developed by Alex Vary at the Lewis Research Center, this technique has shown an ability to determine "weakest link" regions within a structure. AU is performed by injecting a known ultrasonic pulse (or stress wave) into a structure and measuring the relative attenuation or frequency shifts generated as a result of the interactions of that stress wave with the material volume. The similarity of AU to AE is carried over into the data analyses phase since AE hardware and software can be used for signal analysis of AU experiments. The major difference is that AE listens for stress waves emitted by crack or flaw propagation and AU provides its own stress wave energy, measuring the relative ability of the structure to dissipate that energy. Regions in which the energy is highly dissipated/concentrated or where drastic frequency shifting occurs are normally regions in which fracture will ultimately begin.

AU testing will be based on the ASTM standard currently under consensus ballot by ASTM, with the exact sequence of procedures best fitting the vessels under examination being developed during the course of this research effort. The incorporation of AU to map the quality of pressure vessels before pressure loading should provide benefits for interpretation of other NDE test data, as well as demonstrate the capabilities of AU to a broader audience. By performing AU scans on the composite vessels prior to the hydroburst testing and then monitoring the occurrence and location of AE "failure" during the pressure tests, information about how well the stress wave theory of AU predicts where failure will occur can be made. The AE events will provide real time information that fracture is occurring in those regions which were determined to be weaker structurally by AU.

In summary, the purpose of this task is to develop methods to evaluate the structural integrity of composite pressure vessels using both AE and AU techniques. Acousto-ultrasonic evaluation of the extent and effects of impact damage to pressure vessels will be investigated before hydroburst testing. During hydroburst, AE data will be acquired permitting the measurement of active flaw growth and burst pressure prediction models to be developed.

## 2.0 ACOUSTIC EMISSION

Impact damage, experienced in-service, is a problem that plagues the composites industry. Damage that may appear only superficial can often times have a detrimental effect on the performance of a composite structure [1]. Conventional NDE techniques typically map only the locations and shapes of impact damage and are not able to quantify its effects on the structure. Acoustic emission testing on the other hand, which records active flaw growth as the structure is loaded, provides the means to measure the reduction in structural performance that has been produced by an impact load or other abnormality. This research effort demonstrates a method for quantitatively proof testing impact damaged composite pressure vessels at sub-critical loads through a neural network analysis of their cumulative AE amplitude distribution data.

Acoustic emission signal analysis has been used to measure the effects of impact damage on the burst pressure of 5.75 inch diameter filament wound pressure vessels. The AE data were collected from a total of 101 vessels (31 inert propellant filled) constructed from graphite and kevlar fiber with an epoxy matrix. The physical properties of the pressure vessels are described in Section 2.1.2. A summary of the AE test matrix is provided in Table 1.

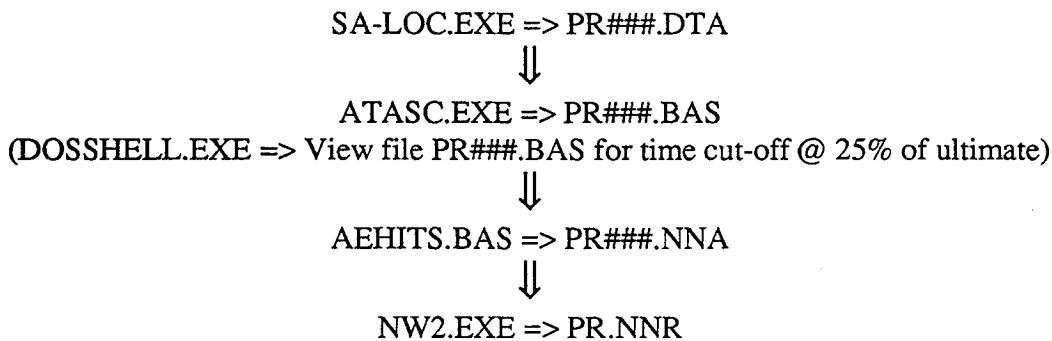
	Inert Propellant Backing	Fiber type	Resin type	Quantity
Graphite/Epoxy	Yes	IM7	3501-6	6
			977-2	6
			X8553-45	5
			Total	17
Graphite/Epoxy	No	IM7	3501-6	12
			977-2	12
			X8553-45	12
			Total	36
Kevlar/Epoxy	Yes	Kevlar 49	DPL862/W	14
Kevlar/Epoxy	No	Kevlar 49	DPL862/W	19
Graphite/Epoxy (Tall)	No	IM7	977-2	15
<b>Grand Total</b>				<b>101</b>

Table 1. Acoustic emission test matrix.

Impact damage was produced by means of a dead weight drop fixture utilizing both 0.5 inch/12.7 mm blunt (BT) and 0.039 inch/1.0 mm sharp (ST) hemispherical impactor tips with impact energies ranging from zero up to twenty ft-lb. Burst pressure prediction models were developed by correlating the cumulative AE amplitude distribution collected during low level hydroproof tests (approximately 25% of the average expected burst pressure for an undamaged vessels) to

known burst pressures using back propagation neural networks. The neural network models were trained from a subset of the vessels from each fiber/resin system and tested using the remaining vessels from that class.

A Physical Acoustics Corporation (PAC) SPARTAN-AT performs the data acquisition during the hydroburst tests. The PAC program SA-LOC.EXE is configured to collect the AE and parametric pressure data during each test. The AE data file "PR###.DTA" is converted to ASCII text format "PR###.BAS" by the PAC program ATASC.EXE. The AE data file is trimmed to contain only the data from the first 25% of loading by running the QuickBasic program AEHITS.BAS. Here, the amplitude distribution is computed and arranged for latter analysis "PR###.NNA". Finally, the neural network model is developed and tested generating the results file "PR.NNR".



Note: PR = Test filename prefix  
### = File number

## 2.1 EXPERIMENTAL

### 2.1.1 Hydroburst Facility

The MSFC "portable" hydroburst chamber was used to test the pressure vessels. The hydroburst facility consists of a test chamber, air driven water pump and instrumentation to provide the pressure level. A schematic of the chamber is shown in Figure 1 along with the AE system and supporting instrumentation. A detail of the pumping system is provided in Figure 2.

During the time that the first thirty-six empty graphite/epoxy vessels were tested (Fall 1993) many problems were encountered with the repeatability and accuracy of the recorded pressures. A lack of a consistent pressure standard and pressurization schedule coupled with the limited number of samples for each test point (consisting of a variable impact energy, impactor and resin) made subsequent AE burst pressure prediction modeling virtually impossible by introducing to many uncontrolled and unknown variables into the already full test matrix.

Measures were taken to overcome these problems by establishing a reference from which to check the output of the pressure transducer against and a computer generated pressurization schedule was established. The pressure standard was facilitated through the use of a high precision

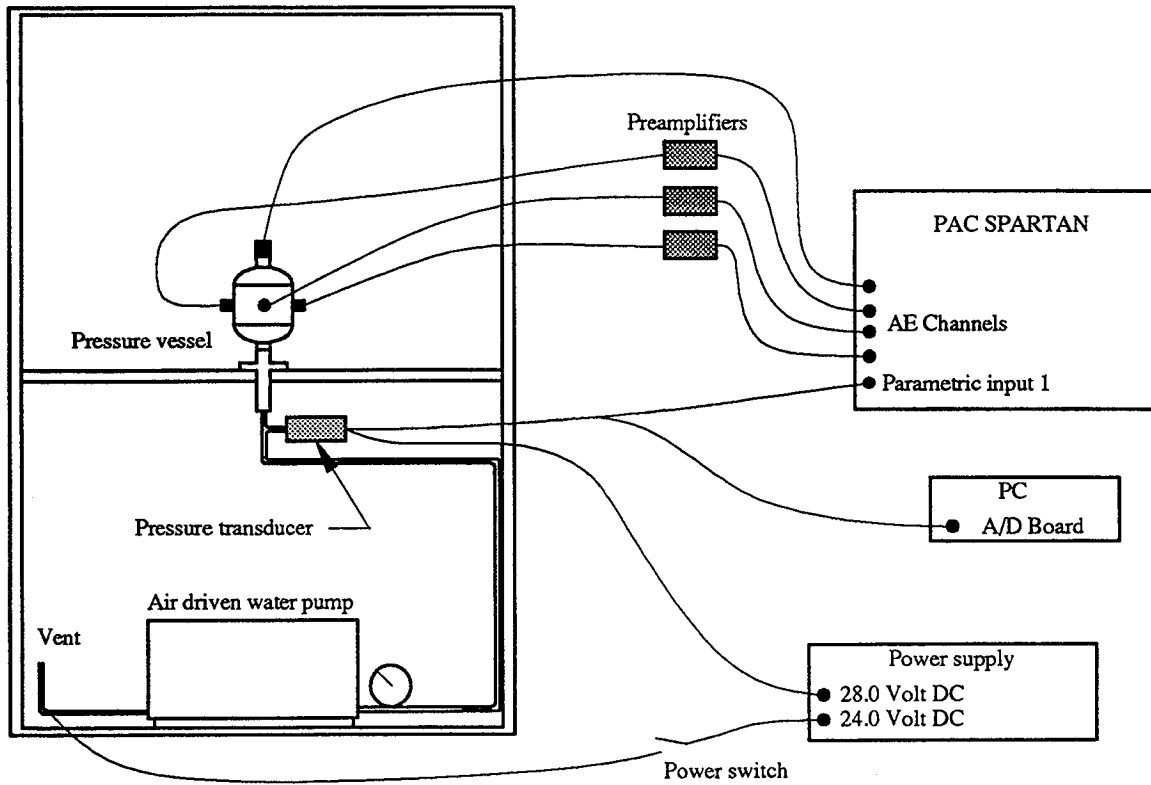


Figure 1. Hardware configuration.

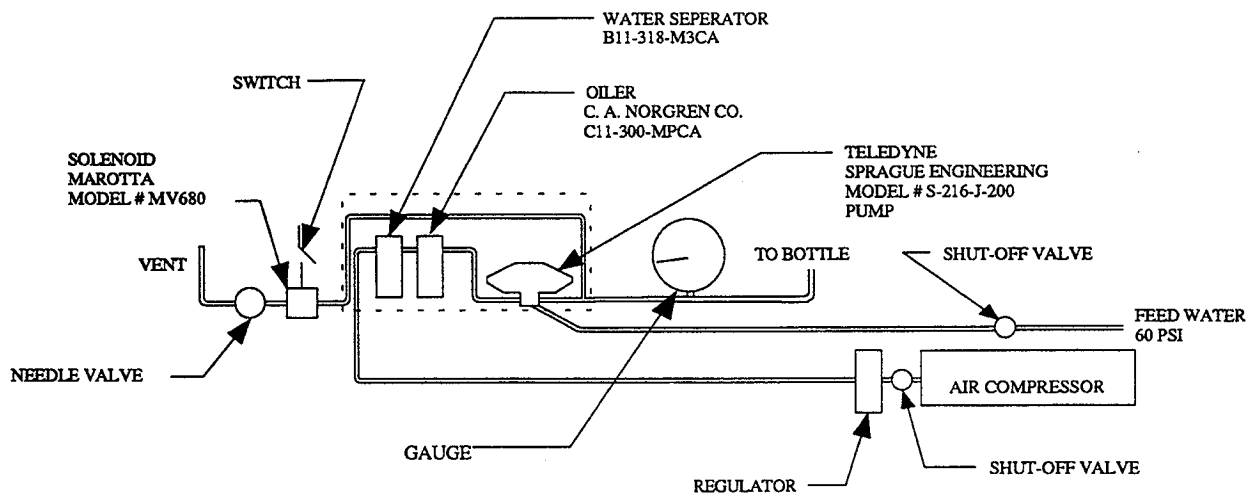


Figure 2. Pressure pump.

Bourdon tube pressure gage. Here, by periodically checking the output of the pressure transducer against the gauge, the correct burst pressures could be confidently measured.

To ensure repeatability in the pressure cycles the output from the pressure transducer was collected by an DAS-8 OMEGA A/D board controlled by a LABTECH NOTEBOOK program. The LABTECH program displayed the desired pressurization ramp and the actual signal from the pressure transducer so that the test operator could regulate the air pressure driving the water pump, matching the desired pressurization ramp. A 10 psig/sec (600 psig/min.) pressurization rate was set for each ramp. The LABTECH program stores the pressure histories with a 10 Hz sampling rate for future reference and to determine the burst pressure of each vessel.

### 2.1.2 Pressure Vessels

The graphite/epoxy vessels included in this work were all tumble wound and rotisserie cured using a Hercules IM-7 graphite fiber prepreg with either a Hercules 3501-6 ATL, Hercules X8553-45 or Fiberite 977-2 epoxy resin. The cure cycle consisted of a one hour 150 °F precure followed by a three hour 350 °F cure, with 5 °F/minute temperature ramps. Inert propellant was packed into seventeen of the vessels, after washing out the sand mandrel, leaving only a one inch diameter cylindrical core through its mid-section (Figure 3).

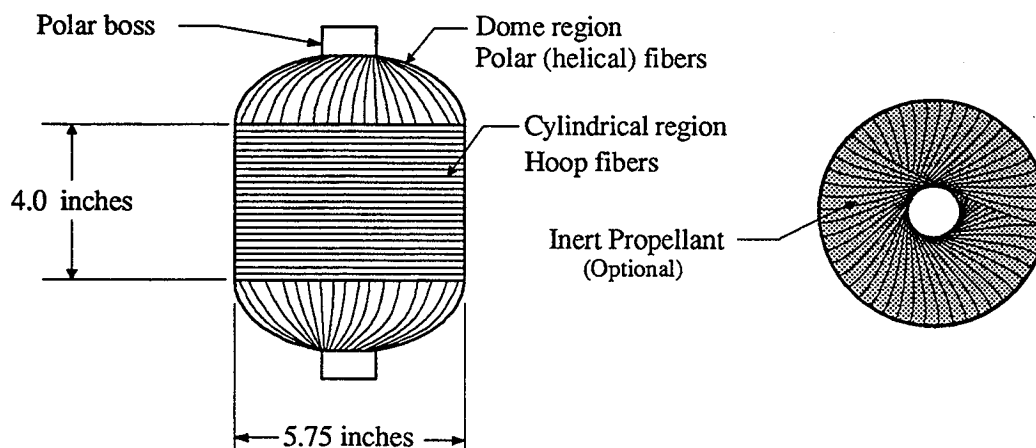


Figure 3. Standard 5.75 inch diameter pressure vessel geometry.

The kevlar/epoxy vessels were tumble wound “wet” and rotisserie cured using Kevlar 49 fiber and Dow DPL862/W resin. Here, the cure cycle consisted of a one hour precure at 250 °F, followed by a three hour cure at 350 °F. The temperature ramps were maintained in the 1 to 5 °F/minute range. Fourteen of the kevlar vessels were packed with inert propellant in a similar manner to the graphite vessels.

One of the problems that had been encountered early on in this program was manufacturing consistency (See Section 2.3). An investigation into optimizing the manufacturing techniques was performed by fabricating tall (12 inch hoop length) graphite/epoxy bottles (Figure 4) made from

IM7 fiber and 977-2 resin. The five manufacturing techniques are presented in Table 7 of Section 2.5.1. As an additional benefit to these tests, the ability to scale the neural network burst pressure prediction models could be investigated. None of the tall vessels were impact damaged.

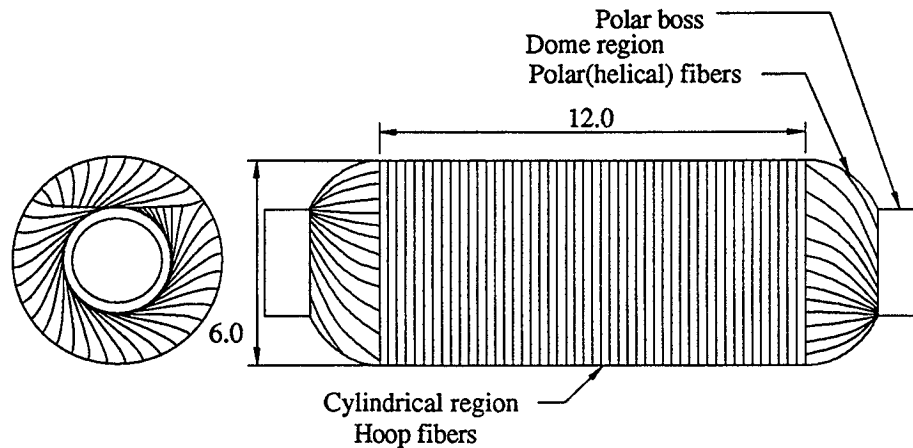


Figure 4. Tall 5.75 inch diameter pressure vessel geometry.

## 2.2 BACKPROPAGATION NEURAL NETWORKS

A back propagation neural network was developed to model the effects of the impact damage on burst pressure using NeuralWorks Professional II/PLUS software, by NeuralWare, Inc. The back propagation neural network paradigm is well suited to the problem of prediction using AE data since it can automatically map the descriptive features from a multidimensional input vector into a desired output response. Processing elements (PE) of the back propagation neural network (Figure 5) are used in a manner analogous to biological *neurons* creating the architecture necessary to provide the basis for learning [3]. The PE performs a simple summation of the weighted input values producing a single output response based upon a continuous transfer function. For this work, a hyperbolic transfer function is used to apply progressively smaller step sizes to the update delta weights as the normalized training error decreases (Figure 6).

The PE in a back-propagation neural network are arranged into an input layer, an output layer and at least one middle, or hidden layer (Figure 7). The input layer provides a way to introduce data into the network. Here, for example the discrete values of the amplitude distribution histogram would be entered as an input vector. Each input processing element is fully connected by a series of weighting factors to the hidden layer and these in turn are fully connected by another series of weighting factors to the output layer. If more than one hidden layer is used, their PE are also fully connected. The middle layers serves to map nonlinear variations in the data set. A bias processing element may also be weight connected to the PE of the hidden and output layers to serve as an offset value in the network. Ultimately, the weighting factors serve as the memory of the trained network by providing a multiplier between a preceding processing element's output value and an ensuing processing element's input value.

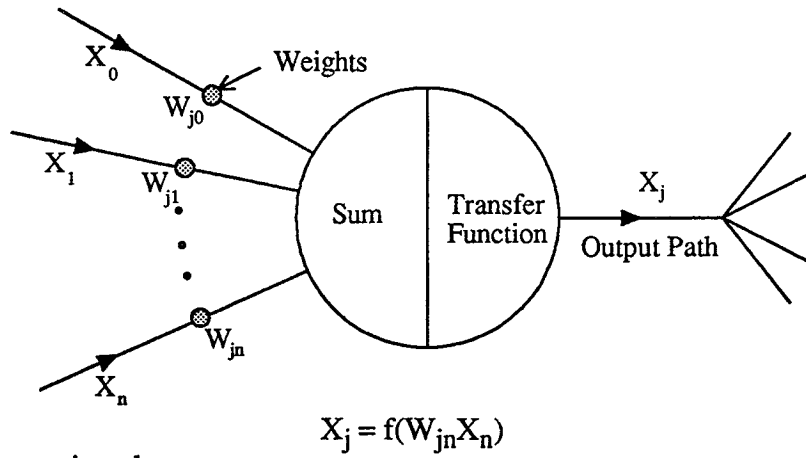


Figure 5. The processing element.

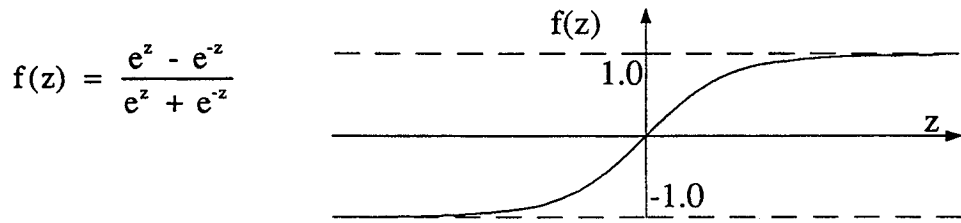


Figure 6. Hyperbolic tangent transfer function.

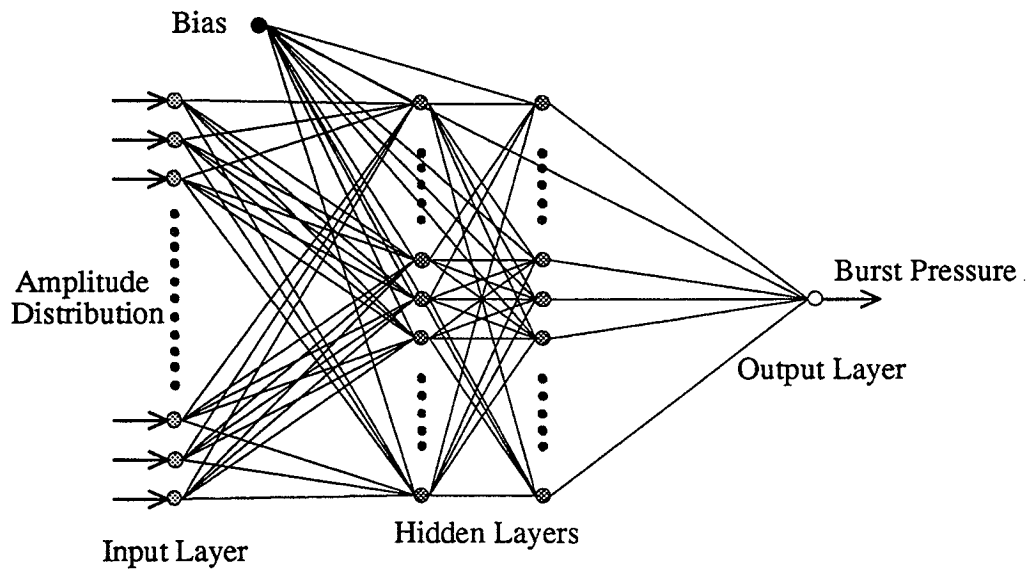


Figure 7. Back propagation neural network.

Fabrication number	Bottle I.D.	Burst (psig)	Resin type	Test code	HLT ( $\mu$ s)	Multiplier (psi/volt)	Impact status
91PV-003	A001-002	1818	3501-6	AA	100	671	High
92PV-005	C065-066	2793	3501-6	AN	300	3325	High
91PV-003	A015-016	1729	3501-6	AO	300	3325	High
92PV-005	C081-082	2509	3501-6	AB	100	671	Medium
92PV-005	C085-086	2776	3501-6	AP	300	3325	Medium
92PV-005	C083-084	2677	3501-6	AQ	300	3325	Medium
91PV-003	A021-022	2616	3501-6	AC	100	671	Low
91PV-003	A019-020	2311	3501-6	AR	300	3325	Low
91PV-003	A011-012	2227	3501-6	BH	300	3325	Low
91PV-003	A009-010	2154	3501-6	AD	100	671	None
92PV-003	C075-076	2842	3501-6	AZ	300	3325	None
92PV-005	C073-074	2676	3501-6	BA	300	3325	None
92PV-007	C133-134	2730	977-2	AE	300	671	High
92PV-007	C153-154	2576	977-2	AH	300	671	High
92PV-007	C123-124	1288	977-2	AI	300	671	High
92PV-007	C147-148	2731	977-2	AG	300	671	Medium
92PV-007	C121-122	3355	977-2	AJ	300	671	Medium
92PV-007	C145-146	2961	977-2	AK	300	3365	Medium
92PV-007	C149-150	3215	977-2	AF	300	671	Low
92PV-007	C111-112	3292	977-2	AL	300	3325	Low
92PV-007	C157-158	2926	977-2	AM	300	3325	Low
92PV-007	C125-126	2975	977-2	BB	300	3325	None
92PV-007	C127-128	3192	977-2	BC	300	3325	None
92PV-007	C143-144	2793	977-2	BD	300	3325	None
92PV-001	A041-042	1995	8553-45	AS	300	3325	High
92PV-006	C097-098	3175	8553-45	AT	300	3325	High
92PV-001	A031-032	2643	8553-45	AU	300	3325	High
92PV-006	C103-104	1962	8553-45	AV	300	3325	Medium
92PV-001	A039-040	2776	8553-45	AW	300	3325	Medium
92PV-001	A037-038	1978	8553-45	BI	300	3325	Medium
92PV-006	C101-102	2876	8553-45	AY	300	3325	Low
92PV-006	C107-108	N.A.	8553-45	BJ	300	3325	Low
92PV-006	C105-106	1978	8553-45	AX	300	3325	Low
92PV-006	C095-096	3308	8553-45	BE	300	3325	None
92PV-006	C089-090	3275	8553-45	BF	300	3325	None
92PV-006	A045-046	3009	8553-45	BG	300	3325	None

High = 7 ft-lb.      Medium = 5 ft-lb.      Low = 3 ft-lb.

All impacted with a 0.5 inch hemispherical tip

Table 2. Summary of unfilled graphite/epoxy pressure vessels.

The vessels were acoustically monitored with four PAC R15I sensors mounted with vacuum bag sealant tape. One sensor was attached to the wave guide pipe plug screwed into the top polar boss, while the remaining three sensors were bonded symmetrically around the mid-hoop line of each vessel. The same AE system setting described in Section 2.4 were used during this series of tests. A pressurization schedule consisting of three phases was used to load the vessels. First, the vessels were ramped (10 psi/sec) to 1000 psig and held for two minutes. During that time AE data was collected for potential burst pressure prediction modeling. After unloading, the vessels were again ramped to 1000 psig and held for a variable time while the shearographic and video image correlation images were acquired. The vessels were then loaded to 2000 psig and held at pressure for another two minutes. Pressure was again released, so that the AE sensors could safely be removed, and the vessel reloaded to failure.

A plot of the final burst pressures versus impact energy is provided in Figure 8.

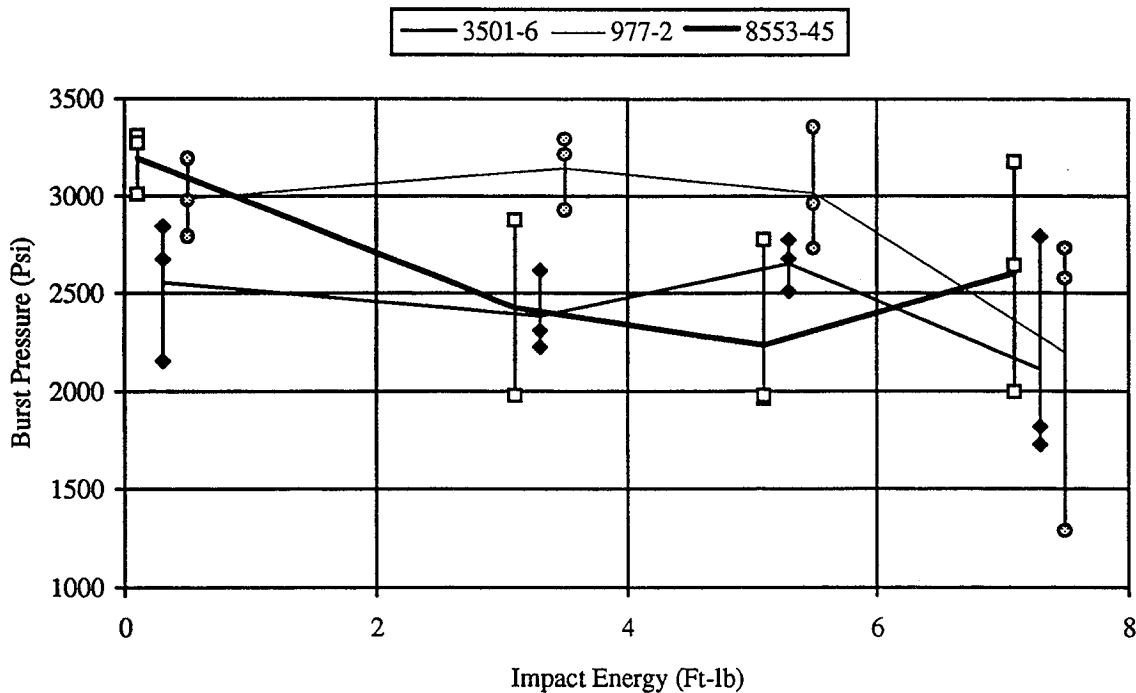


Figure 8. Burst pressure results of unfilled graphite/epoxy pressure vessels.

#### 2.4 INERT FILLED GRAPHITE/EPOXY 5.75 INCH DIAMETER VESSELS

The acoustic activity produced during hydroproof testing of seventeen inert propellant filled 5.75 inch diameter graphite/epoxy pressure vessels is presented. Four AE sensors were used to monitor the acoustic activity, three located symmetrically around the mid-line of the hoop region and one on the top polar boss (Figure 9). The sensors were all bonded to the vessel with hot melt glue. All of the pressure vessels were constructed from a Hercules IM-7 graphite fiber, while the resins types were split evenly into three groups using either a Hercules 3501-6 ATL, Hercules X8553-45 or a Fiberite 977-2 resin.

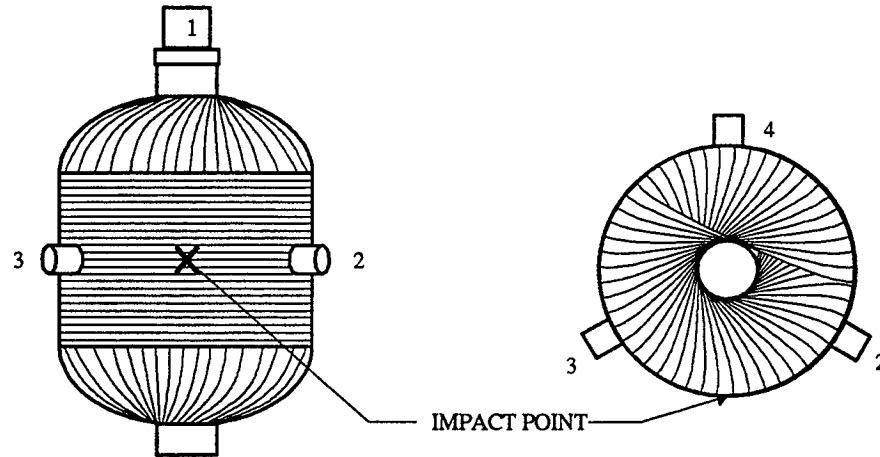


Figure 9. Transducer placement.

A pressurization cycle was selected that would be convenient for the AE testing, as well as for the optical NDE techniques (shearography and sub-pixel video image correlation) also used to monitor the vessels (Figure 10). The first proof cycle to 800 psig (approximately 25% of the expected burst pressure) provided a consistent AE data set for later use in developing burst pressure prediction models and to ensure that the containment chamber door could be safely opened for the optical NDE techniques. By monitoring the continuation of AE activity during a two minute hold at 800 psig the level of creep damage could be measured. Here, a large amount of AE activity during a hold would signify that the vessel was near failure making it unsafe to continue pressurization with the chamber door open. The vessels were then unloaded by opening the pump vent switch, the containment door opened, and the vessels stepped back up to 750 psig. in 250 psig. increments. Five minute holds were allowed between each pressure ramp to allow time to collect the optical data for each step. After the 750 psig hold the chamber door was closed and the vessels were proofed to 1000 psig. Following a two minute hold at 1000 psig to allow time for any creep activity to stabilize (noted by the absence of AE) the door was reopened and the final optical measurements made. The vessels were then unloaded, the hoop AE sensors removed, the door re-shut and a final pressure ramp straight to failure applied.

The pressure vessels' acoustic activities were collected during the hydroburst with the PAC SPARTAN AE system. A PAC R15I (150 kHz, 40 dB integral preamplifier, 100 kHz to 300 kHz bandpass filter) transducer was bonded with hot melt glue on the pipe plug used to seal the upper polar boss (Figure 9). Three PAC R15 (150 kHz) transducers were bonded symmetrically around the mid-hoop line and connected to external PAC 1220A preamplifiers (40 dB gain, 100 kHz to 300 kHz bandpass filter). A 20 dB internal gain and 60 dB signal threshold were used to establish the system's sensitivity. The AE system's timing parameters defined the acoustic hits with a 30  $\mu$ s peak detection time, 80  $\mu$ s hit detection time and a 300  $\mu$ s hit lock-out time. With these settings, lead breaks performed approximately two inches from each sensor produced signal amplitudes in the 80 dB range, verifying good sensor coupling.

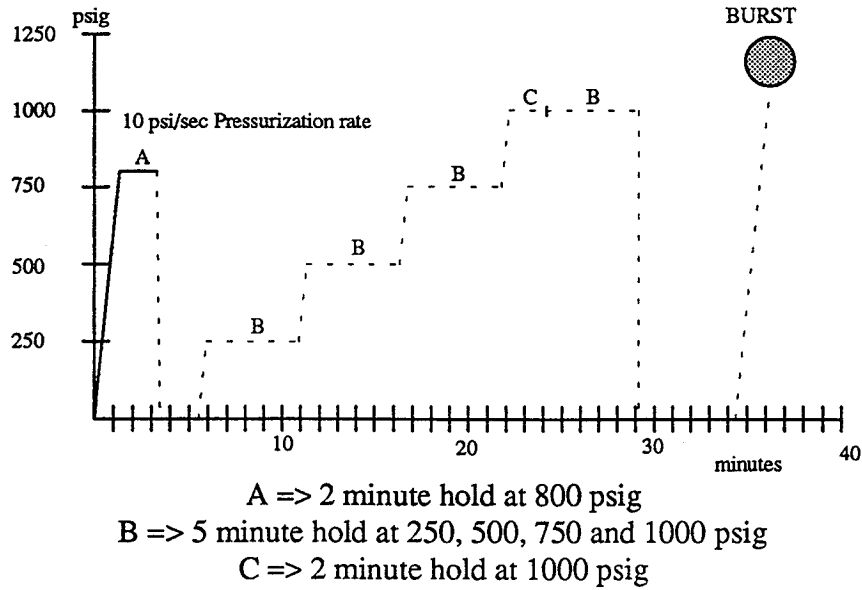


Figure 10. Pressurization schedule.

AE Parameters	Peak definition time (PDT)	30 $\mu$ s
	Hit definition time (HDT)	80 $\mu$ s
	Hit lockout time (HLT)	300 $\mu$ s
	Total system gain	60 dB
	Threshold	60 dB
External Parameters	Parametric multiplier	2020 psi/volt
Location Parameters	Wave speed	200000 inch/sec
	Lockout	18 inch
	Over calibration	1 inch

Table 3. System test parameters.

A calibrated dead weight drop fixture produced impact damage in the mid-hoop region of each vessel ranging from that which was barely visible to obvious fiber breakage. One vessel from each resin class was used as a control sample and left undamaged. The remaining vessels were split into equal groups and impacted with either the sharp or blunt hemispherical tip described in beginning of Section 2.0. Two impact levels were used with each tip (1.2 ft-lb. and 2.6 ft-lb. for the sharp tip, 5.0 ft-lb. and 8.1 ft-lb. for the blunt tip) to produce a broad range of damage conditions. Electronic shearography (ES) and sub-pixel digital video image correlation (SDVIC) techniques showed that the blunt tipped impactors generally produced a wide damaged zone with some localized delaminations while the sharp tip tended to break fibers at the impact point [2]. Typical, full field strain measurements generated using the SDVIC system are provided in Figure 11, demonstrating the extent and effect of impact induced fiber damage. Delamination zones are shown in Figure 12, for both blunt and sharp tipped impactors, as detected by the ES system.

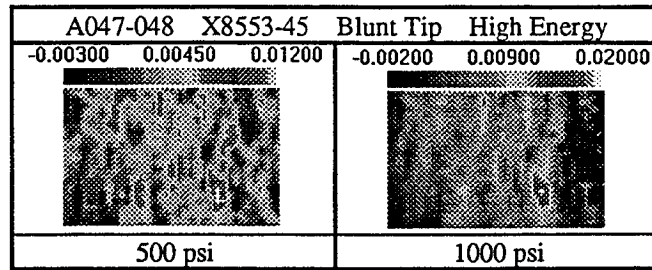


Figure 11. Full field strain measurements indicating regions of fiber damage using SDVIC.

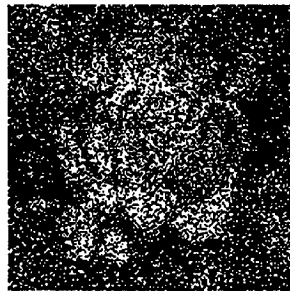


Figure 12. Delamination zone as imaged from the ES system.

#### 2.4.1 Test Summary

The three resin systems were acoustically very different. The amount of AE activity recorded on channel 1, for example, through the end of the first hold at 800 psig varied from an average of 517 hits for the 3501-6 resin, to 118 hits for the 977-2 resin, to only 11 hits for the 8553-45 resin (Figure 13). These results were expected, since the 977-2 and X8553-45 resin systems were formulated to be tougher than the brittle 3501-6 resin system, thereby providing a structure that could better redistribute stresses around stress concentrations rather than failing.

Based upon the limited test data collected, the 977-2 resin system appears to provide the highest burst pressures and the least sensitivity to impact damage. In the undamaged state the 977-2 resin produces a vessel that is 5% stronger than one fabricated from the 8553-45 resin system and 20% stronger than one fabricated from the 3501-6 resin system. The impacted vessels made from the 977-2 resin are on average 32% stronger than those made from the 3501-6 resin and 21% stronger than those made from the 8553-45 resin. Even with the small sample size these percentages are significant and warrant future study.

The burst pressures are plotted versus impact energy in Figure 14 for the seventeen vessels. Overall, the 977 resin system produced the greatest burst pressures and showed the least sensitivity to impact damage. As expected the burst pressures decreased with increasing sharp tip impact energy. The blunt tip impacted vessels though, showed an increase in burst pressure with larger impact energies. The delaminations generated during these impacts appear to be stress relieving the individual hoop plies, creating a more uniform overall stress state, and thus producing a higher net burst pressure.

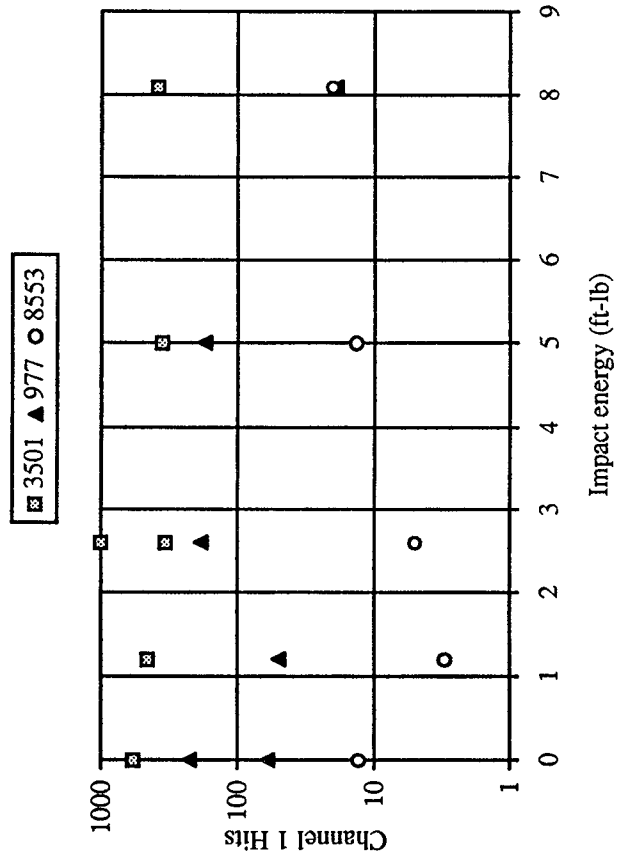


Figure 13. Acoustic activity versus impact energy.

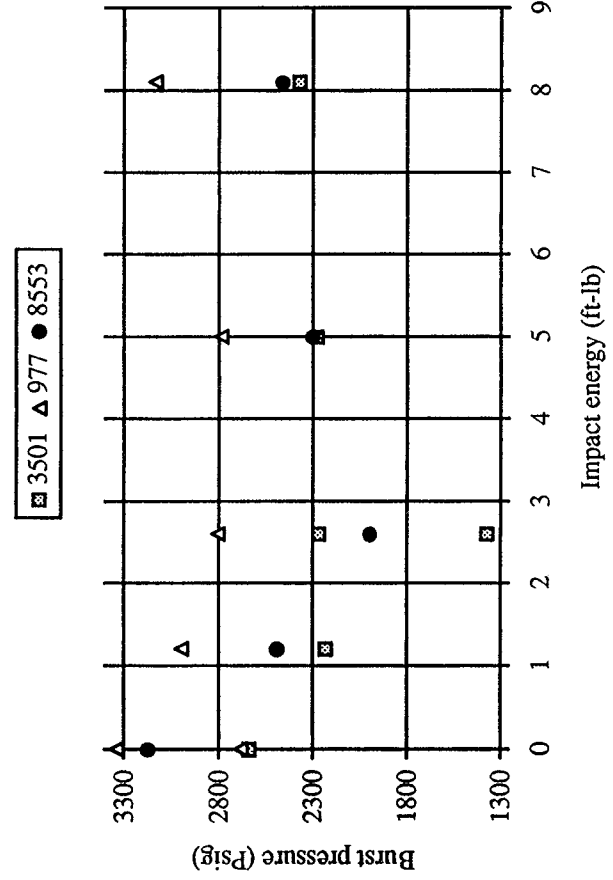


Figure 14. Burst pressure results.

Resin type	Bottle I.D.	Impact status	AE Code	Burst pressure (psig)
Hercules 3501-6	A003-004	None	GBIA003	2639
	C077-078	BT-8.1 ft-lb.	GBIC077	2373
	C069-070	BT-5.0 ft-lb.	GBIC069	2279
	A013-014	ST-1.2 ft-lb.	GBIA013	2232
	A023-024	ST-2.6 ft-lb.	GBIA023	2266
	A017-018	ST-2.6 ft-lb.	GBIA017	1371*
Fiberite 977-2	C115-116	None	GBIC115	3335
	C139-140	None	GBIC139	2682
	C117-118	BT-8.1 ft-lb.	GBIC155	3133
	C155-156	ST-2.6 ft-lb.	GBIC155	2804
	C141-142	BT-5.0 ft-lb.	GBIC141	2786
	C131-132	ST-1.2 ft-lb.	GBIC131	2996
Hercules X8553-45	A025-026	None	GBIA025	3171
	A029-030	BT-5.0 ft-lb.	GBIA029	2302
	C087-088	ST-1.2 ft-lb.	GBIC087	2489
	A047-048	BT-8.1 ft-lb.	GBIA047	2463
	C093-094	ST-2.6 ft-lb.	GBIC093	1995

\* Dome Failure

Table 4. Summary of burst pressures for inert filled graphite/epoxy vessels.

#### 2.4.2 Neural Network Analysis

A back propagation neural network was developed to model the effects of the impact damage on burst pressure using NeuralWorks Professional II/PLUS software. The amplitude distribution data from channel one, between 60 dB and 100 dB were introduced to the network through a 41 neuron input layer. The first of the two 13 neuron middle layers was fully connected by a series of weighting factors to the input layer, and then to each other. Burst pressure values were generated by a single output neuron that was fully weight connected to the second hidden layer. Finally, a bias neuron was weight connected to the hidden and output layer neurons to serve as a constant reference or offset value in the network. Since the network was expected to search for subtle variations between the individual sample data sets a small learning coefficient, 0.001, and momentum, 0.1, were necessary. The epoch size was set at 3, to match the number of training set vectors, permitting an average of the entire training error to be used for each delta weight calculation. A hyperbolic tangent transfer function was utilized to keep the output of the PE in check, i.e. between -1.0 and 1.0.

Three independent, yet similar, networks were trained using three vessels from each resin class by choosing a high, medium and low burst pressure. Each network was trained until a 5% convergence criteria was met on the modeled burst pressures. In all cases, less than 5000 training cycles were required to reach the convergence criteria. The results of this training exercise is presented in table 5.

Once trained, the networks were tested on the remaining vessels from each resin class. A summary of the predicted burst pressure values are provided in Table 6. Burst predictions were made with an average prediction error of only 5.0% including an outlier with an error of over 19%. Excluding this outlier the average prediction error drops to a low 2.9%.

Resin Type	Bottle I.D.	Actual Burst (psig)	Predicted Burst (psig)	% Error
Hercules 3501-6	A003-004	2639	2600	-1.5
	C077-078	2373	2381	0.4
	A017-018	1371*	1426	4.0
Fiberite 977-2	C115-116	3335	3308	-0.8
	C141-142	2786	2785	-0.00
	C131-132	2996	3008	0.4
Hercules X8553-45	A025-026	3171	3123	-1.5
	A047-048	2463	2467	-0.1
	C093-094	1995	2037	2.1
Abs(Average)				1.2

Table 5. Neural network training results.

Resin Type	Bottle I.D.	Actual Burst (psig)	Predicted Burst (psig)	% Error
Hercules 3501-6	C069-070	2279	2226	-2.3
	A013-014	2232	2356	5.6
	A023-024	2266	2712	19.7
Fiberite 977-2	C139-140	2682	2792	4.1
	C117-118	3133	3113	-0.6
	C155-156	2804	2935	4.7
Hercules X8553-45	A029-030	2302	2283	-0.8
	C087-088	2489	2551	2.5
Abs(Average)				5.0 (2.9)*

\* Average error excluding outlier

Table 6. Neural network prediction results.

## 2.5 TALL GRAPHITE/EPOXY 5.75 INCH DIAMETER VESSELS

The burst pressures of fifteen “un-filled” 12 inch tall IM7/977-2 (graphite/epoxy) vessels were predicted using the neural network model developed for the short (Section 2.4) 977-2 class vessels. The primary purpose for these tests were to investigate the effects of different manufacturing techniques on burst pressure. As a side benefit, the ability to “scale” a neural network model from subscale to larger structures could be investigated.

The vessels were not impacted, and as such shearography and SDVIC were not performed. Since the optical NDE techniques were not used a slightly modified pressure cycle (Figure 15) could be used. Instead of the ramp to 800 psig, hold, unload and reramp to 1000 psig; the vessels were

directly ramped to 1000 psig, held, unloaded and finally ramped to failure. The same sensor pattern as used on the standard size 5.75 inch diameter graphite/epoxy bottles was incorporated with the tall vessel tests (Figure 16). The network was tested using the cumulative AE amplitude distribution data collected during the initial pressure ramp to 800 psig from the dome sensor (channel 1).

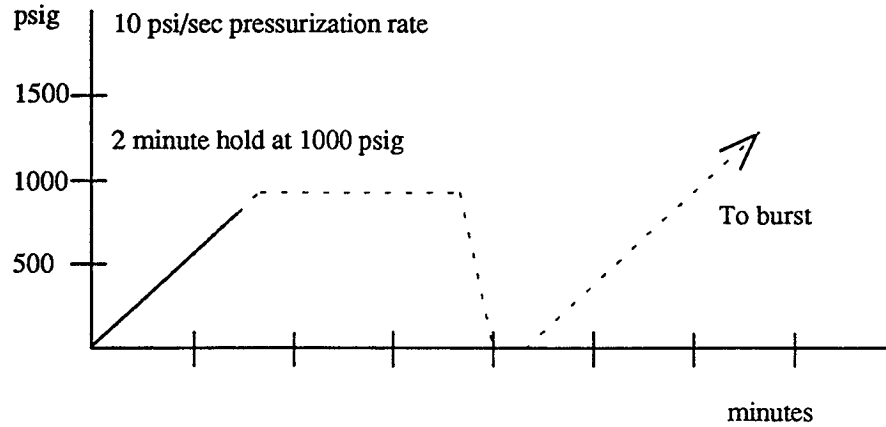


Figure 15. Pressurization cycle for tall graphite/epoxy vessels.

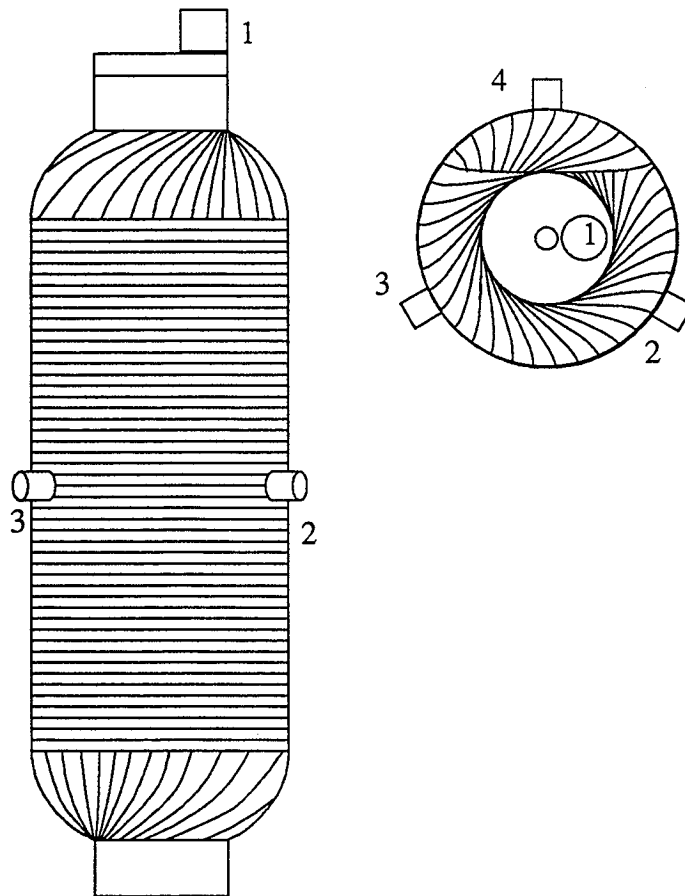


Figure 16. Sensor locations for tall graphite/epoxy vessels.

### 2.5.1 Test Summary

The burst pressures are summarized in Table 7 along with a description of the manufacturing process and failure location. The failure location is determined by the circumferential distance, measured clockwise from the vessel label. Post burst examination of the vessels indicated that failure initiated in the mid-hoop region for eight of the vessels and near one dome for the remaining seven vessels. The dome failures resulted in the ejection of the polar boss, splitting of the vessels along a longitudinal axis and buckling of the polar plies (created by the rapid unloading of the fibers at failure) radially from the initiation point. Vessels that failed in the mid-hoop region first, behaved in a similar fashion except that the domes remained intact after failure.

Overall, the series 5 vacuum bagged and oven cured vessels had the best “highest” burst pressures, averaging 3253 psig. The rotisserie cured series 6 vessels though, yielded only slightly lower burst pressures, averaging 3146 psig for a 3.3 % reduction in overall strength. The series 6 vessels were also the only ones to not have at least one dome failure. Figure 17 illustrates the burst pressure results for the five manufacturing processes.

Bottle I.D.	Burst (psig)	AE Test code	Bottle series	Failure Loc.	Pramp/Pfail
A	2989	GBT4A	94PV0004 Autoclaved	0.5 D	T1.PRN
B	3055	GBT4B		11.5	T2.PRN
C	2290	GBT4C		16.0 D	T3.PRN
Average	2778				
A	3326	GBT5A	94PV0005 Vacuum Bag Oven cure	6.5 D	T4.PRN
B	3268	GBT5B		5.0 D	T5.PRN
C	3162	GBT5C		8.0 D	T6.PRN
Average	3252				
A	3033	GBT6A	94PV0006 Rotisserie	17.5	T7.PRN
B	3240	GBT6B		0.5	T8.PRN
C	3166	GBT6C		0.5	T9.PRN
Average	3146				
A	2591	GBT7A	94PV0007 Low temp cure- PVA washed out- final cure	12.0	T10.PRN
B	2573	GBT7B		16.0	T11.PRN
C	2328	GBT7C		14.5D	T12.PRN
Average	2497				
A	3034	GBT8A	94PV0008 Rotisserie 350° and cured	3.0	T13.PRN
B	3104	GBT8B		14.0 D	T14.PRN
C	2948	GBT8C		5.0	T15.PRN
Average	3029				

D = Dome Failure

Table 7. Test summary for tall graphite/epoxy vessels.

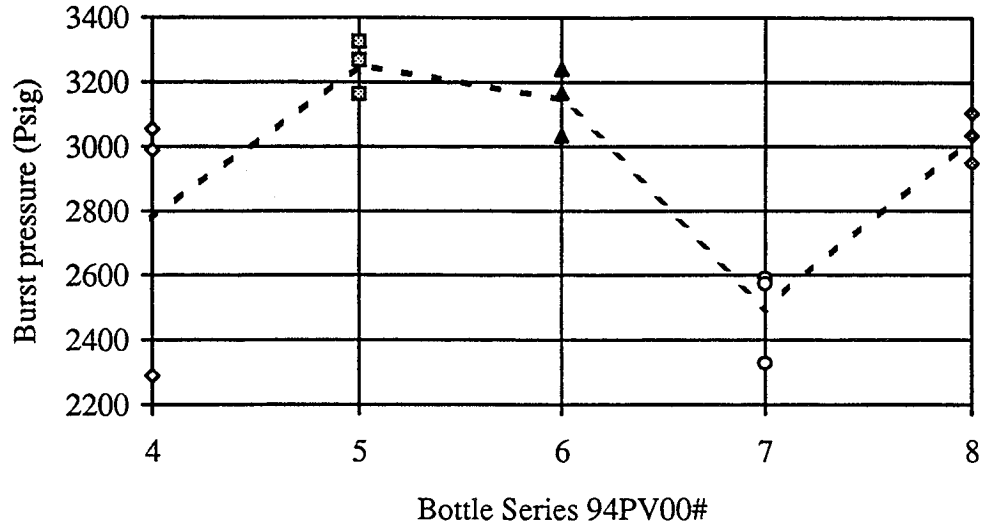


Figure 17. Burst pressure summary for the tall graphite/epoxy vessels.

### 2.5.2 Neural Network Analysis

The neural network results for the tall graphite/epoxy vessels show that provided the manufacturing processes are similar, good overall burst pressure predictions can be made from the trained network of the standard size vessels. Table 8 provides the prediction errors for all of the tall vessels along with the average error computed by the absolute value of prediction error for each vessel series. The lowest average error, 4.9 %, was found for the series 6 vessels were the same material and manufacturing processes were used as with the standard size vessels. A fair prediction error was also produced with the series 5 and 8 vessels. The network model had the most problem predicting the burst pressures of the series 7 vessels. Apparently, the cure changed the mechanical properties of the vessels enough that their acoustic signature was unrecognizable by the model. Besides that series, only one outlier was found. The third vessel in the series 4 class of vessels has a burst pressure 700 psi lower than the other two of that class. The network model was not able to pick up this variation netting an error of over 37 %.

Bottle series	AE test code	Failure location	Actual burst pressure (psig)	Predicted burst pressure (psig)	Prediction error
94PV0004 Autoclaved	GBT4A	0.5 D	2989	2877.4	-3.7
	GBT4B	11.5	3055	3110.4	1.8
	GBT4C	16.0 D	2290	3154.9	37.8
				<b>Abs(Average)</b>	<b>14.4</b>
94PV0005 Vacuum bag Oven cure	GBT5A	6.5 D	3326	3182.2	-4.3
	GBT5B	5.0 D	3268	2923.7	-10.5
	GBT5C	8.0 D	3162	3050.3	-3.5
				<b>Abs(Average)</b>	<b>6.1</b>
<b>94PV0006*</b> <b>Rotisserie</b> <b>cure</b>	<b>GBT6A</b>	<b>17.5</b>	<b>3033</b>	<b>2955.4</b>	<b>-2.6</b>
	<b>GBT6B</b>	<b>0.5</b>	<b>3240</b>	<b>2947.3</b>	<b>-9.0</b>
	<b>GBT6C</b>	<b>0.5</b>	<b>3166</b>	<b>3070.4</b>	<b>-3.0</b>
				<b>Abs(Average)</b>	<b>4.9</b>
94PV0007 Low temp cure- PVA removed- final cure	GBT7A	12.0	2591	3000.5	15.8
	GBT7B	16.0	2573	2835.8	10.2
	GBT7C	14.5D	2328	2741.6	17.8
				<b>Abs(Average)</b>	<b>14.6</b>
94PV0008 Rotisserie cured at 350°	GBT8A	3.0	3034	2788.1	-8.1
	GBT8B	14.0 D	3104	3306.4	6.5
	GBT8C	5.0	2948	2794.3	-5.2
				<b>Abs(Average)</b>	<b>6.6</b>

D = Dome Failure

\* = Similar manufacturing process to short inert filled vessels.

Table 8. Neural network results.

## 2.6 UN-FILLED KEVLAR/EPOXY 5.75 INCH DIAMETER VESSELS

Nineteen “un-filled” 5.75 inch diameter kevlar/epoxy pressure vessels were acoustically monitored during hydroburst with four AE sensors. Just as with the graphite/epoxy vessels, three AE sensors were mounted symmetrically around the mid-line of the hoop region with one sensor on the top polar boss (Figure 9) with hot melt glue. All of the pressure vessels were wet wound and rotisserie cured from a Dupont Kevlar fiber and Dow DPL862/W epoxy resin.

The pressure cycle was shortened slightly from the one used with the graphite/epoxy vessels by decreasing the hold at each 250 psig step (labeled B in Figure 10 of Section 2.4) to only 2 minutes, as compared to the previous 5 minute holds. The reduction in the hold time was permitted as a result of not conducting shearography during the proof tests.

The system parameters of the PAC SPARTAN were kept the same as for the graphite/epoxy vessels except that the threshold was reduced to 50 dB. The reduction in threshold was deemed necessary due to the larger attenuation of the kevlar vessels over the graphite vessels and the lower overall acoustic nature of the kevlar/epoxy material system. Six (3 each filled and unfilled)

kevlar/epoxy vessels were tested before the threshold was changed to the lower value. With these settings, lead breaks performed approximately two inches from each sensors produced signal amplitudes in the 70 dB range, verifying good sensor coupling.

A calibrated dead weight drop fixture produced impact damage in the mid-hoop region of each vessel ranging from that which was barely visible to obvious fiber breakage. Two vessels were used as a control sample and left undamaged. The remaining vessels were somewhat randomly impacted with either the sharp and blunt hemispherical tip. Overall, impacts ranged up to 11.91 ft-lb. with the sharp tip and 15.5 ft-lb. with the blunt tip. Just as with the graphite/epoxy vessels ES and SDVIC techniques showed that the blunt tipped impactors generally produced a wide damaged zone with some localized delaminations while the sharp tip tended to break fibers at the impact point. The major difference between the two fiber/resin systems was that the delaminations appeared more pronounced in the kevlar vessels, but fewer fiber breaks were apparent.

### 2.6.1 Test Summary

A summary of the burst pressures, threshold, impact status and number of channel one hits are presented in Table 9. The burst pressures are plotted versus impact energy in Figure 18 for the nineteen kevlar vessels. It should be noted that vessel D254-255 was impacted twice, and is represented in the figure at a position denoted by the sum of the two impact energies. The summed energy value for D254 should not be taken literally, as the energy from multiple impacts are not additive. The value shown is strictly for reference.

Bottle I.D.	Burst (psig)	Threshold (dB)	AE code	Impact Status (Ft-lb.)	Channel 1 Hits	Pramp/Pfail
D179-180	2561	60	KBD179	ST-10.00	21	K4
D227-228	2275	60	KBD227	BT-12.00	38	K5
D165-166	2353	60	KBD165	ST-7.00	52	K6
D239-240	1796	50	KBD239	BT-15.50	143	K7
D213-214	2356	50	KBD213	ST-11.00	87	K9
D235-236	1701	50	KBD235	BT-14.41	35	K16
D254-255	1541	50	KBD254	BT-13.09/14.41	102	K13
D169-170	2608	50	KBD169	ST-8.83	42	K12
D187-188	2407	50	KBD187	BT-11.80	43	K11
D241-242	2354	50	KBD241	BT-9.00	271	K14
D177-178	2237	50	KBD177	ST-11.91	52	K10
D225-226	2149	50	KBD225	ST-11.80	39	K15
D201-202	2597	50	KBD201	ST-6.90	92	K23
D233-234	3057	50	KBD233	NONE	201	K25
D237-238	2314	50	KBD237	ST-9.80	7	K26
D161-162	2249	50	KBD161	?	26	K27
D221-222	2867	50	KBD221	NONE	31	K31
D215-216	2503	50	KBD215	ST-7.10	122	K32
D163-164	2194	50	KBD163	BT-10.90	24	K33

Table 9. Data summary for un-filled kevlar/epoxy vessels.

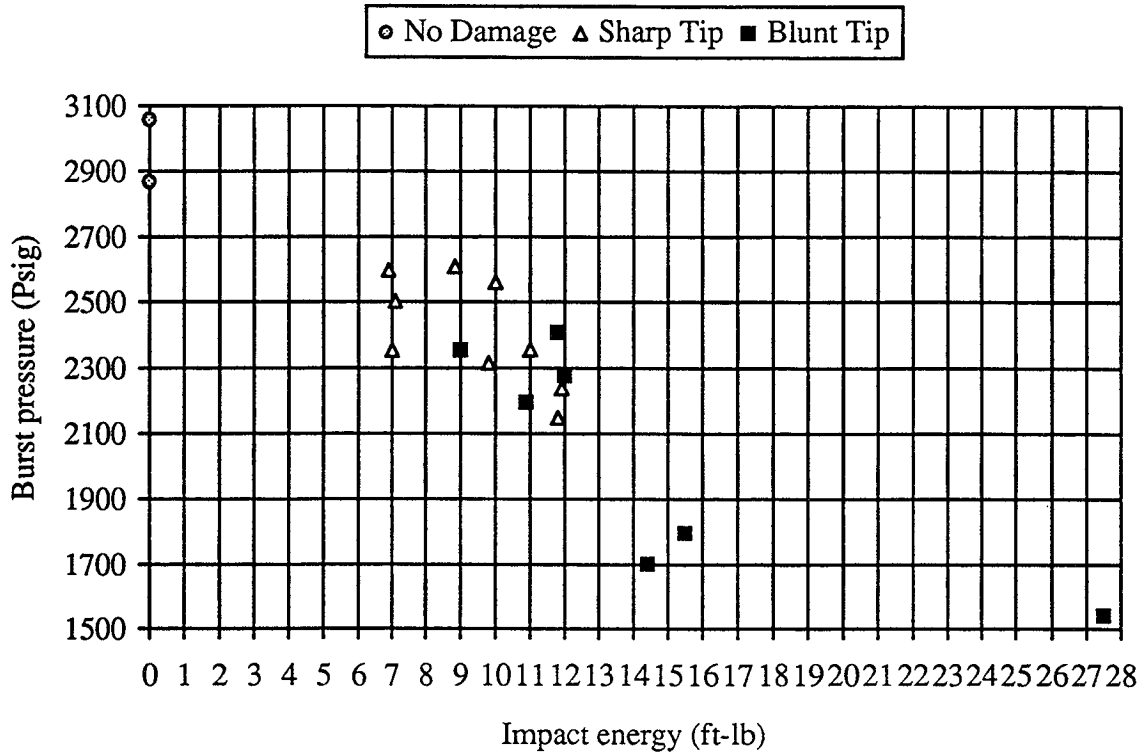


Figure 18. Burst pressure results for un-filled kevlar/epoxy vessels.

### 2.6.2 Neural Network Analysis

Many different back propagation neural network architectures were attempted to model the effects of the impact damage on burst pressure in the kevlar bottles using the NeuralWorks Professional II/PLUS software. The amplitude distribution data between 50 dB and 100 dB from both channel one and the combination of channels 2, 3 and 4 were introduced to the network through a 51 neuron input layer. Due to the low cumulative hit count from channel one it was thought that the benefit of including all the hoop sensors to provide an adequate statistical base would outweigh the problems with source location dependence on the cumulative AE data. The number of hidden layer neurons was varied from as low as 3 to as high as 50 while keeping the learning coefficient fixed at 0.001, and momentum equal to 0.4. The epoch and hyperbolic tangent transfer function were set the same as for the graphite/epoxy vessels.

Three of the first six vessels tested were selected for the initial training phase. Here, the network was allowed to train on a sample high, medium and low burst pressure. Once trained, the networks were presented with two trial vessel data sets to check the training phase. When the error level was sufficiently low, below 6 % for the training and trial bottles, additional *blind* prediction data was tested. These preliminary results show that much more work is required to generate robust neural network models.

Bottle I.D.	Impact Status (Ft-lb.)	Actual burst (psig)	Predicted burst (psig)	% error
Training results				
D254-255	BT-13.09/14.41	1541	1584.6	2.83
D213-214	ST-11.00	2356	2351.3	-0.20
D169-170	ST-8.83	2608	2571.0	-1.42
Trial results				
D187-188	BT-11.80	2407	2262.0	-6.04
D239-240	BT-15.50	1796	1846.0	2.78
Test results				
D235-236	BT-14.41	1701	2399.8	41.08
D241-242	BT-9.00	2354	1782.9	-24.26
D177-178	ST-11.91	2237	2109.7	-5.69
D225-226	ST-11.80	2149	1898.0	-11.68
D201-202	ST-6.90	2597	1884.0	-27.50
D233-234	NONE	3057	1491.9	-51.20
D237-238	ST-9.80	2314	2287.3	-1.15
D161-162	?	2249	2350.6	4.52
D221-222	NONE	2867	2035.9	-29.0
D215-216	ST-7.10	2503	2400.0	-4.11
D163-164	BT-10.90	2194	2210.5	-0.75

Table 10. Burst pressure prediction results.

## 2.7 INERT FILLED KEVLAR/EPOXY 5.75 INCH DIAMETER VESSELS

A similar test procedure was conducted on the inert propellant filled vessels as was done for the empty vessels.

### 2.7.1 Test Summary

Bottle I.D.	Burst (psig)	Threshold (dB)	AE code	Impact Status (Ft-lb.)	Channel 1 Hits	Pramp/Pfail
D197-198	2319	60	KBID197	ST-4.23	66	K1
D229-230	2196	60	KBID229	BT-17.00	33	K2
D247-248	2541	60	KBID247	BT-10.90	31	K3
D243-244	2588	50	KBID243	ST-2.17	305	K4
D249-250	2560	50	KBID249	ST-3.82	55	K17
D231-232	2072	50	KBID231	ST-4.85	109	K18
D181-182	2390	50	KBID181	ST-2.89	73	K19
D223-224	2978	50	KBID223	NONE	135	K24
D191-192	2099	50	KBID191	BT-20.28	58	K20
D205-206	3071	50	KBID205	BT-4.95	102	K22
D245-246	2249	50	KBID245	BT-13.29	33	K21
D185-186	3025	50	KBID185	NONE	52	K28
D175-176	1997	50	KBID175	BT-16.50	69	K29
D255-256	2682	50	KBID255	ST-4.10	108	K30

Table 11. Data summary for inert propellant filled kevlar/epoxy vessels.

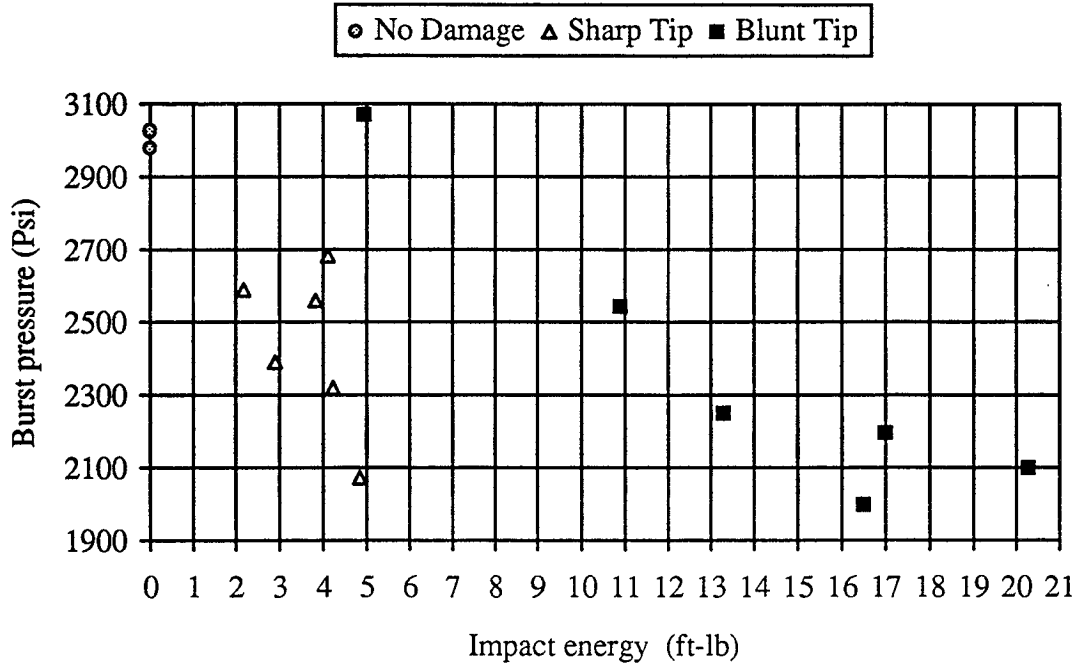


Figure 19. Burst pressure results for un-filled kevlar/epoxy vessels.

### 2.7.2 Neural Network Analysis

Bottle I.D.	Impact Status (Ft-lb.)	Actual burst (psig)	Predicted burst (psig)	% error
Training results				
D249-250	ST-3.82	2560	2018.5	1.08
D191-192	BT-20.28	2099	2125.7	1.27
D205-206	BT-4.95	3071	2024.4	-1.52
Trail results				
D243-244	ST-2.17	2588	2453.5	-5.20
D245-246	BT-13.29	2249	2297.0	2.14
Test results				
D231-232	ST-4.85	2072	2563.0	23.70
D181-182	ST-2.89	2390	2577.7	7.85
D223-224	NONE	2978	3158.8	6.07
D185-186	NONE	3025	2096.9	-30.68
D175-176	BT-16.50	1997	2010.1	-.065
D255-256	ST-4.10	2682	2362.9	-11.90

Table 12. Burst pressure prediction results.

## 2.8 CONCLUSIONS (AE)

- This research effort provides a means for quantitatively proof testing composite pressure vessels that have experienced some form of impact damage in service.

- The result of this work shows that the effects of impact damage on the burst pressures of graphite/epoxy vessels can be made using a four layered back propagation neural network.
- The neural network models developed for the kevlar/epoxy vessels can only be used in a limited sense to predict burst pressures. The current network was only capable of predicting the burst pressure of a portion of the vessels tested.
- The potential to scale the neural network model for a particular manufacturing process shows promise.

## **2.9 RECOMMENDATIONS (AE)**

To date, the neural network models for the kevlar vessels “filled or un-filled” are not robust enough to accurately predict burst pressures outside the trial data set. Possible solutions to this problem include; (1) Normalizing the amplitude distribution data before it is presented to the network, (2) Entering other AE parameters, such as energy or duration, along with the amplitude distribution to the network during training, and (3) Working with different network architectures such as the self organizing map.

The effects of scale on the network models needs to be addressed in greater detail by conducting scaled tensile tests and hydroburst tests of larger diameter vessels.

## 3.0 ACOUSTO-ULTRASONICS

### 3.1 THEORY

Acousto-ultrasonics serves as a NDE tool by combining the technologies of AE and ultrasonics. The AU system records the response of a structure to an ultrasonic pulse, similar to that of through-transmission ultrasonics. A pulser driving an ultrasonic transducer is configured to inject a single strain wave (acoustic signal) into the structure. The signal passes through the structure and is transformed by the complex interactions of itself with the material volume and then is received by a broadband AE transducer. The parameters of the recorded acoustic signal, or event, then carries with it a fingerprint of the integrity and quality of the material between the pulser and receiver. By analyzing the frequency (power) spectrum of the received signal a correlation with the material properties and overall residual strength of the structure can often be deduced.

A stress wave factor (SWF) is defined as a measure of the received signals strength. The stress wave factor can take on many forms ranging from a simple amplitude measurement to an integration of the power spectrum. Researchers have devised many different ways to calculate the SWF for specific structural cases. For this work the energy associated with specific frequency bands of the power spectrum was chosen to represent the SWF. The SWF (waveform energy) for the inert filled graphite/epoxy vessels were computed on two intervals selected in the range from 25 to 375 kHz and 375 to 700 kHz, based on an apparent grouping in the power spectrum curves. The kevlar/epoxy vessels were tested utilizing a system with a larger bandpass, allowing the frequency spectra be investigated up to 2.0 MHz. The 750 kHz to 1250 kHz portion of the frequency spectra provided the best resolution for measuring the extent of damage in the kevlar/epoxy vessels and locating the ultimate failure location.

The basic requirement for a valid SWF is that it provide an indication as to the structural quality of a pressure vessel before an impact as well as be directly related to the amount of damage attained from an impact. The SWF will also be related to manufacturing variations such as voids in the resin or misaligned fibers and experimental variables including contact pressure and degree of sensor coupling.

### 3.2 AURES

A basic requirement for AU testing is that sensor contact pressure be uniform and that a sufficient number of measurements be made to completely map the region of interest. As described in Section 3.3, the process of taking AU measurements by hand is not only time consuming but also lacks resolution and repeatability. These problems were partially solved by developing a acousto-ultrasonic robotic evaluation system (AURES). The AURES incorporates the robotic controls from a Rhino<sup>®</sup> robot with a PC based ultrasonic measurement system to create an automated AU measurement system. With the AURES many more measurements can be made over the surface of the vessels, in less time and with more repeatability, than were done by hand. The AURES has

proven to be very versatile, allowing AU mapping of drone wing panels, compressed gas container welds, powder formed impact cages as well as the pressure vessels described in this report. A schematic of the AURES configured for the 5.75 inch diameter pressure is shown in Figure 20.

The program RBTBOT.M controlling the AURES was written in the MATLAB working environment. MATLAB essentially works as a batch driver, allowing execution of the robot control, data acquisition and FFT programs. Robot control is facilitated through three QuickBasic executable files. The programs UPRBT.EXE and SPINBT.EXE are both position oriented programs not requiring feedback from the load cell. UPRBT simply lifts the sensor pair two inches after each measurement, while the program SPINBT steps the bottle through 40 equally spaced angular ( $9^\circ$  each) positions. The third program, DOWNRBT.EXE, works in conjunction with a load cell to ensure that contact pressure remains constant for each measurement. The ultrasonic receiver of the AURES is instrumented with a Omega Engineering, Inc. subminiature LCK series 1 kg capacity compression type load cell. A balance beam type arm is adjusted so that the same contact pressure is also applied to the pulse transducer. The load cell output is feed to an instrumentation amplifier (1000x gain) which intern is input to one side of a comparator. The other side of the comparator is regulated by a simple voltage divider so that the load (voltage) from the load cell can be used to turn the comparator on and off. The DOWNRBT program moves the robot arm down until it either reaches its travel limit or compresses the load cell enough to trip the comparator and shut itself "the robot" down. The procedures for running and calibrating the AURES are presented in the Appendix.

The AU signal is recorded by a Digital Wave broadband receiver. The signal is amplified by a Digital wave PA2040G 40 dB preamplifier powered by a 28 volt DC supply. The input signal is generated by a Harrisonic 1.0 MHz (0.5 inch diameter) ultrasonic sensor driven by a Panametrics pulser/receiver unit. The signals are recorded by a Physical Acoustics Corp. (PAC) A/D board running in a 90 MHz Pentium PC. The A/D is configured to digitize the waveforms with a 32 MHz sampling rate over 4096 points or 128  $\mu$ s window.

A summary of the AURES instrumentation system is provided in Figure 21.

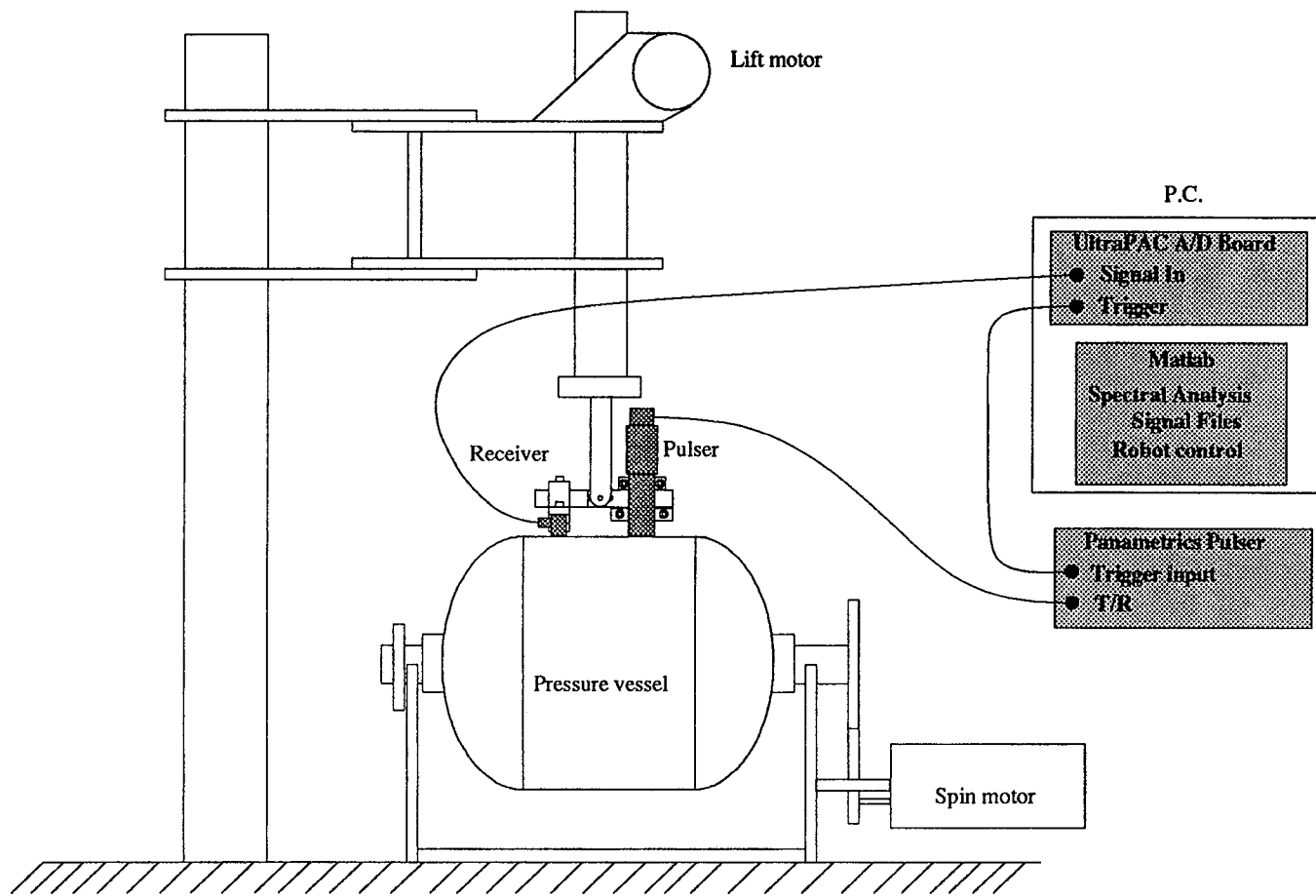


Figure 20. The AURES.

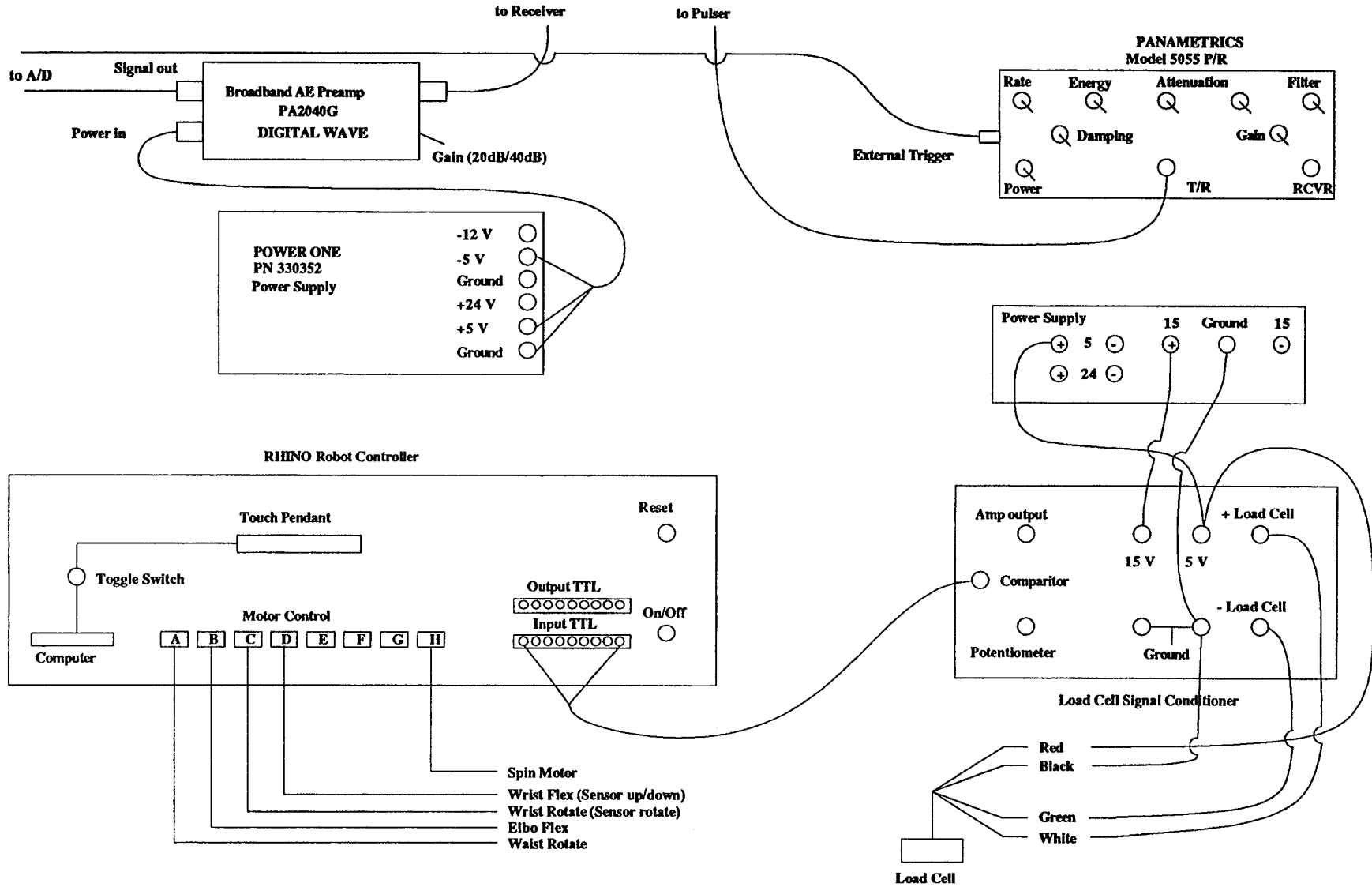


Figure 21. AURES instrumentation.

### 3.3 INERT FILLED GRAPHITE/EPOXY 5.75 INCH DIAMETER VESSELS

The AURES was not completed at the time the first of the filled graphite/epoxy vessels were scheduled for hydroburst. Instead, an AU system was assembled to map the inert filled graphite/epoxy vessels by combining a standard ultrasonic pulser and AE recording system. The heart of the AU system was a PAC SPARTAN AE system which measured and stored the AE signal parameters as well as the signal waveform. A PAC model W4I (100 to 1000 kHz) broadband receiver was used to record the response of the material to an ultrasonic pulse generated by a Harrisonic 500 kHz ultrasonic transducer driven by a Panametrics model 5055PR pulser. The receiver and pulser were coupled to the surface using Sonotrace ultrasonic couplant. The pulser was triggered by a signal from a Wavetek Pulse/Function generator so as to generate a single waveform. The AU system is shown in Figure 22.

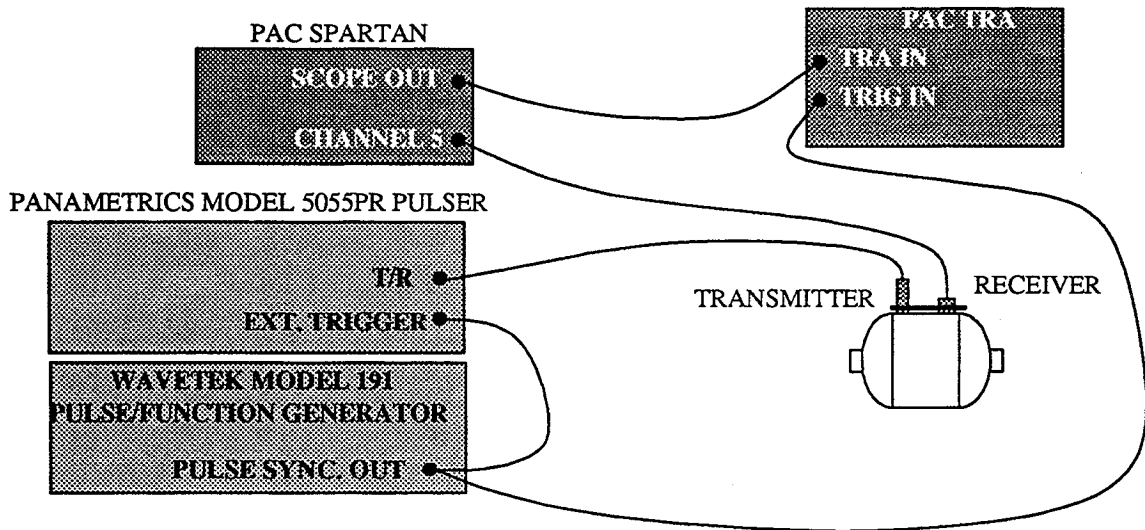


Figure 22. Acousto-Ultrasonic system schematic.

Twelve graphite/epoxy vessels (Table 13) were mapped with this system to determine the extent of damage in the impact zone. Measurements were taken by hand along and perpendicular to the hoop fiber direction for these twelve bottles. The power spectrum and resulting spectral energy were tabulated for each acoustic signal. The energy was then plotted versus bottle location as a test of the AU system to quantify the extent of impact damage.

Transducer spacing and contact pressure is often a problem associated with AU measurements. To help overcome these problems two simple holders were constructed from 1/4 inch thick Plexiglas providing a means to both position the transducers relative to each other and press them to the structure. A simple flat holder (Figure 23) was used for making measurements perpendicular to the hoop direction while a hinged version (Figure 24) was constructed for making measurements around the hoop direction of the vessel. A two pound steel weight was bonded to each holder to provide the required constant contact pressure. The holders were designed to maintain a 1.5 inch sensor spacing.

Fabrication number	Bottle I.D.	Resin type	Impact status
92PV005	C069-070	3501-6	BT-5.0 ft-lb.
92PV005	C077-078	3501-6	BT-8.1 ft-lb.
92PV003	A013-014	3501-6	ST-1.2 ft-lb.
92PV003	A017-018	3501-6	ST-2.6 ft-lb.
92PV007	C141-142	977-2	BT-5.0 ft-lb.
92PV007	C117-118	977-2	BT-8.1 ft-lb.
92PV007	C131-132	977-2	ST-1.2 ft-lb.
92PV007	C155-156	977-2	ST-2.6 ft-lb.
92PV001	A029-030	8553-45	BT-5.0 ft-lb.
92PV001	A047-048	8553-45	BT-8.1 ft-lb.
92PV006	C087-088	8553-45	ST-1.2 ft-lb.
92PV006	C093-094	8553-45	ST-2.6 ft-lb.

Table 13. Graphite/epoxy vessels mapped by acousto-ultrasonics.

The recorded AU signals were first converted to ASCII format through the PAC program TRA2DAD.EXE. This program generates a data file consisting of a seven line header followed by a sequential string of values representing the digitized waveforms. For this work the sampling rate was set at 16 MHz for a total of 8192 points, a 512  $\mu$ s window. The ASCII data file is then run through the BASIC program "TRA2MLAB.BAS" which eliminates the header and puts the file into MATLAB format. The program "ENGYDATA.M" is executed by MATLAB to compute the power spectra and resulting energy for the two frequency bands (25 to 375 kHz and 375 to 700 kHz). Finally, the energy table from MATLAB is processed by another BASIC program "OUTPUT.BAS" which computes the average of the readings for one position and orders the data into a convenient form. The programs just described can be found in the Appendix of this report.

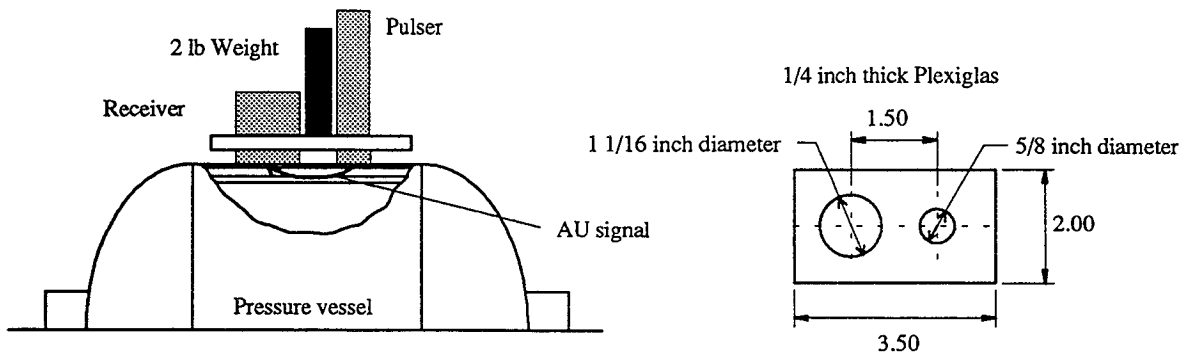


Figure 23. Flat transducer holder.

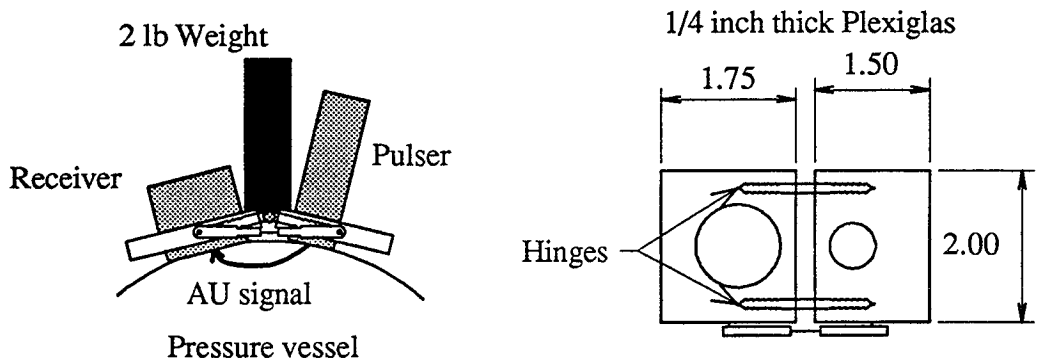


Figure 24. Hinged transducer holder.

### 3.3.1 Data Summary

Three measurements were made at each sensor position in an attempt to reduce the effects of contact pressure variations and local surface roughness on the data set. For the longitudinal direction, measurements were taken on 1.0 inch circumferential spacing in the vicinity of the impact point and 2.0 inch spacing elsewhere (Figure 25). Three sets of measurements were taken at each circumferential position (top, middle, bottom) to measure the extent of damage along the length of the vessels.

The AU signal was also taken from top to bottom along the hoop region in the damage zone. Here, AU measurements were taken at seven positions spaced 1/2 inch apart through the impact point (Figure 26). Again three measurements were taken at each location and averaged.

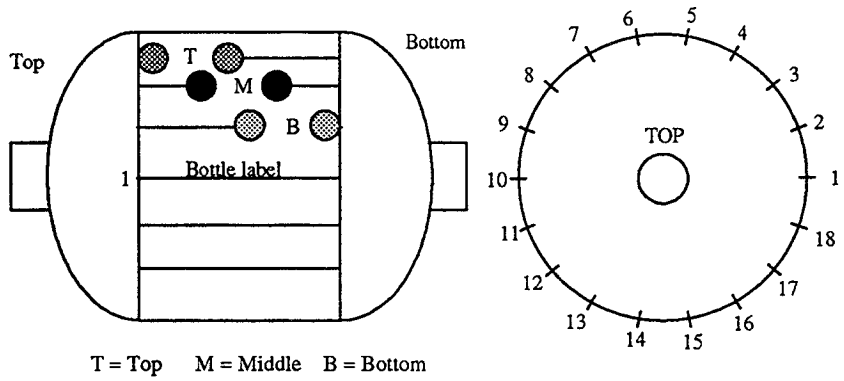


Figure 25. Bottle position and sensor locations for longitudinal measurements.

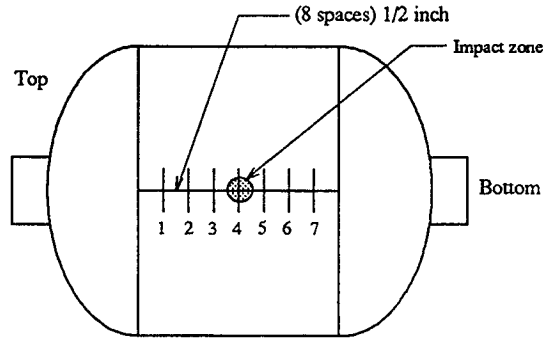


Figure 26. Hoop data transducer positions.

### 3.3.2 Energy/Location Plots and Discussion

The results presented in Figures 27 through 38 depict the average partitioned energies for each hoop and middle circumferential position. The top and bottom energy values have been omitted from the circumferential measurement graphs as they provided no additional information. A open circle indicates the impact point for the circumferential measurements. The impact point for the hoop direction is always at position number four.

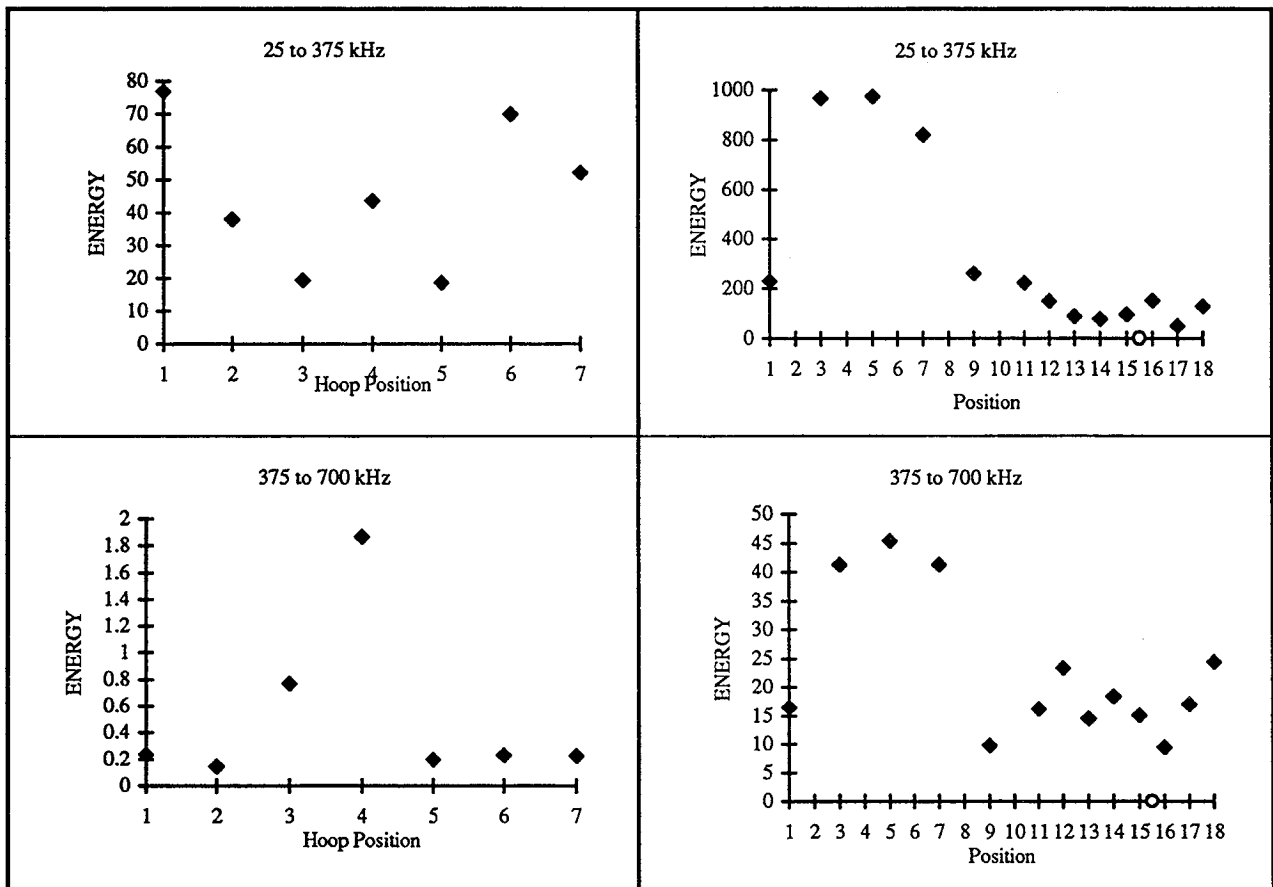


Figure 27. Energies for vessel A029-030 (8553-BT-5.0).

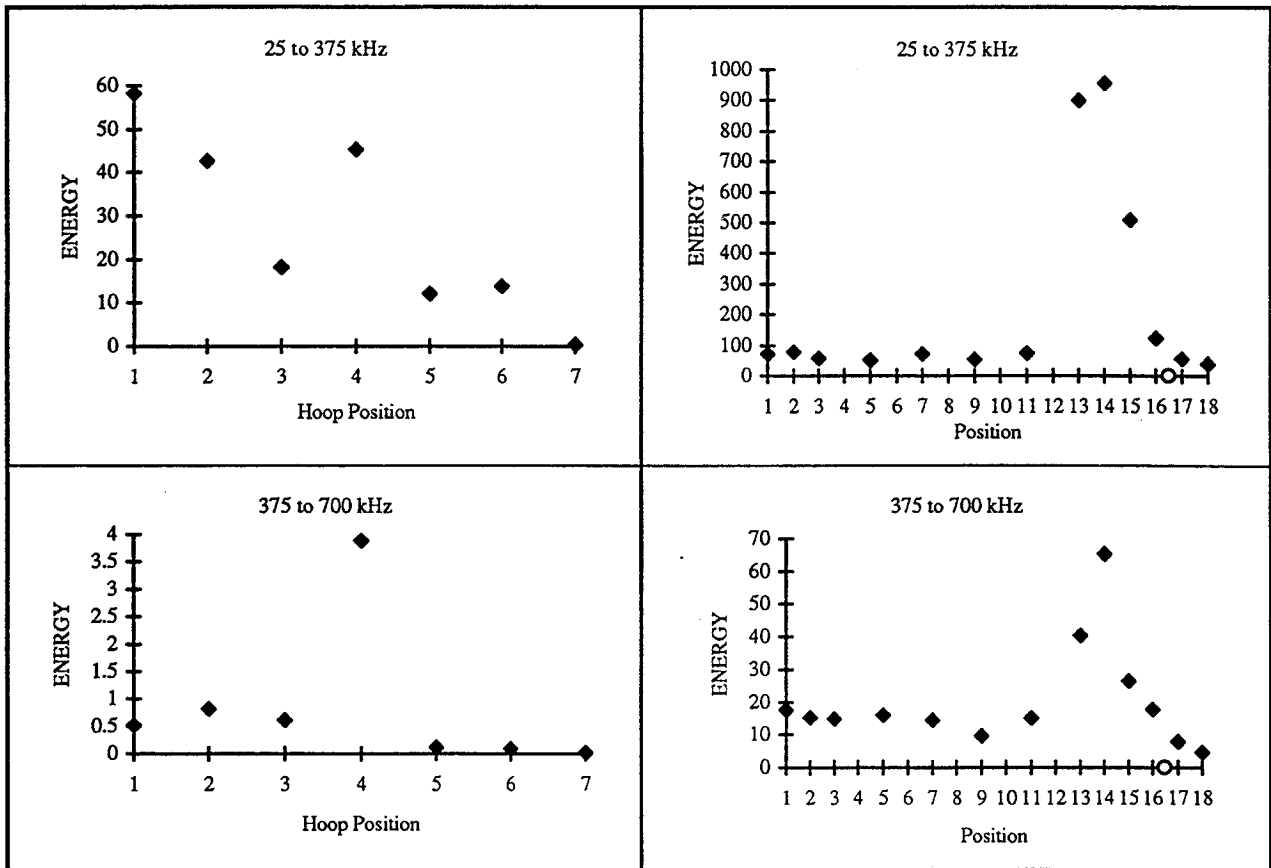


Figure 28. Energies for vessel A047-048 (8553-BT-8.1).

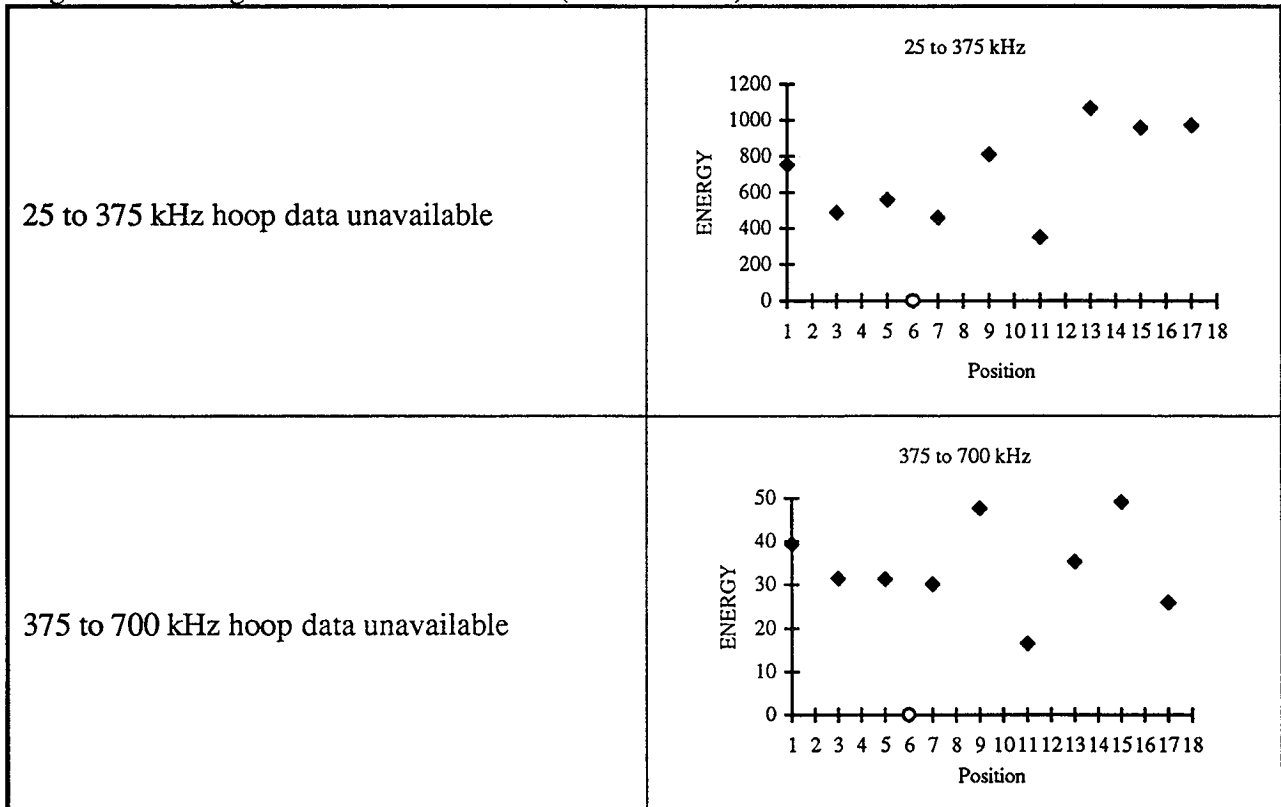


Figure 29. Energies for vessel C087-088 (8553-ST-1.2).

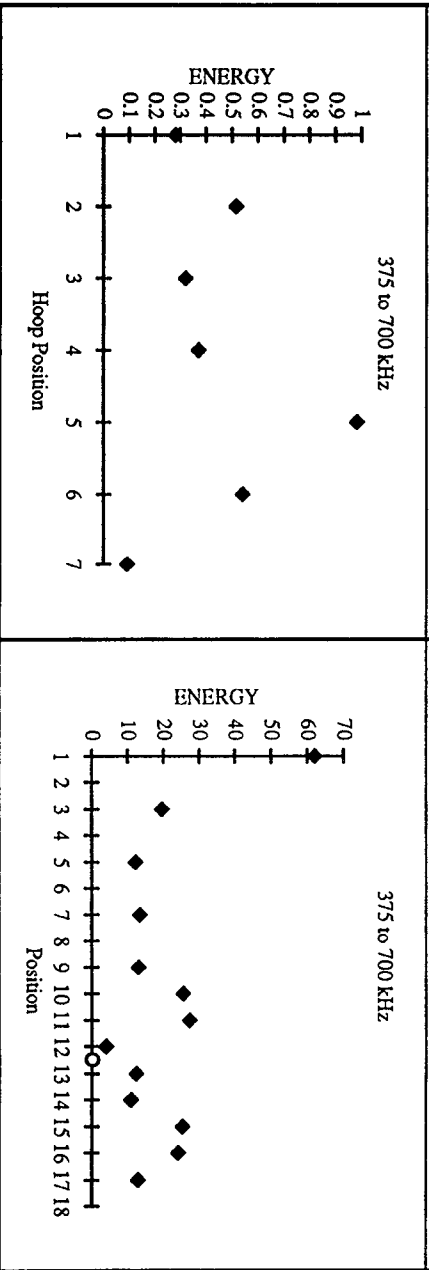
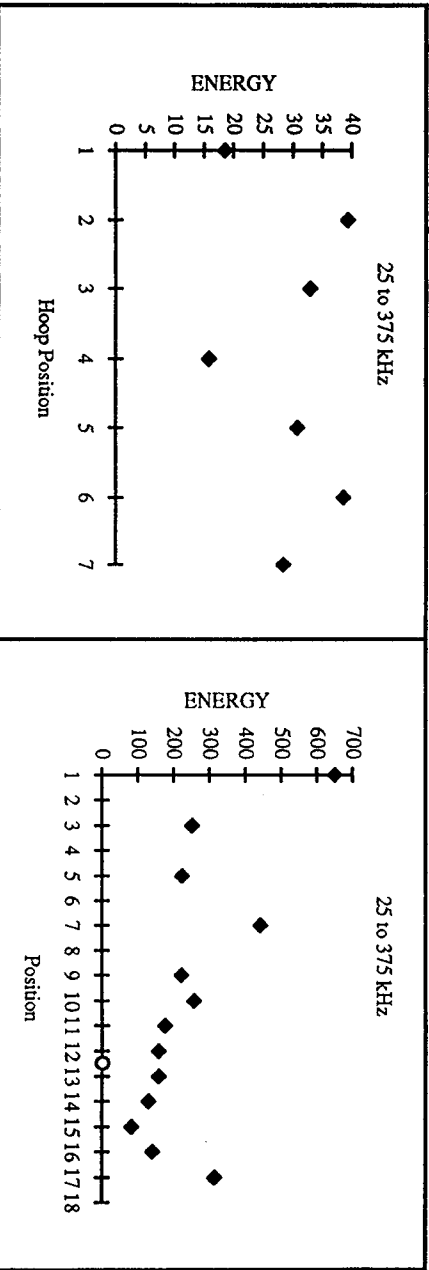
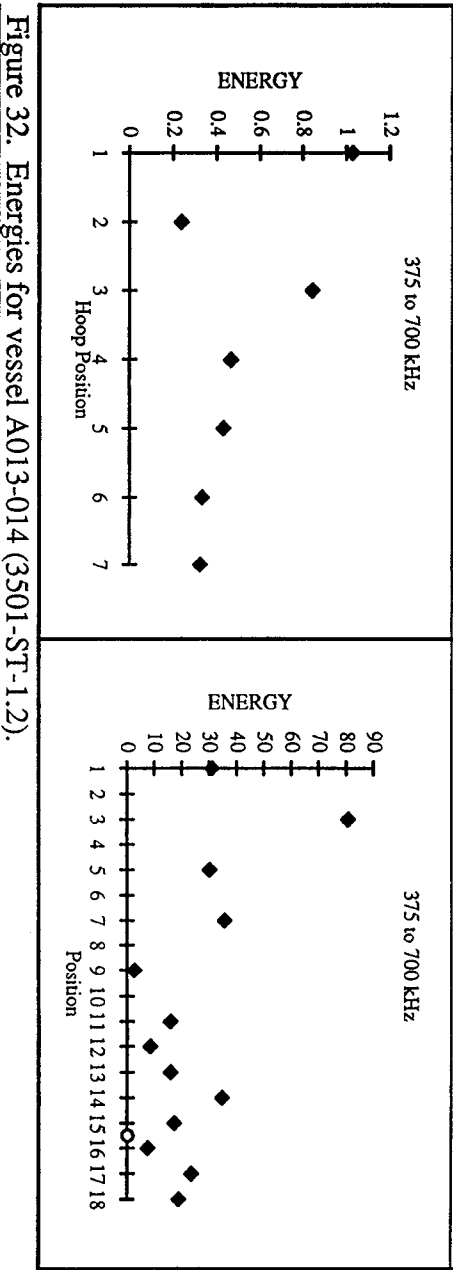
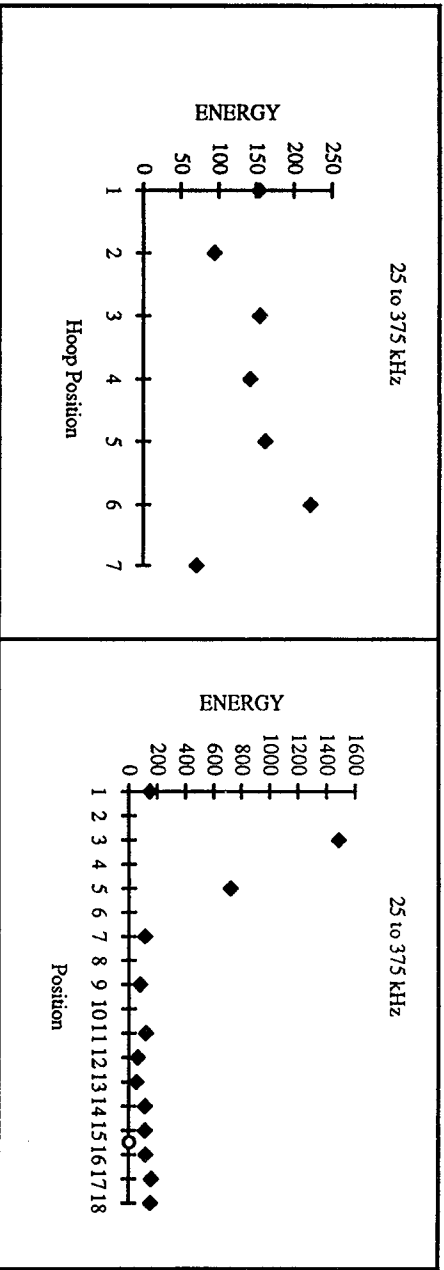


Figure 33. Energies for vessel A017-018 (3501-ST-2.6).

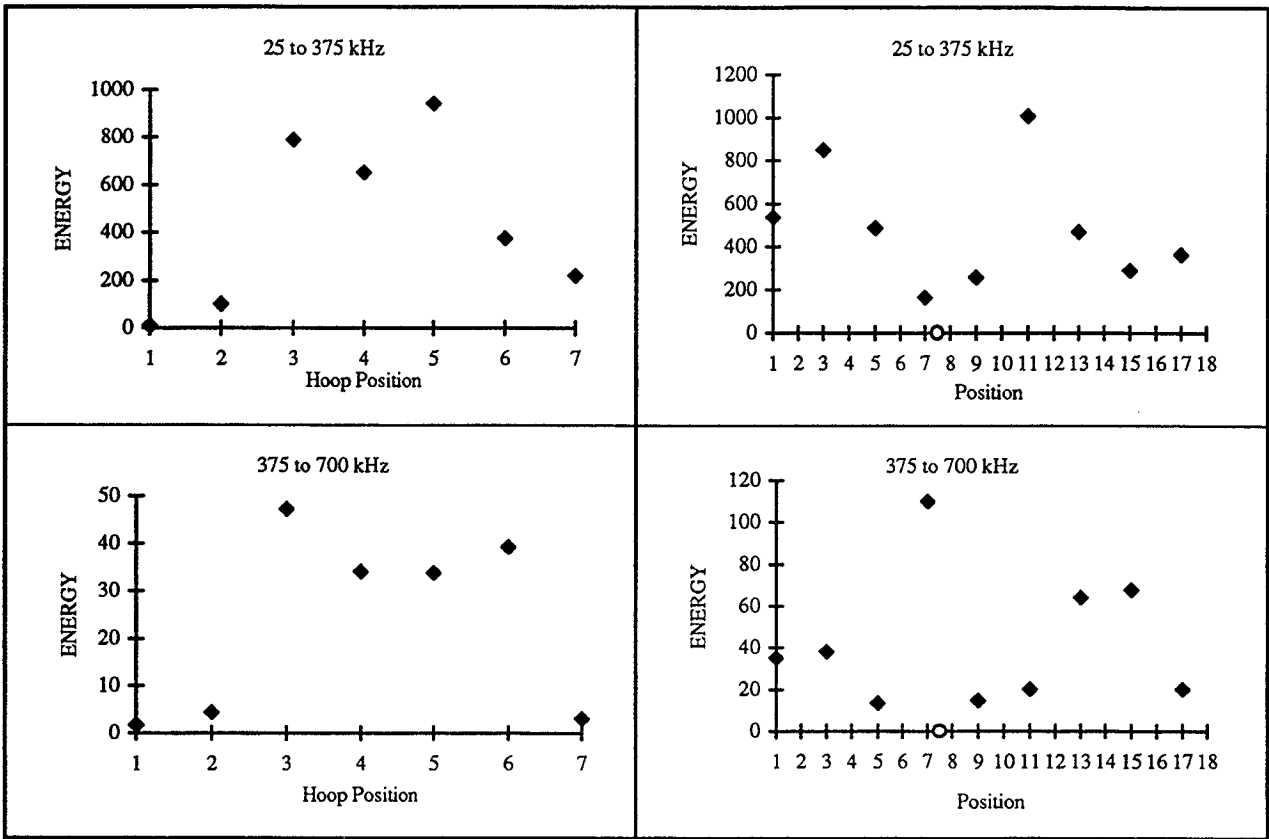


Figure 34. Energies for vessel C077-078 (3501-BT-8.1).

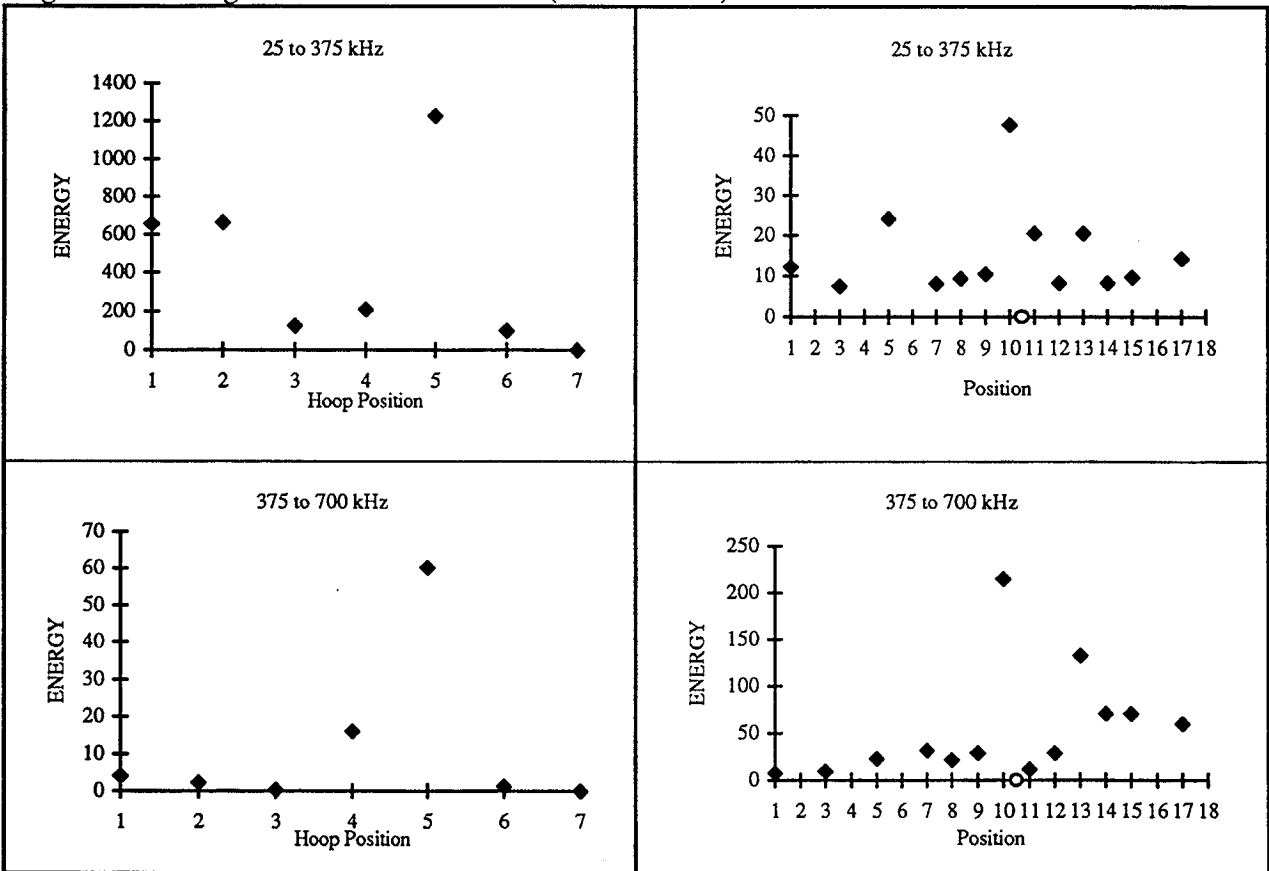


Figure 35. Energies for vessel C117-118 (977-BT-8.1).

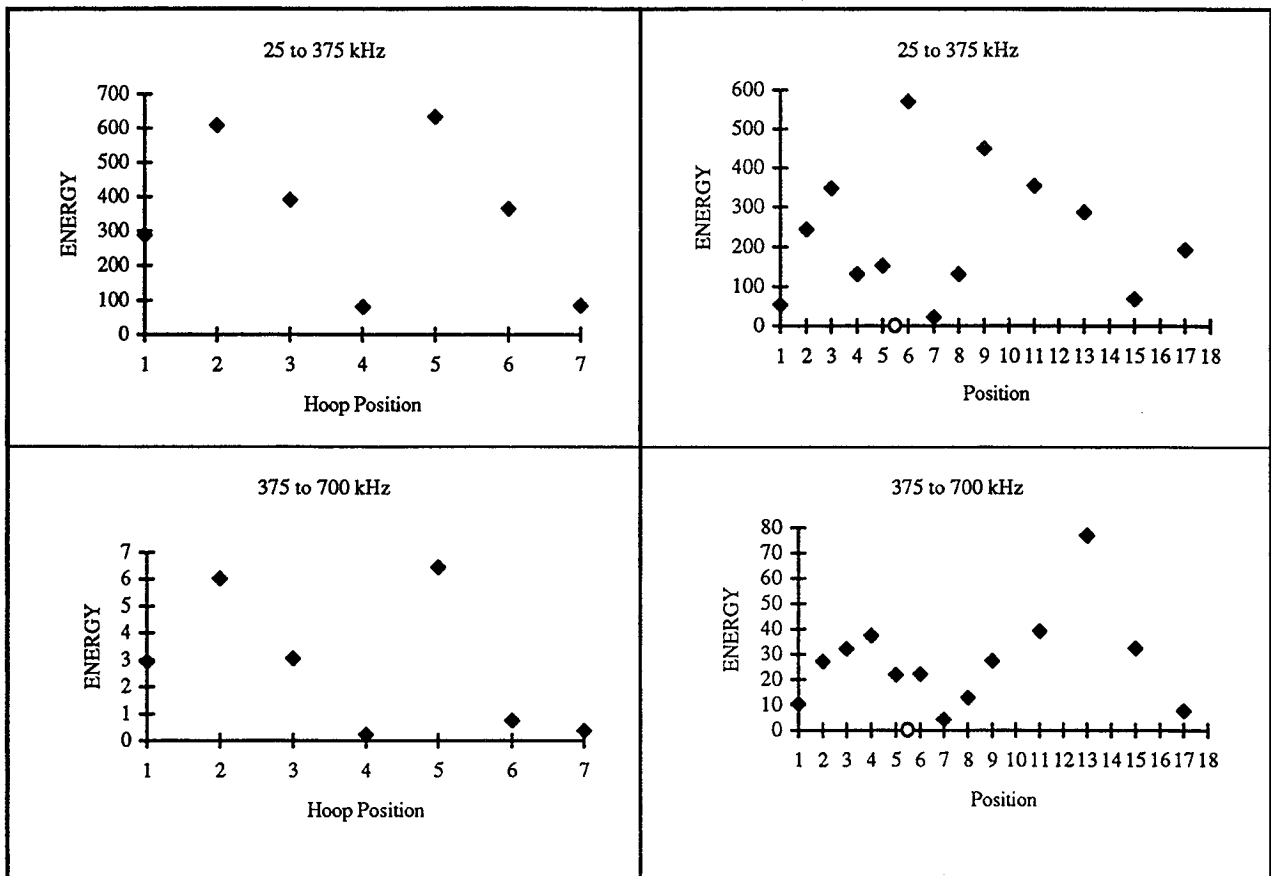


Figure 36. Energies for vessel C131-132 (977-ST-1.2).

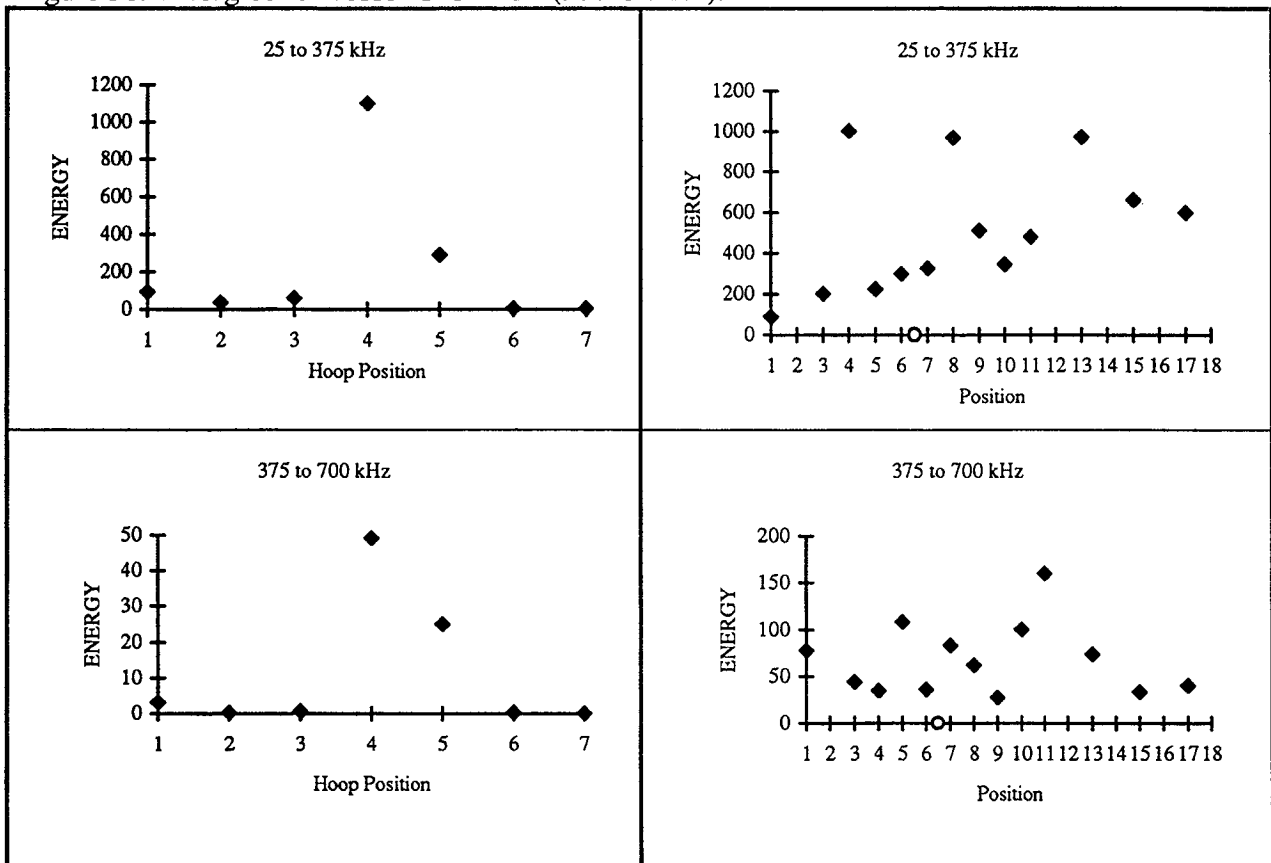


Figure 37. Energies for vessel C141-142 (977-BT-5.0).

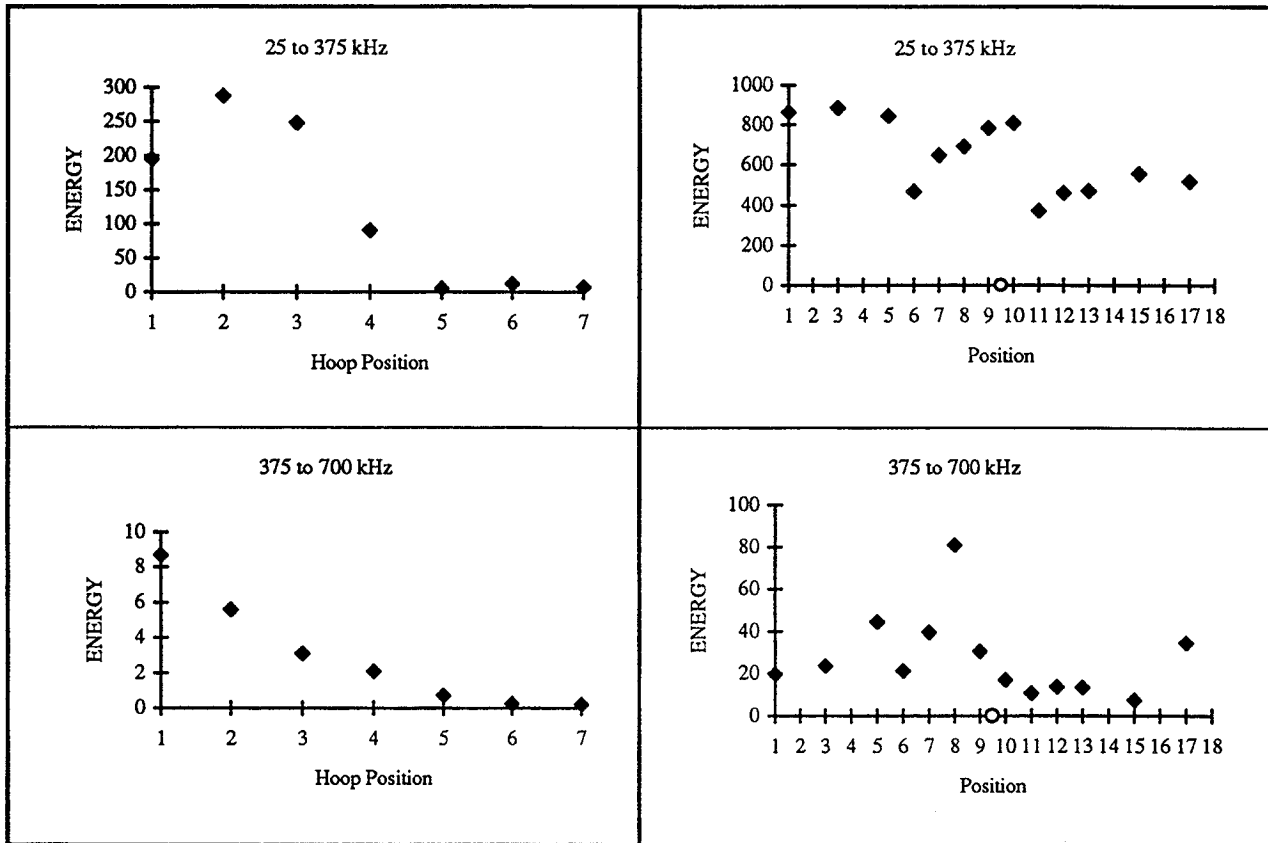


Figure 38. Energies for vessel C155-156 (977-ST-2.6).

The energy bands selected for this preliminary study did not provide an adequate SWF for identifying the impacted regions of the pressure vessels. In general, the energy values for the circumferential measurements tended to decrease in the damage zone while the hoop energy values tended to increase at the impact point. Overall, no conclusive trends could be found in the energy profiles to establish a measurement of the impact position or severity.

There were two major sources for the inability of this AU system to detect the flawed regions. First, a high degree of surface roughness and curvature combined with a large sensor contact area lead to poor couplant repeatability. The individual values used to compute the averages produced variations greater than 100% in some cases. Wave guides were constructed from brass and Plexiglas to reduce the footprint of the transducers in an attempt to help reduce the problem of local surface roughness. The combined attenuation of the wave guides and the bottles reduced the already weak AU signal to an impractical level though, such that the background noise dominated the power spectrum. Figure 39 illustrates the wave guides that were constructed for the study.

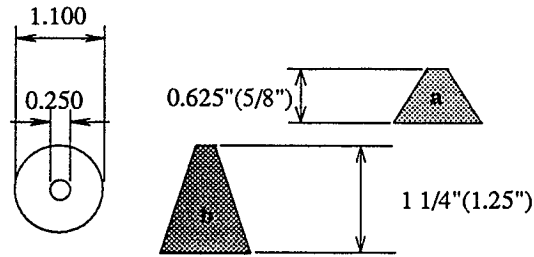


Figure 39. Wave guides.

The second reason that the system was not able to detect the damage zone was that the AU signal had to pass through a "filtered" channel board of the AE system before it could be stored by the TRA system. This meant that the 100 to 300 kHz bandpass filter located on the channel board would block some if not all of the high frequency information of the AU signal. Since the signal was already weak due to the attenuation of the pressure vessel, very little of the high frequency components were recorded. The damage detection threshold of an AU system is directly related to the frequency of the transmitted signal. A small crack or discontinuity acts as a low pass filter, blocking high frequency components of the signal. The lower frequency components will pass through a damaged region with little or no effect to its attenuation while higher frequencies will be blocked by the damage. Therefore, since what is being measured by an AU system is the variation in the signals characteristics from one location on the structure to another, if the higher frequencies are attenuated by the recording system no variations will be measured. The amount that a signal will be attenuated by the filter can be seen in the amplitude frequency response of the channel board shown in Figure 40.

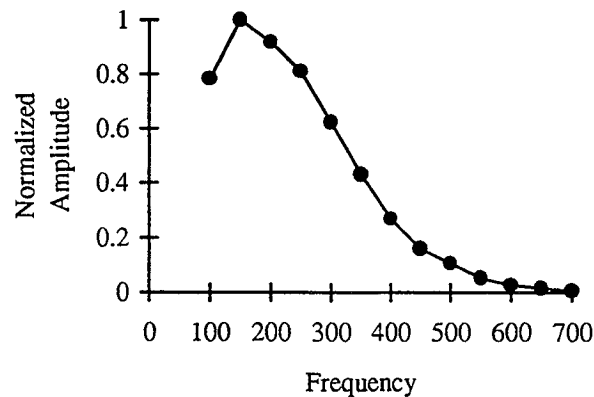


Figure 40. Amplitude frequency response of SPARTAN system.

The problems encountered with this preliminary work led to the development of the AURES. The AURES eliminates virtually all of the sensor contact repeatability and tedium problems found when taking measurements by hand. The ultrasonic receiver used with the AURES (0.25 inch diameter) is less effected by surface roughness than the 1.0 inch diameter WDI sensor. By using load cell feedback consistent pressure could be maintained for each measurement with the AURES. Also, the bandwidth of the AURES permits frequency analysis up to 2 MHz, which greatly enhances the potential of the AU signal analysis.

Two inert filled graphite/epoxy vessels were mapped using the AURES system (Table 14). Two hundred measurements were taken over forty equally spaced circumferential positions (5 measurements per position) to map the damage state of the vessels. The results are presented in Figures 41 and 42.

Fabrication number	Bottle I.D.	Resin type	Impact status
92PV003	A007-008	3501-6	ST-2.1 ft-lb.
92PV001	A033-034	8553-45	BT-5.0 ft-lb.

Table 14. Graphite/epoxy vessels mapped by acousto-ultrasonics.

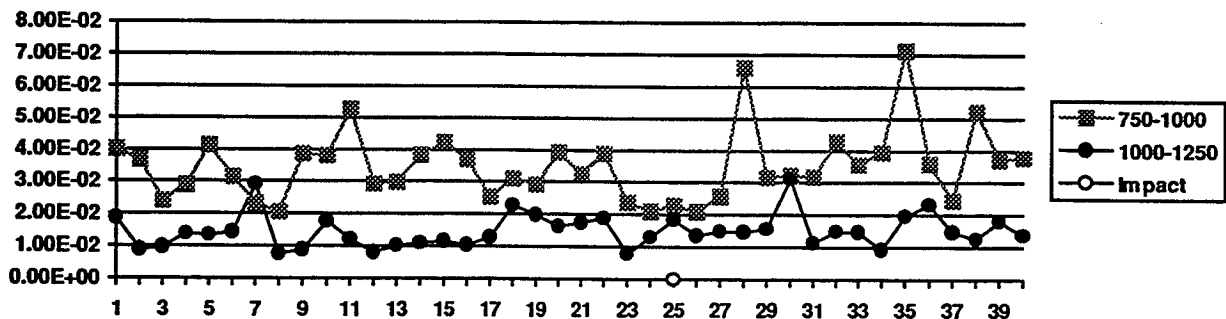


Figure 41. Energies for vessel A007 - Sharp Tip 2.1 ft-lb.

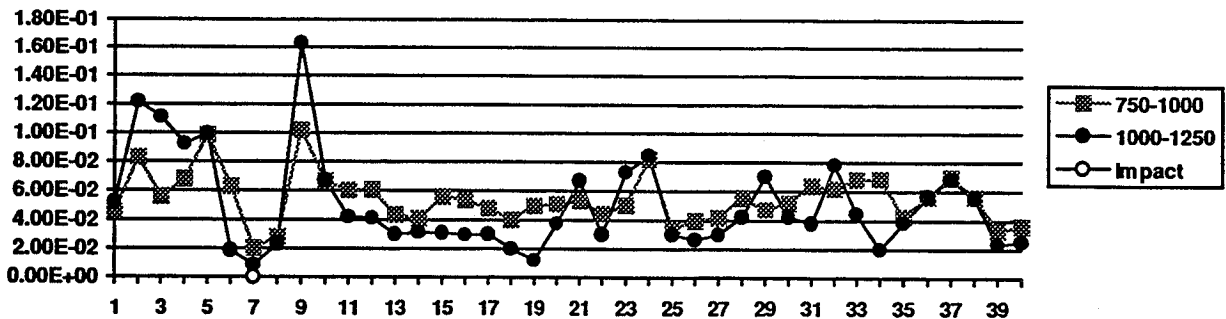


Figure 42. Energies for vessel A033 - Blunt Tip 5.0 ft-lb.

The energy computed from the 750 to 1000 kHz frequency interval showed the same trend as was found using the hybrid AE/ultrasonic system. That is, the AU energy associated with the damage zone is less than that of the remaining vessel. To a lesser degree, the 1000 to 1250 kHz zone could also be used to locate damage. It is interesting to note that a second region of lower energy is found nearly 180° from the impact site. Although, the energy reduction is not as great, the results indicate that secondary damage may exist. This damage may be a side effect of the way the vessels were cradled during impact, with the cradle-vessel contact producing some damage at impact.

### 3.4 INERT FILLED KEVLAR/EPOXY 5.75 INCH DIAMETER VESSELS

The AURES was used to AU map 13 inert propellant filled vessels featuring various levels of impact energies. A Harrisonic 1.0 MHz pulser injected the ultrasonic energy into the vessel while a Digital Wave broadband receiver recorded the AU signal. The sensors were spaced two inches apart along the longitudinal axis of the vessels and were centered on the bottles length. A thin bead of Soundsafe ultrasonic couplant was applied around the vessels in the path of the sensors and a 4.5 psi (0.25 volt) contact pressure was set into the comparator. The pulse energy of the Panametric pulser unit was set to 4 (400 volt).

#### 3.4.1 Data Summary

The vessels are identified in Table 15 along with the impact locations, AU code and impact status. The impact locations provide the approximate center of the impact point. When three digits are given the impact point is nearly centered on the middle digit, while two digits implies that the impact point is centered between those values.

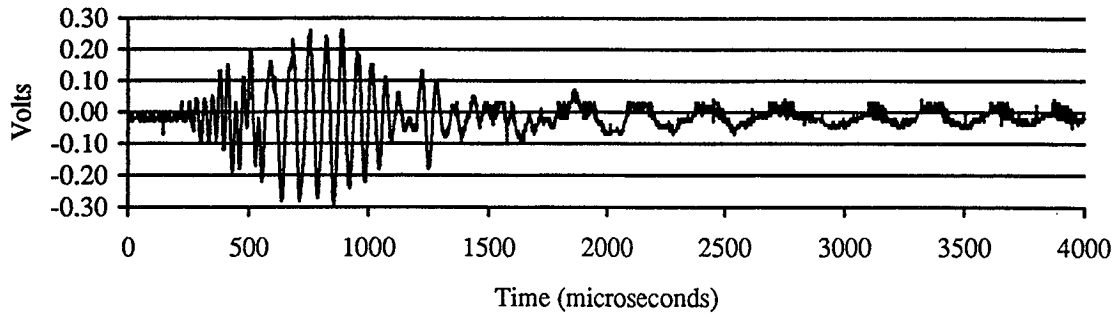
Bottle I.D.	Impact Location	Test date	AU test code	Impact Status (Ft-lb.)
D249-250	7-8-9	4-17-95	I	ST-3.82
D231-232	37-38	4-17-95	J	ST-4.85
D181-182	37-38	4-17-95	K	ST-2.89
D223-224	none	4-9-95	N	none
D191-192	5-6-7	4-9-95	O	BT-20.28
D205-206	8-9-10	4-9-95	P	BT-4.95
D245-246	35-36	4-9-95	Q	BT-13.29
D175-176	6-7	7-31-95	U	BT-16.5
D185-186	none	8-1-95	W	none
D255-256	3-4	7-31-95	X	ST-4.10
D257-258	4-5	8-1-95	Y	BT-10.9
D159-160	33-34	10-25-95	AB	ST-3.92
D219-220	27-29-31	10-25-95	AD	BT-15.04

BT = Blunt Tip (0.5 inch) ST = Sharp Tip (1 mm)

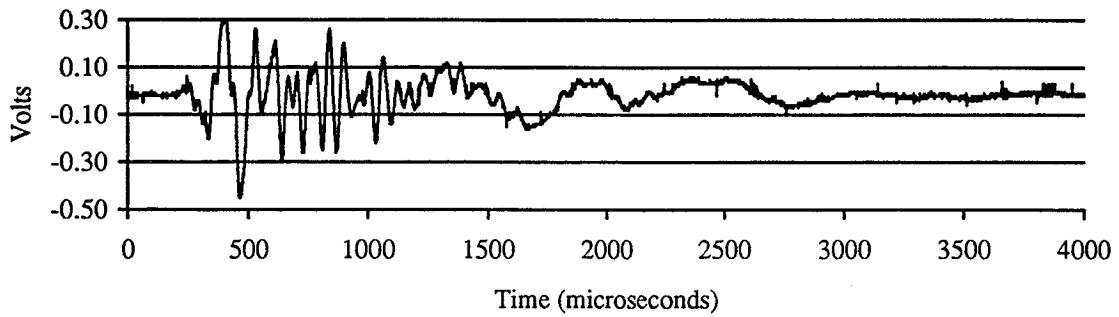
Table 15. Inert filled vessel AU data summary.

#### 3.4.2 Energy/Location Plots and Discussion

The spectral energies were computed over eight, 250 kHz, intervals, from nearly DC up to 2.0 MHz. Of these bands, the 750 kHz to 1000 kHz and 1000 kHz to 1250 kHz bands provided the best resolution to measure the extent of the impact damage. Typical signals and their power spectra are given in Figure 43 for a damaged and undamaged zone. The results of the AU analysis are presented in Figures 44 through 56.



Signal at damage zone



Signal away from damage zone

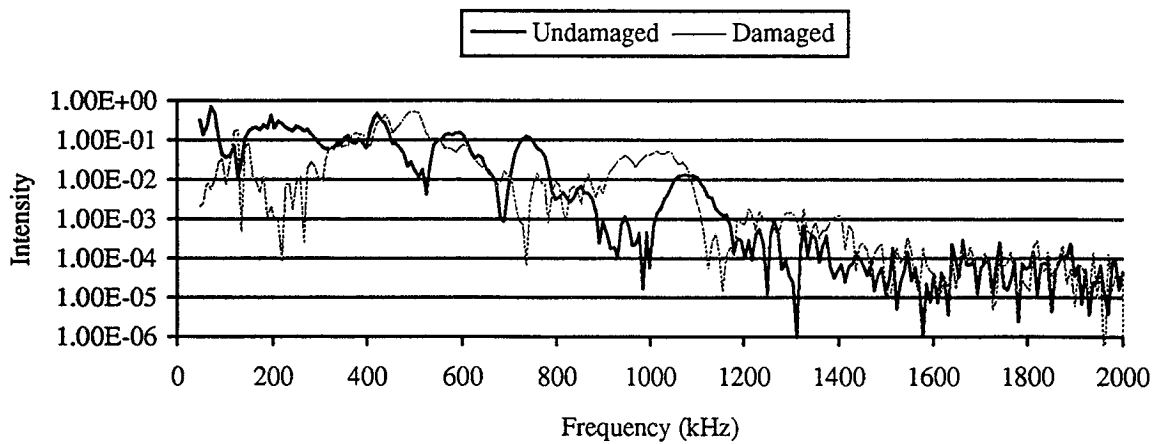


Figure 43. Signal variations between damaged and undamaged zones.

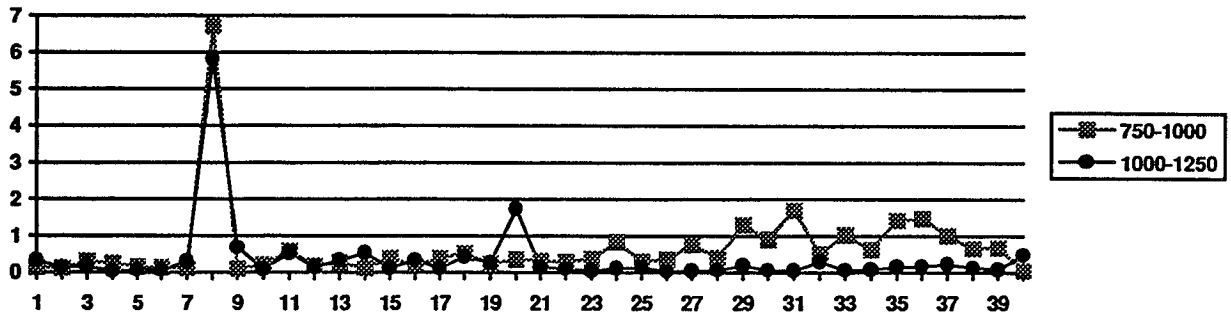


Figure 44. Energies for vessel D249 - Impact at position 8 - Sharp Tip 3.82 ft-lb.

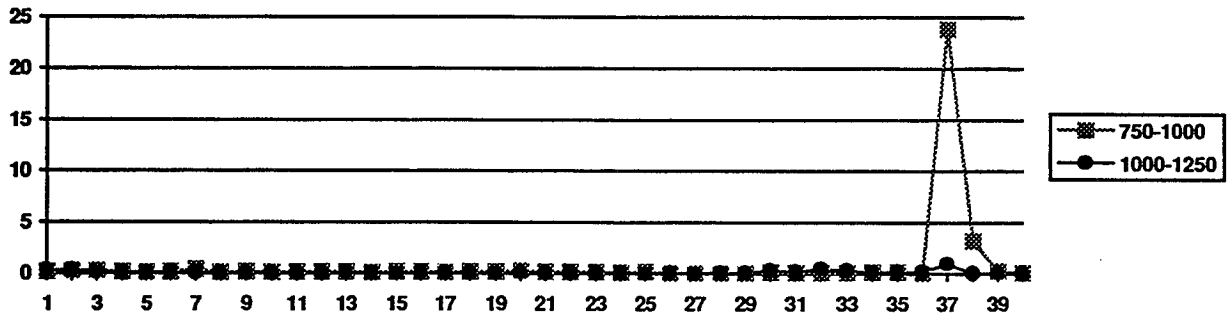


Figure 45. Energies for vessel D231 - Impact at position 37.5 - Sharp Tip 4.85 ft-lb.

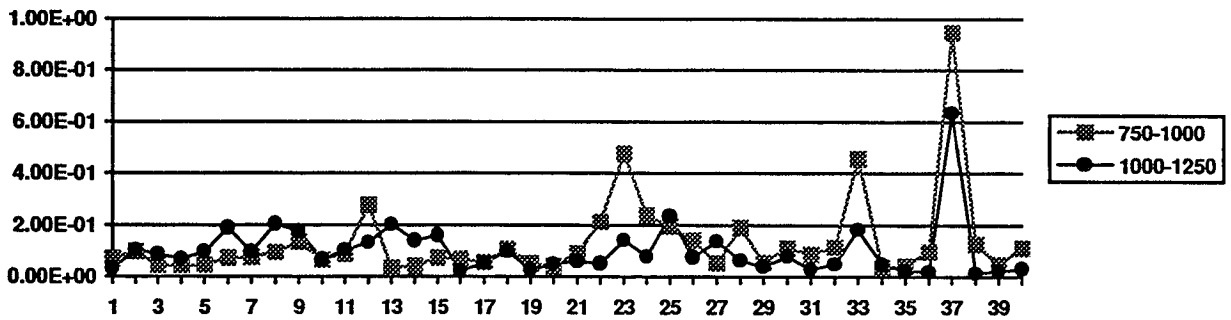


Figure 46. Energies for vessel D181 - Impact at position 37.5- Sharp Tip 2.89 ft-lb.

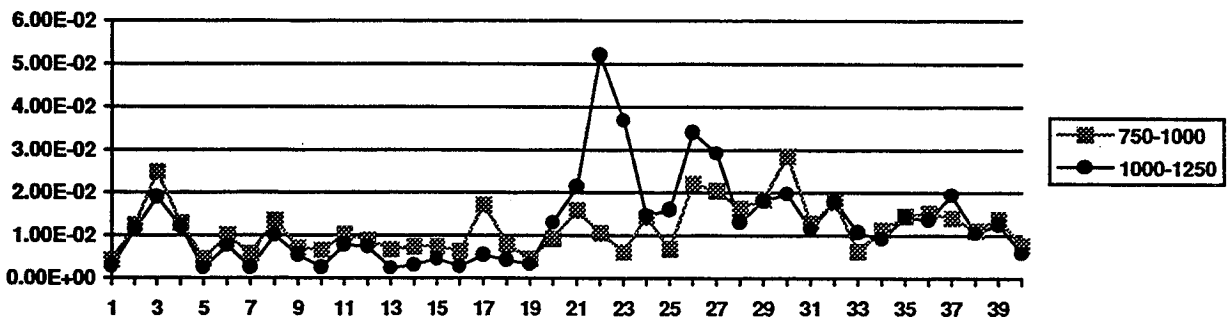


Figure 47. Energies for vessel D223 - No impact - Failure at position 30.

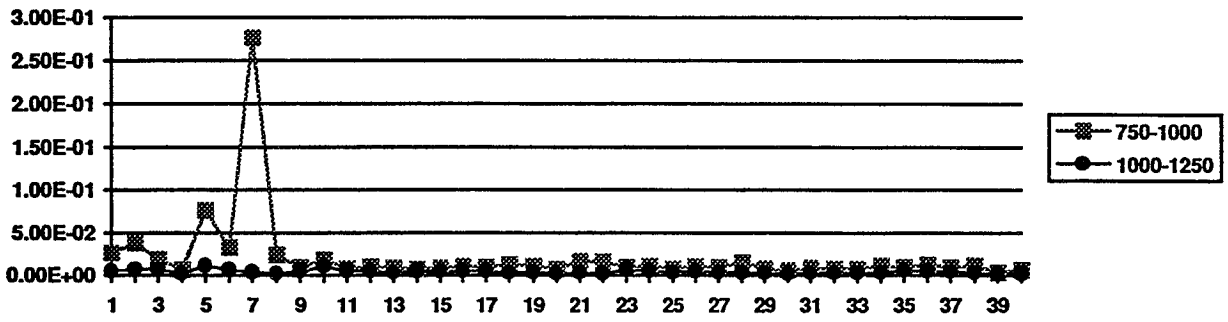


Figure 48. Energies for vessel D191 - Impact at position 6 - Blunt Tip 20.28 ft-lb.

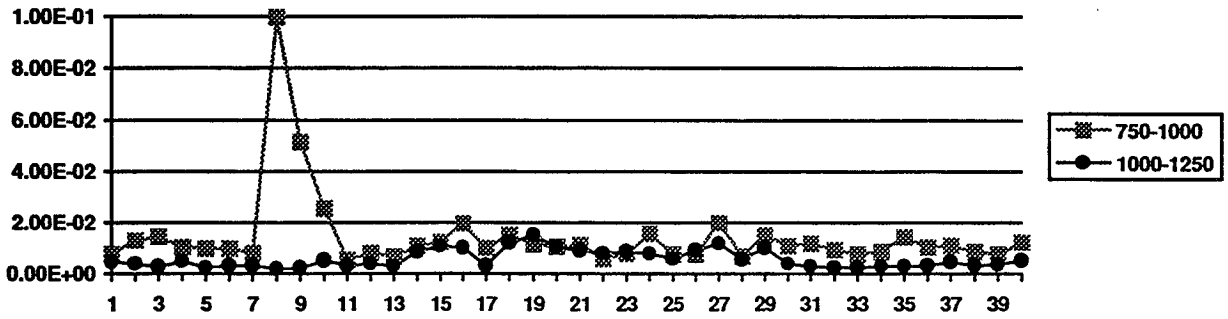


Figure 49. Energies for vessel D205 - Impact at position 9 - Blunt Tip 4.95 ft-lb.

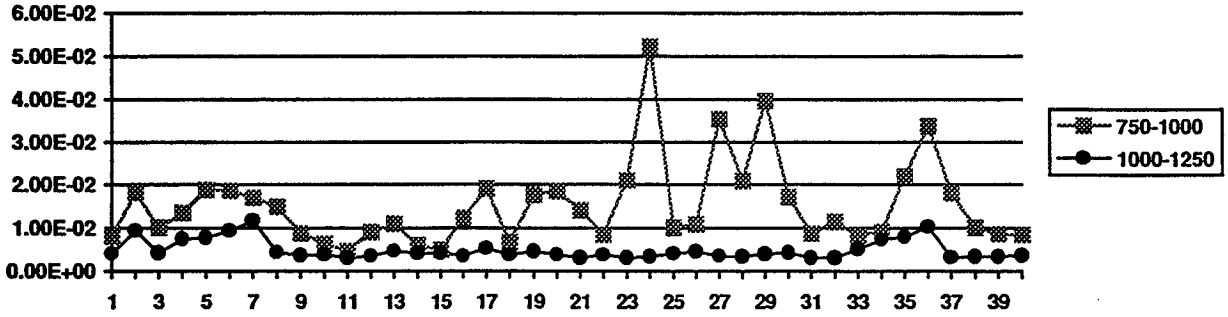


Figure 50. Energies for vessel D245 - Impact at position 35.5 - Blunt Tip 13.29 ft-lb.

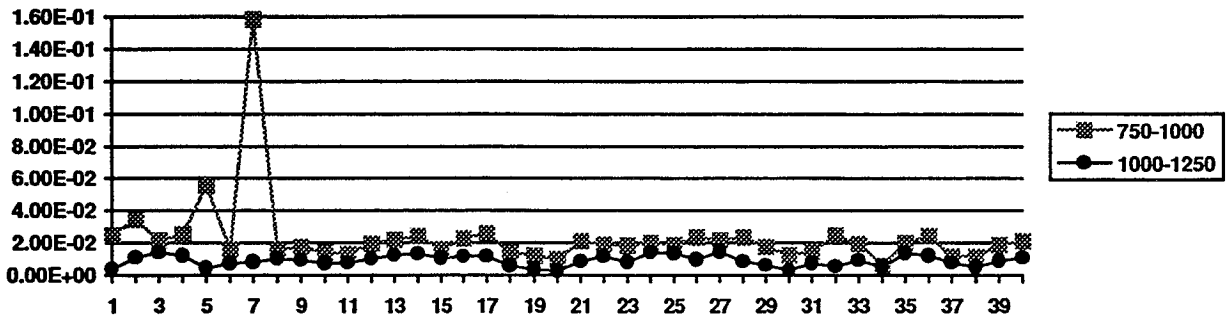


Figure 51. Energies for vessel D175 - Impact at position 6.5 - Blunt Tip 16.5 ft-lb.

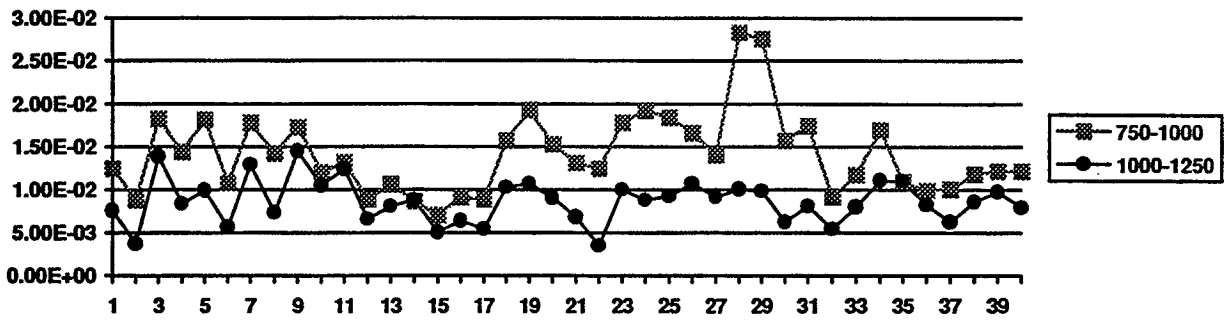


Figure 52. Energies for vessel D185 - No impact - Failure at position 28.

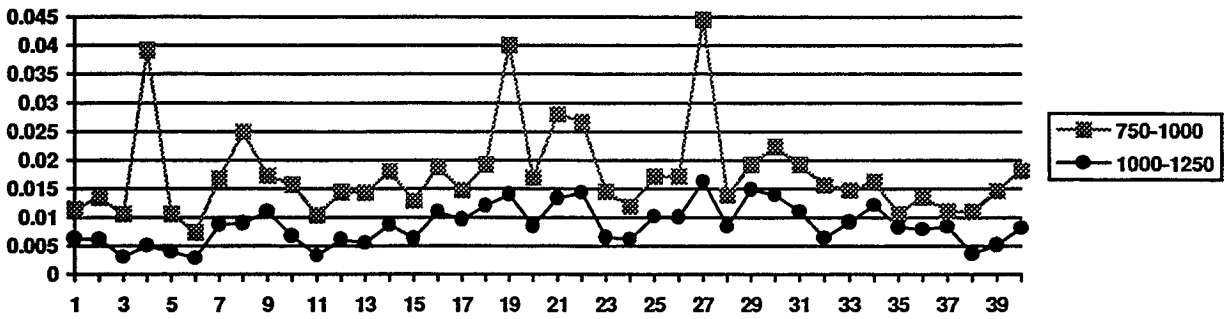


Figure 53. Energies for vessel D255 - Impact at position 3.5 - Sharp Tip 4.10 ft-lb.

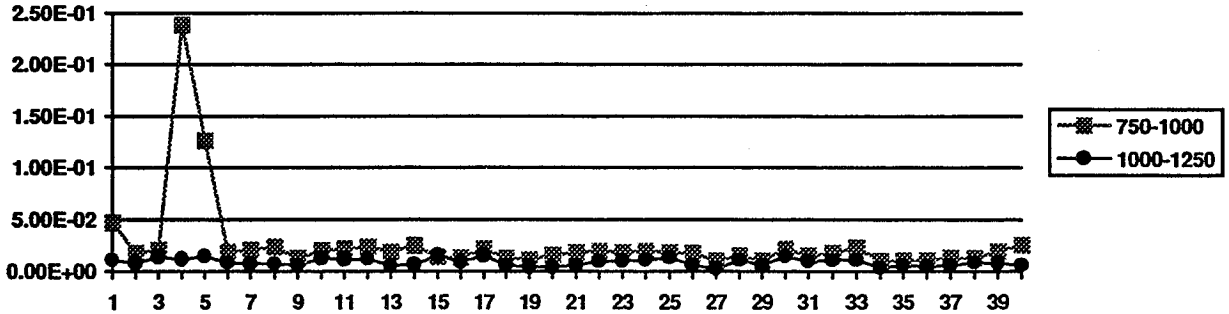


Figure 54. Energies for vessel D257 - Impact at position 4.5 - Blunt Tip 10.90 ft-lb.

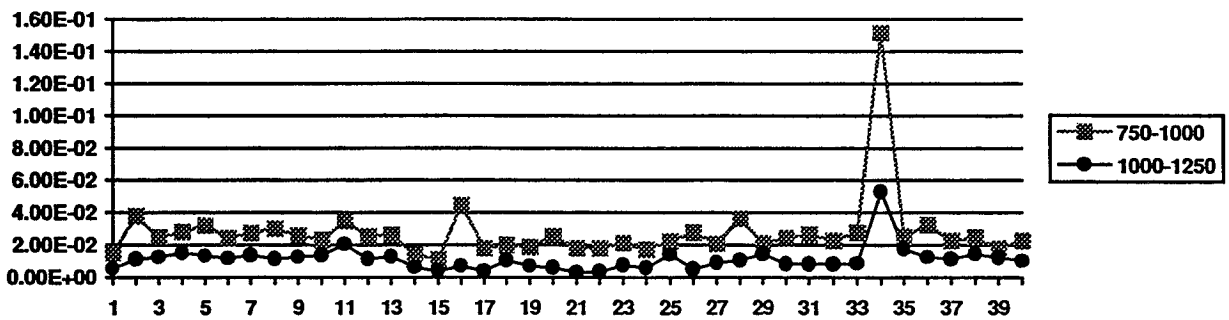


Figure 55. Energies for vessel D159 - Impact at position 33.5 - Sharp Tip 3.92 ft-lb.

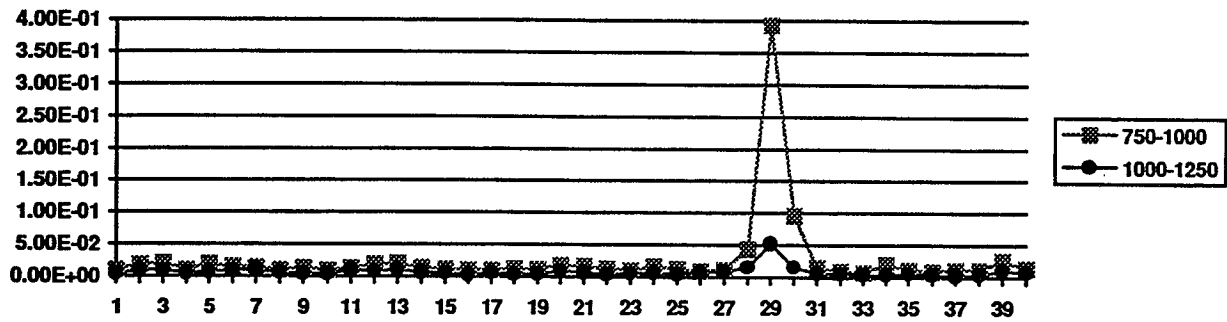


Figure 56. Energies for vessel D219 - Impact at position 29 - Blunt Tip 15.04 ft-lb.

The impact locations were very pronounced in the energy plots for the kevlar vessels. In every case, the energy from the 750 to 1000 kHz band increased several orders of magnitude at and around the impact site. The 1000 to 1250 kHz frequency band was not as good a measure of the impact location but it did provide additional information when the lower frequency interval was not as clear.

Most important to note though, was the capability of the AU system to locate the failure initiation point of the unimpacted vessels. The overall energy magnitudes were the same for the damaged and undamaged vessels, with only slight increases in energy around suspect zones for the undamaged vessels. For example, the AU system mapped regions of high energy for vessel D185 at position 28, and vessel D223 at position 30; in both cases failure initiated at or near those regions.

### 3.5 EMPTY KEVLAR/EPOXY 5.75 INCH DIAMETER VESSELS

The AURES was used to AU map 17 empty kevlar/epoxy vessels featuring various levels of impact energies. A Harrisonic 1.0 MHz pulser injected the ultrasonic energy into the vessel while a Digital Wave broadband receiver recorded the AU signal. The sensors were spaced two inches apart along the longitudinal axis of the vessels and were centered on the bottles length. A thin bead of Soundsafe ultrasonic couplant was applied around the vessels in the path of the sensors and a 4.5 psi (0.25 volt) contact pressure was set into the comparator. The pulse energy of the Panametric pulser unit was set to 4 (400 volt).

#### 3.5.1 Data Summary

The vessels are identified in Table 16 along with the impact locations, AU code and impact status. The same impact location code as for the inert filled vessels was followed.

#### 3.5.2 Energy/Location Plots and Discussion

The spectral energies were computed over eight, 250 kHz, intervals, from nearly DC up to 2.0 MHz. Of these bands, the 750 kHz to 1000 kHz and 1000 kHz to 1250 kHz bands provided the best resolution to measure the extent of the impact damage. The results (Figures 57 through 73) of these tests were the same as for the empty kevlar vessels in that the energy values increased drastically around the impact site.

Bottle I.D.	Impact Location	Test date	AU test code	Impact Status (Ft.-lb.)
D171-172	23-24	4-13-95	A	?
D235-236	38-39	4-13-95	B	BT-14.41
D254-255	4-8-12	4-13-95	C	BT-13.09/14.41
D169-170	33-34-35	4-14-95	D	ST-8.83
D187-188	7-8	4-14-95	E	BT-11.80
D241-242	9-10-11	4-14-95	F	BT-9.00
D177-178	36-37	4-14-95	G	ST-11.91
D225-226	36-37	4-14-95	H	ST-11.80
D201-202	3-4	6-8-95	L	ST-6.90
D233-234	none	6-9-95	M	none
D237-238	4-5	7-28-95	R	ST-9.8
D163-164	4-5-6	7-28-95	S	BT-10.9
D215-216	4-5	7-28-95	T	ST-7.1
D221-222	none	7-28-95	V	none
D161-162	35-36	8-21-95	Z	?
D207-208	29-30-31	10-25-95	AA	ST-9.40
D203-204	9-10	10-25-95	AC	BT-11.47

Table 16. AU data summary.

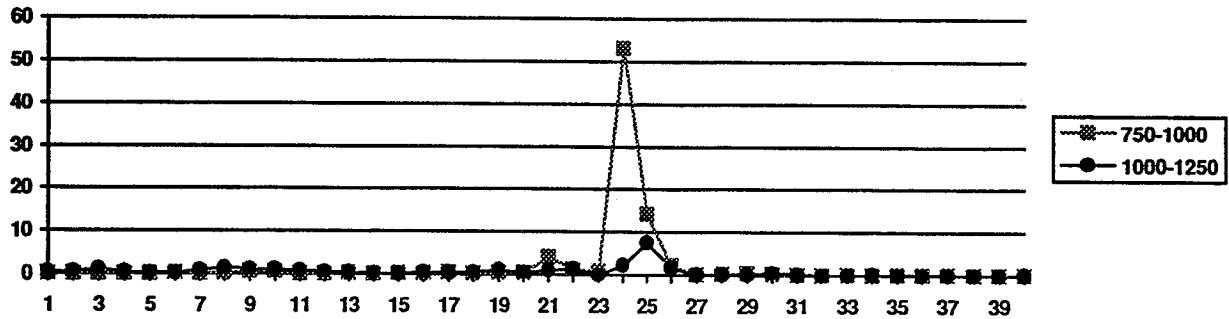


Figure 57. Energies for vessel D171 - Impact at position 23.5.

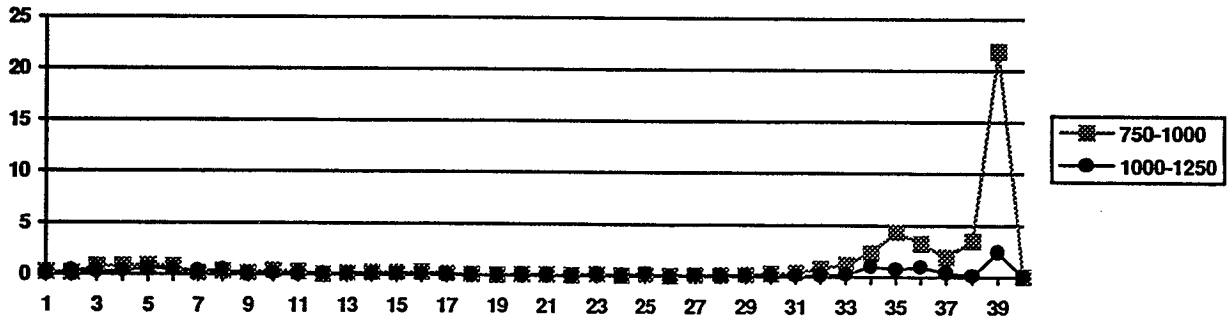


Figure 58. Energies for vessel D235 - Impact at position 38.5 - Blunt Tip 14.41 ft.-lb.

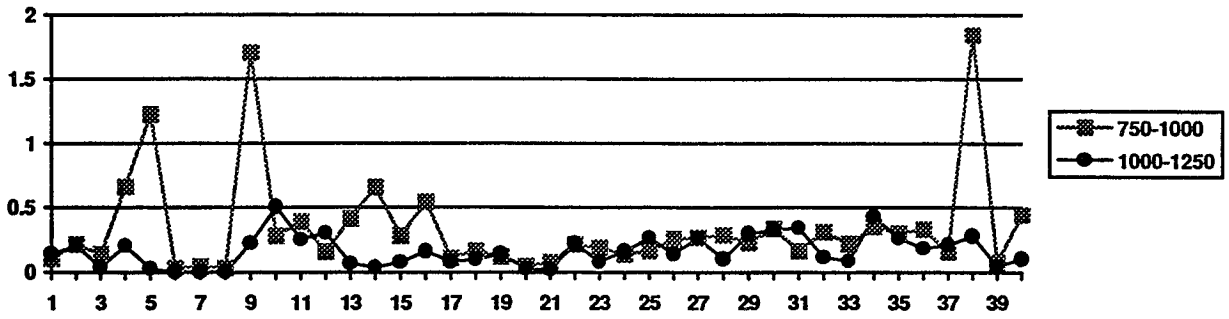


Figure 59. Energies for vessel D254 - Impact at position 8 - Blunt Tip 13.09/14.41 ft-lb.

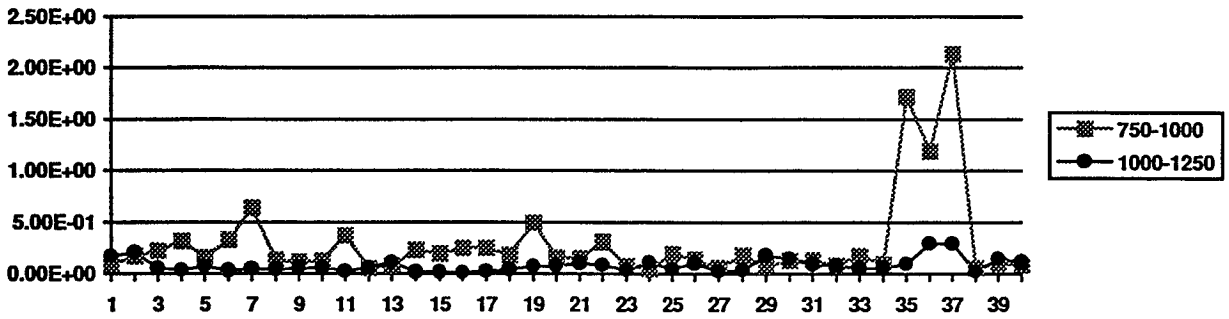


Figure 60. Energies for vessel D169 - Impact at position 34 - Sharp Tip 8.83 ft-lb.

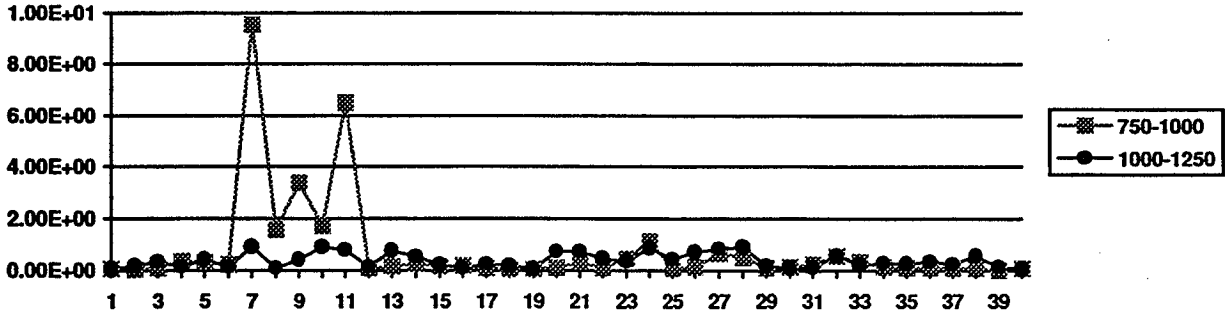


Figure 61. Energies for vessel D187 - Impact at position 7.5 - Blunt Tip 11.80 ft-lb.

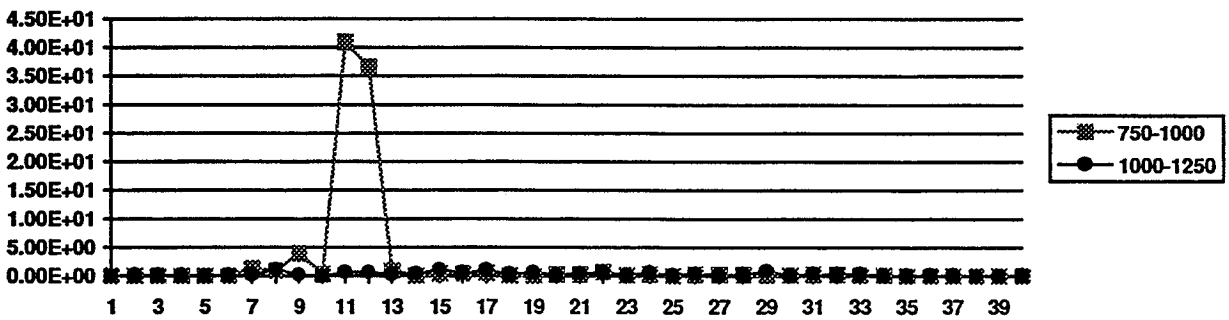


Figure 62. Energies for vessel D241 - Impact at position 10 - Blunt Tip 9.00 ft-lb.

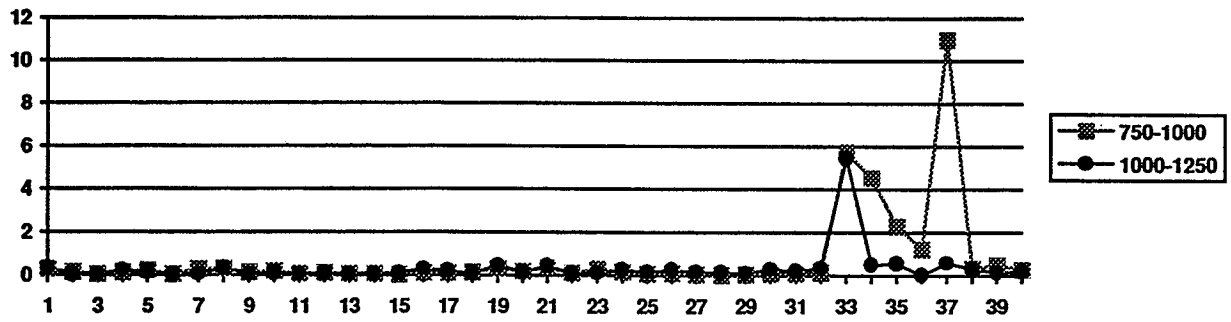


Figure 63. Energies for vessel D177 - Impact at position 36.5 - Sharp Tip 11.91 ft-lb.

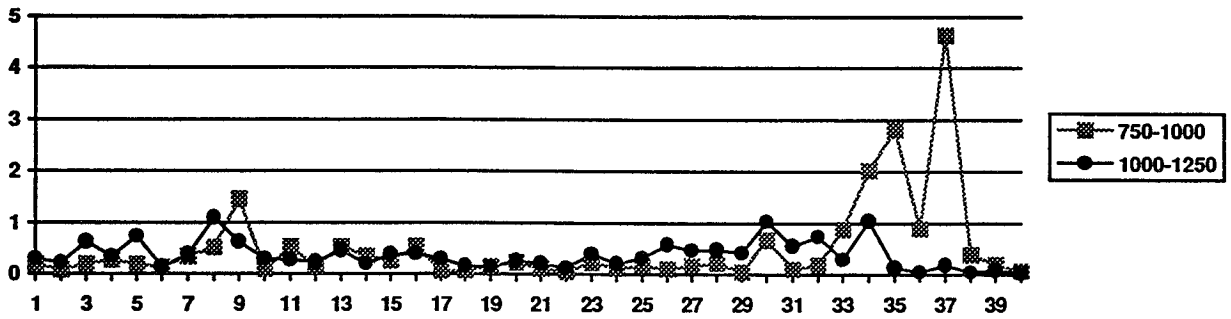


Figure 64. Energies for vessel D225 - Impact at position 36.5 - Sharp Tip 11.80 ft-lb.

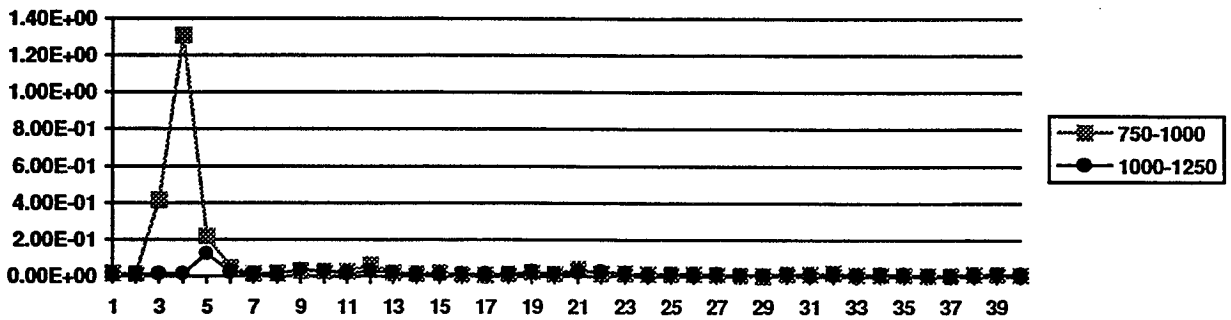


Figure 65. Energies for vessel D201 - Impact at position 3.5 - Sharp Tip 6.90 ft-lb.

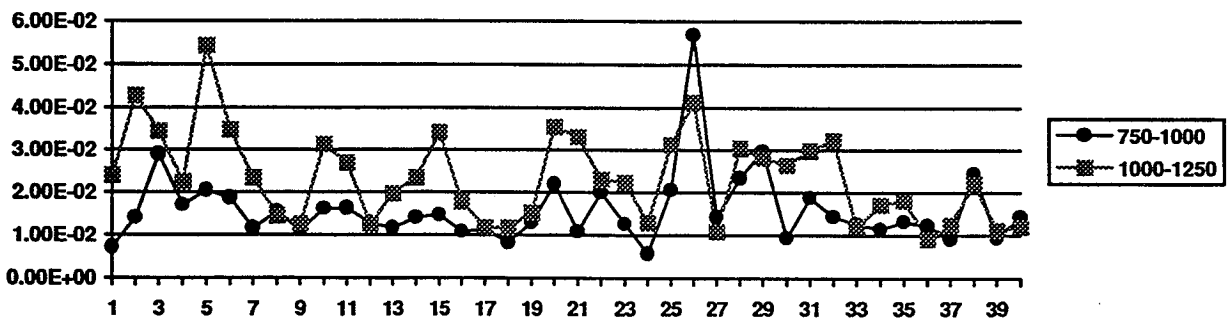


Figure 66. Energies for vessel D233 - No impact - No identifiable failure initiation point.

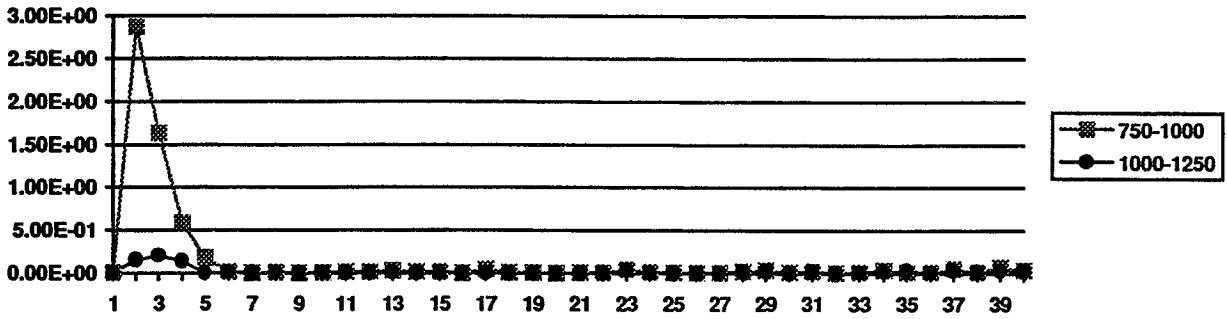


Figure 67. Energies for vessel D237 - Impact at position 4.5 - Sharp Tip 9.80 ft-lb.

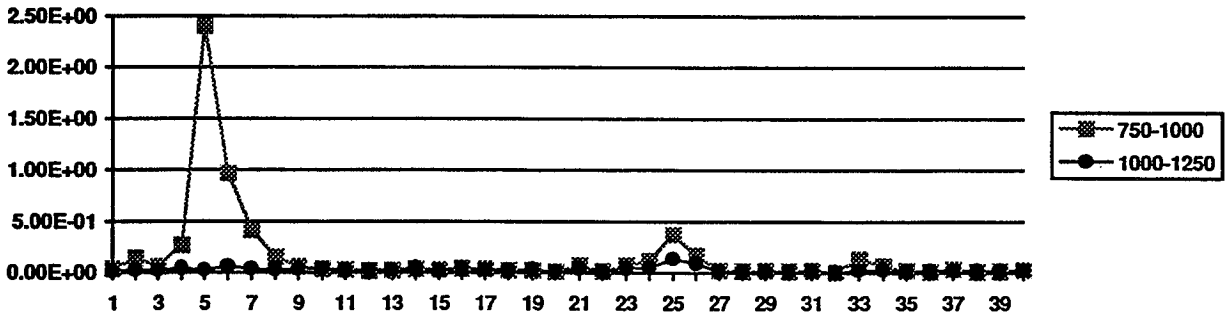


Figure 68. Energies for vessel D163 - Impact at position 5 - Blunt Tip 10.90 ft-lb.

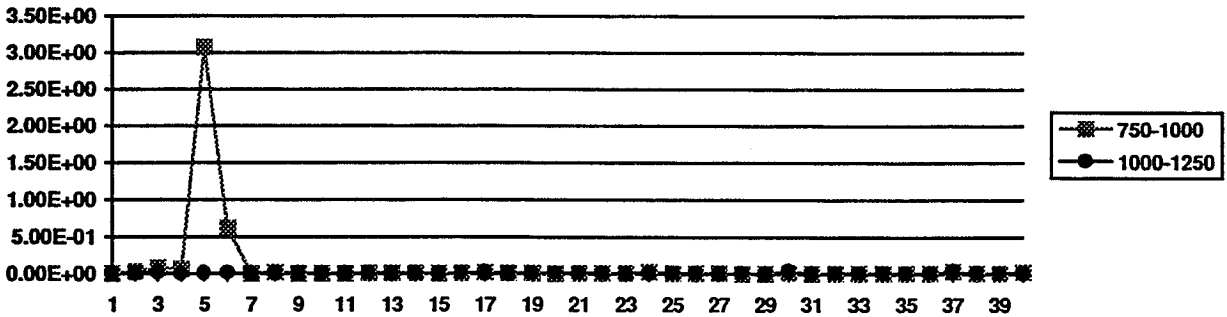


Figure 69. Energies for vessel D215 - Impact at position 4.5 - Sharp Tip 7.10 ft-lb.

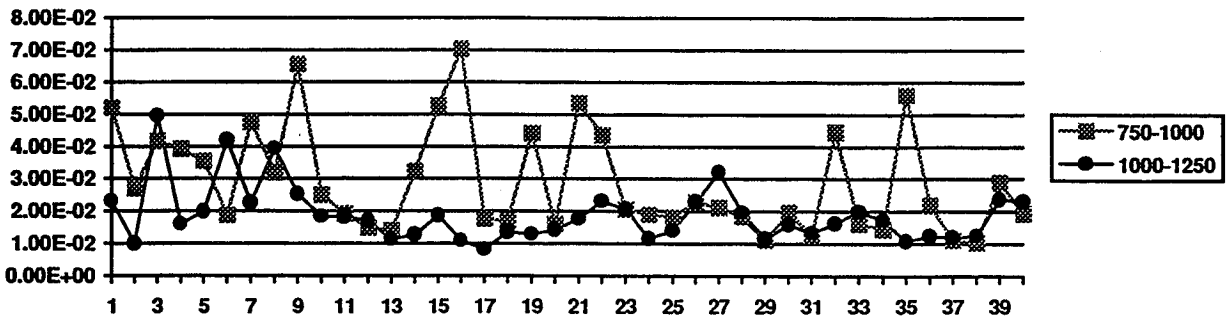


Figure 70. Energies for vessel D221 - No impact - Failure initiation at location 16.

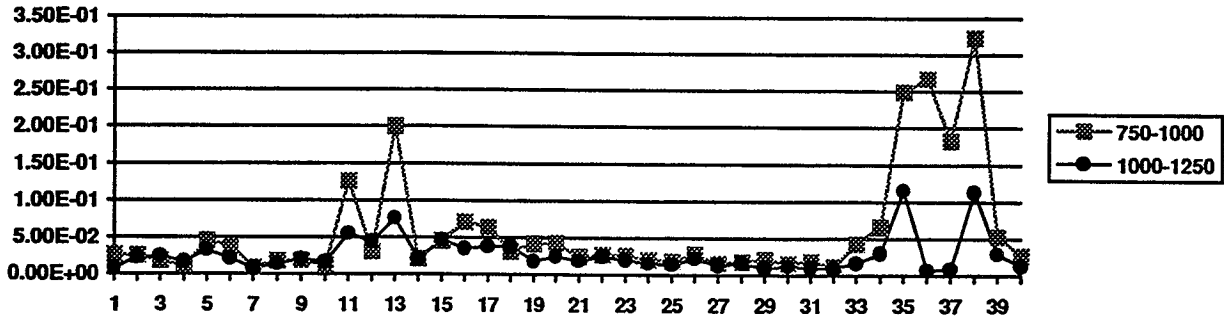


Figure 71. Energies for vessel D161 - Impact at position 35.5 - Unknown energy.

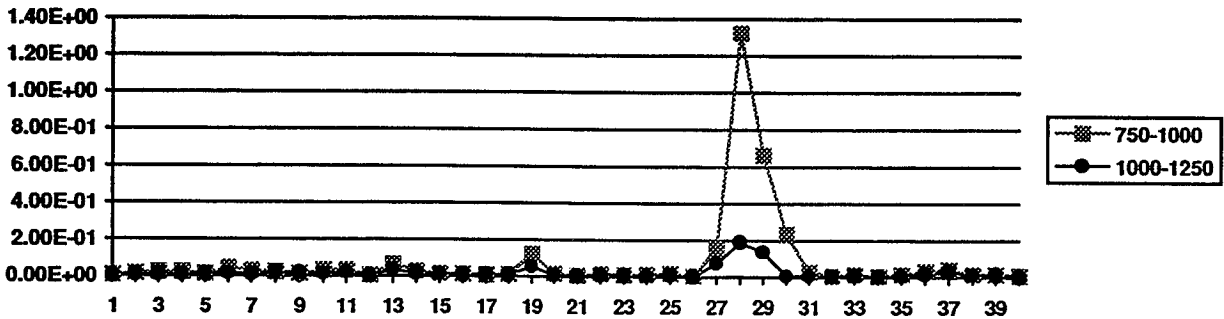


Figure 72. Energies for vessel D207 - Impact at position 30 - Sharp Tip 9.40 ft-lb.

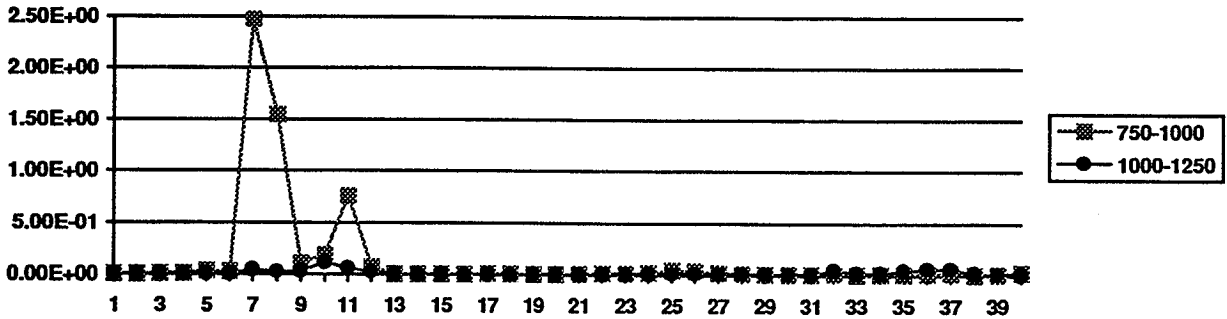


Figure 73. Energies for vessel D203 - Impact at position 9.5 - Blunt Tip 11.47 ft-lb.

Just as with the inert propellant filled kevlar vessels, a large increase in the energy of the 750 to 1000 kHz frequency band was found in and around the impact site. In certain instances such as for vessels D161, D225 and D163, secondary damage sites were located nearly 180 ° from the impact site, similar to the results found with the filled graphite/epoxy vessels (Section 3.3).

### 3.6 CONCLUSIONS (AU)

- The SWF formulated by the energy content of the frequency band between 750 and 1000 kHz can be used to locate critical zones in kevlar/epoxy pressure vessels.
- The SWF increases drastically in the damage zone for the kevlar/epoxy vessels.

- The SWF decreases only slightly in the impact zone for the graphite/epoxy vessels.
- The AURES has demonstrated the ability to determine the position where potential failure would occur in damaged and undamaged filament wound pressure vessels.

### **3.7 RECOMMENDATIONS (AU)**

The AURES should be reconfigured to map the entire pressure vessel. The vessels tested in this report were designed to fail in the mid hoop region, but since the failure location may vary for vessels of a different geometry the AURES should be given the flexibility to search any portion of the vessel. This flexibility will most likely come from the use of two robots, instead of one, to independently control the positioning of the pulser and receiver.

The AU spectra and resulting energies should be analyzed for the potential to measure the residual vessel strength. The AU waveforms will have to be normalized so that the power spectra is not biased by the natural variation in attenuation resulting from contact pressure and local surface conditions.

### **4.0 CONCLUSIONS**

The methods outlined in this report demonstrate that the quality of small FWPV can be determined nondestructively. Combining robotics and acousto-ultrasonics allows for vessel integrity to be checked without having to apply any form of loading other than the ultrasonic pulse. The automated technique works very well on the kevlar vessels and to a lesser degree on graphite/epoxy with or without an inert propellant liner. Once the critical area of interest is found with AU, other NDE methods such as SDVIC or ES should be employed to map the zone and determine the type of damage present.

By recording, "active" flaw growth, and not just the size of a flaw, AE has shown the potential for quantitatively determining the quality of a pressure vessel. AE signal analysis, through backpropagation neural networks, show the potential for developing burst pressure prediction models. The models can then be used to access the residual life of a vessel, at low proof loads, where fiber damage is at a minima.

### **5.0 REFERENCES**

1. Hoskin, B. C. and Baker, A. A., Editors, Composite Materials for Aircraft Structures, American Institute of Aeronautics and Astronautics, New York, NY, 1986.

2. Walker, J. L., Lansing, M. L., Russell, S. S., Workman, G. L. and Nettles A., "Materials Characterization of Damage in Filament Wound Composite Pressure Vessels.", Proceedings from the ASNT 1995 Spring Conference, Las Vegas, Nevada, March 20-24.
3. Caudill, M. and Butler C., Understanding Neural Networks, Volume 1: Basic Networks, Massachusetts Institute of Technology, Cambridge, MA, 1992.
4. Ely, T. E. and Hill, E. v. K., "Longitudinal Splitting and Fiber Breakage Characterization in Graphite Epoxy Using Acoustic Emission Data", Materials Evaluation, pp.288-294, February 1995, ASNT.

## 6.0 APPENDIX

### 6.1 TRA2MLAB.BAS

' This program converts a file from the TRA format to a MATLAB format.  
' The user should specify the upper limit on the loop before executing  
' the program.

```
FOR r = 0 TO 20
  IF r < 10 THEN
    w$ = "ch.00" + LTRIM$(STR$(r))
  END IF
  IF r > 9 AND r < 100 THEN
    w$ = "ch.0" + LTRIM$(STR$(r))
  END IF
  IF r > 99 THEN
    w$ = "ch." + LTRIM$(STR$(r))
  END IF
  ww$ = "ch" + LTRIM$(STR$(r)) + ".m"
  PRINT w$, ww$
  OPEN "i", 1, w$
  OPEN "o", 2, ww$
  FOR y = 1 TO 9
  LINE INPUT #1, q$
  NEXT y
  PRINT #2, "a=["
  FOR y = 1 TO 8191
    INPUT #1, z
    PRINT #2, z
  NEXT y
  INPUT #1, z
  PRINT #2, z,
  PRINT #2, "];"
CLOSE #1
CLOSE #2
NEXT r
END
```

### 6.2 ENGYDATA.M

% This program computes the energy content as measured by the area under  
% the power spectral density curve for a series of user defined PAC TRA  
% files. The input files should first be organized into sequentially  
% numbered ".m" files before running this program. The program "TRA2MLAB.BAS"  
% can be used to create the ".m" files.

```
!cls
clear % Clear all variables.
for k=0:20, % The range of "m" files.
eval(['ch',int2str(k)]); % Load the file into MATLAB.
k % Indicate the current file number.
a=a*.01; % Scale the signal amplitude to volts.
y = fft(a,8192); % Calculate the FFT for the signal.
```

```

Pyy = y.*conj(y)/8192;      % Calculate the power spectral density.
low(k+1)=sum(Pyy(25:192));  % Low energy for file (k+1).
high(k+1)=sum(Pyy(193:359)); % High energy for file (k+1).
end
save low.bas low -ascii     % Save energy data in an ASCII file.
save high.bas high -ascii

```

### 6.3 OUTPUT.BAS

```

' This program is used to organize the energy files from MATLAB.
' The input files "low.bas" and "high.bas" are created in MATLAB for a given
' TRA file. The user needs to supply an output filename for files 3 and 4
' and the upper limit on the loop.
OPEN "i", 1, "low.bas"
OPEN "i", 2, "high.bas"
OPEN "o", 3, "a029hl.bas"
OPEN "o", 4, "a029hh.bas"
FOR x = 1 TO 21 STEP 3
  INPUT #1, 1, I2, I3
  INPUT #2, h, h2, h3
  avgl = (I2 + I3) / 3
  avgh = (h + h2 + h3) / 3
  WRITE #3, I2, I3, avgl
  WRITE #4, h, h2, h3, avgh
NEXT x
CLOSE
END

```

### 6.4 AEHITS.BAS

```

CLEAR
REM ***** AMPLITUDE SORTING ROUTINE *****
PRINT "THIS ROUTINE WILL SORT AN AE DATA FILE TO FIND THE NUMBER OF HITS"
PRINT "FOR A GIVEN AMPLITUDE."
PRINT " "
CLEAR
DIM AMP1(100), AMP3(100), AMP4(100), AMP5(100)
PRINT "ENTER THE TEST FILE NAME AND PATHING INSTRUCTIONS"
INPUT FILES
OPEN "I", 1, FILES
PRINT " "
MINAMP = 60
MAX1 = 0
MAX3 = 0
MAX4 = 0
MAX5 = 0
PRINT "ENTER THE CUT-OFF TIME LIMIT FOR THIS TEST"
INPUT TCUT
150 INPUT #1, TIME, P1, CH, RISE, COUN, ENER, DUR, A
   IF TIME <= TCUT THEN
     IF A >= MINAMP THEN
       IF CH = 1 THEN

```

```

AMP1(A) = AMP1(A) + 1
IF A > MAX1 THEN MAX1 = A
I1 = I1 + 1
GOTO 150
END IF
IF CH = 3 THEN
AMP3(A) = AMP3(A) + 1
IF A > MAX3 THEN MAX3 = A
I3 = I3 + 1
GOTO 150
END IF
IF CH = 4 THEN
AMP4(A) = AMP4(A) + 1
IF A > MAX4 THEN MAX4 = A
I4 = I4 + 1
GOTO 150
END IF
IF CH = 5 THEN
AMP5(A) = AMP5(A) + 1
IF A > MAX5 THEN MAX5 = A
I5 = I5 + 1
GOTO 150
END IF
END IF
END IF
CLOSE #1
REM ***** AMPLITUDE OUTPUT ROUTINE *****
PRINT "THIS ROUTINE WILL LIST THE HITS FOR A RANGE OF AMPLITUDES FROM 60 TO
100dB."
PRINT " "
PRINT " AMP EVENTS   AMP EVENTS   AMP EVENTS   AMP EVENTS"
FOR Y = 1 TO 10
PRINT USING "### ####   ### ####   ### ####   ### ####"; Y + 60; AMP1(Y + 60); Y + 60;
AMP1(Y + 70); Y + 80; AMP1(Y + 80); Y + 90; AMP1(Y + 90)
NEXT Y
PRINT " "
PRINT " AMP EVENTS   AMP EVENTS   AMP EVENTS   AMP EVENTS"
FOR Y = 1 TO 10
PRINT USING "### ####   ### ####   ### ####   ### ####"; Y + 60; AMP3(Y + 60); Y + 70;
AMP3(Y + 70); Y + 80; AMP3(Y + 80); Y + 90; AMP3(Y + 90)
NEXT Y
PRINT " "
PRINT " AMP EVENTS   AMP EVENTS   AMP EVENTS   AMP EVENTS"
FOR Y = 1 TO 10
PRINT USING "### ####   ### ####   ### ####   ### ####"; Y + 60; AMP4(Y + 60); Y + 70;
AMP4(Y + 70); Y + 80; AMP4(Y + 80); Y + 90; AMP4(Y + 90)
NEXT Y
PRINT " "
PRINT " AMP EVENTS   AMP EVENTS   AMP EVENTS   AMP EVENTS"
FOR Y = 1 TO 10
PRINT USING "### ####   ### ####   ### ####   ### ####"; Y + 60; AMP5(Y + 60); Y + 70;
AMP5(Y + 70); Y + 80; AMP5(Y + 80); Y + 90; AMP5(Y + 90)
NEXT Y
PRINT " "

```

```

PRINT "OUTPUT DATA TO A SPECIFIED DIRECTORY. Y/N"
INPUT Q$
IF Q$ = "N" OR Q$ = "n" THEN GOTO 301
PRINT " "
PRINT "ENTER THE OUPUT FILENAME AND EXTENSION"
INPUT OUTFILES$
PRINT " "
PRINT "ENTER THE BURST PRESSURE OF THE BOTTLE IN PSI."
INPUT ULTSTR
OPEN "O", 2, OUTFILES$
FOR Y = 60 TO 100
  PRINT #2, AMP1(Y),
NEXT Y
PRINT #2, ULTSTR
FOR Y = 60 TO 100
  PRINT #2, AMP3(Y),
NEXT Y
PRINT #2, ULTSTR
FOR Y = 60 TO 100
  PRINT #2, AMP4(Y),
NEXT Y
PRINT #2, ULTSTR
FOR Y = 60 TO 100
  PRINT #2, AMP5(Y),
NEXT Y
PRINT #2, ULTSTR
CLOSE #2
301  REM ***** WEIBULL ANALYSIS ROUTINE *****
DIM R(100), XAXIS(100), YAXIS(100)
PARSUMS = 0
FOR Y = MINAMP TO MAXAMP
  PARSUMS = PARSUMS + AMP(Y) / I
  R(Y) = 1 - PARSUMS + AMP(Y) / (I * 2)
NEXT Y
PRINT USING "THE THRESHOLD AMPLITUDE IS SET TO ##."; MINAMP
THRESHOLD = MINAMP
PRINT " "
FOR Y = MINAMP TO MAXAMP
  IF (Y - THRESHOLD) > 0 GOTO 350
  XAXIS(Y) = 0
  YAXIS(Y) = 0
  C = C + 1
  GOTO 360
350  XAXIS(Y) = LOG(Y - THRESHOLD)
  IF R(Y) > 0 THEN GOTO 355
  CC = CC + 1
  GOTO 360
355  YAXIS(Y) = LOG(LOG(1 / R(Y)))
360  NEXT Y
REM ***** LINEAR REGRESSION ROUTINE *****
N = 0
SX = 0
SY = 0
SXY = 0

```

```

SXS = 0
SYS = 0
SSXX = 0
SSXY = 0
SSYY = 0
TMIN = MINAMP + C
TMAX = MAXAMP - CC
FOR Y = TMIN TO TMAX
  SX = SX + XAXIS(Y)
  SY = SY + YAXIS(Y)
  SXY = SXY + XAXIS(Y) * YAXIS(Y)
  SXS = SXS + XAXIS(Y) ^ 2
  SYS = SYS + YAXIS(Y) ^ 2
  N = N + 1
NEXT Y
SSXY = SSXY + SXY - (SX * SY) / N
SSXX = SSXX + SXS - (SX ^ 2) / N
SSYY = SSYY + SYS - (SY ^ 2) / N
B1H = SSXY / SSXX
BOH = SY / N - B1H * (SX / N)
THETA = EXP(ABS(BOH / B1H)) + THRESHOLD
REM ***** RESIDUAL ANALYSIS *****
SUMRESID = 0
SSE = 0
FOR Y = TMIN TO TMAX
  SSE = SSE + (((XAXIS(Y) * B1H) + BOH) - YAXIS(Y)) ^ 2
NEXT Y
S = SQR(SSE / (N - 2))
SSR = SSYY - SSE
K = 2
DFR = K - 1
DFE = N - K
DFT = DFR + DFE
MSR = SSR / DFR
MSE = SSE / DFE
F = MSR / MSE
RSQ = 100 * (1 - (SSE / SSYY))
RSA = 100 * (1 - (SSE / DFE) / (SSYY / DFT))
REM ***** STATISTICAL OUTPUT *****
CLS
PRINT " "
PRINT USING " THE REGRESSION EQUATION IS Y = ####.#### + ####.####X."; BOH; B1H
PRINT " "
PRINT USING " AO = ###  b = ###.###  THETA = ###.###"; THRESHOLD; B1H; THETA
PRINT " "
PRINT "ANALYSIS OF VARIANCE"
PRINT " "
PRINT "SOURCE      DF      SS      MS      F"
PRINT USING " REGRESSION  ###  #####.####  #####.####  #####.####"; DFR; SSR; MSR; F
PRINT USING " ERROR      ###  #####.####  #####.####"; DFE; SSE; MSE
PRINT USING " TOTAL      ###  #####.####"; DFT; SST
PRINT " "
PRINT USING " S = ####.####  R-SQ = ##.##%  R-SQa = ##.##%"; S; RSQ; RSA
PRINT " "

```

```

PRINT "CR TO RETURN TO MAIN MENU"
INPUT QS
END

```

## 6.5 ROBOT OPERATIONS

1. Plug in power supply for PA2040G (receiver) preamplifier
2. Turn on pulser (set rep rate = EXT., Energy = 4, Damping = 0)
3. Turn on RHINO Controller (set Mode select to Teach Pendant)
4. Turn on power supply for load cell.
5. Calibrate load cell circuit.
6. Mount pressure vessel in fixture (Bottle ID letter on side opposite motor and label up).
7. While spinning bottle with teach pendant, apply a small bead of Soundsafe couplant
8. Confirm proper send/receive by;
  - lower sensor => C:\MATLAB\BINSPECTRUM\ Type **DOWNRBT**
  - activate A/D => C:\MATLAB\BINSPECTRUM\ Type **SCOPE**
  - Press "esc" to exit SCOPE
  - raise sensor => C:\MATLAB\BINSPECTRUM\ Type **UPRBT**
9. Taking AU data.
  - C:\MATLAB\BINSPECTRUM\ Type **MATLAB**
  - >> Type **RBTBOT**
  - Output Filename => **RB** (Enter a 1 to 5 character filename)
  - Sample Size => **3** (Enter a number up to 999)
  - To lower sensor press **ENTER**
  - To exit MATLAB type **exit**

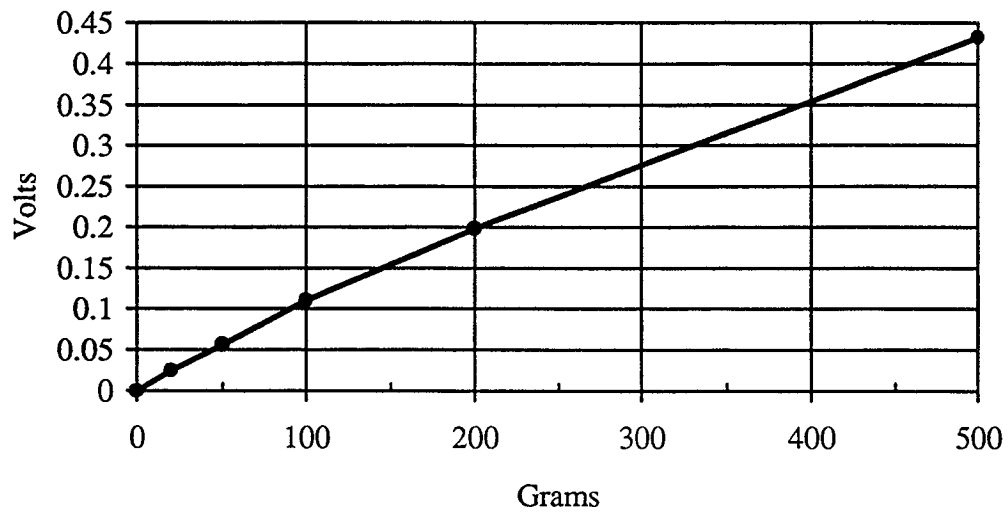
## 6.6 CALIBRATION PROCEDURE FOR ROBOT LOAD CELL

1. Calculate force required for sensor pressure
2. Measure voltage across CD (Box 9 - 2) with no load (CDNL)
3. Measure voltage across CD with load (CDL)
4. Subtract CDL - CDNL to get X
5. Measure voltage across BD (Box 4 - 2)
6. Adjust potentiometer until voltage across BD is equal to voltage across CD (no load) minus X/2 [BD = CDNL + X/2] (Clockwise decreases BD output voltage)
7. Measure voltage across ED. No load should equal 5 volts; Load should equal 0 volts. (External connections not installed)

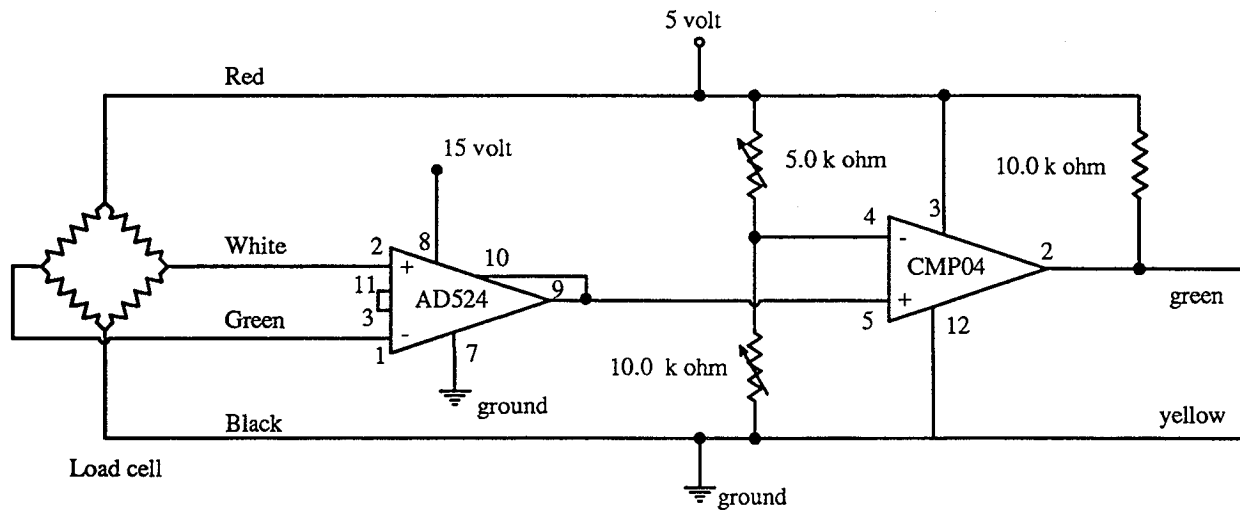
$$P(\text{psi}) = \frac{F}{A} = \frac{m \cdot a}{A} = \frac{x(\text{kg})}{1 \text{ kg}} * \frac{1 \text{ Ns}^2/\text{m}}{1 \text{ N}} * \frac{0.225 \text{ lb}}{1 \text{ N}} * \frac{9.81 \text{ m/s}^2}{0.1104 \text{ in}^2} = 20.0 x(\text{kg})$$

$$P(\text{psi}) = 20.0 x(\text{kg}) * \frac{1 \text{ volt}}{1.157 \text{ kg}} = 17.29 x(\text{volt})$$

1.157 kg/volt with offset 2.908 volt



## 6.7 LOAD CELL CIRCUIT



## 6.8 RBTBOT.M

```

% Program RBTBOT.M
% This program automates the acousto-ultrasonic pressure vessel inspection
% process by controlling the robot and A/D data acquisition board.
% Make sure that the sampling rate and size are the correct size for the A/D.
!cls
clear
h=4096;           % Sample size
s=32;            % Sampling rate (Mhz)
q=input('Enter the output filename. ','s'); % Enter an output filename
    
```

```

disp(' ')
n=input('Enter the sample size. ');      % Enter a samples                               % Number of samples to read
disp(' ')
tt=input('Press enter when ready to start. '); % Confirm program start
disp(' ')
ptime=input('Enter the time to pause during data display. '); % Pause time                               % Number of
samples to read
disp(' ')
uf=input('Enter upper frequency limit (1 = 1Mhz, 2 = 2Mhz, 3 = 3Mhz). ');
disp(' ')
if uf==1
    uf = 128;          % 4096/32
end
if uf==2
    uf = 256;
end
if uf==3
    uf = 384;
end
lb=1;                % File number counter
for ps=1:40          % Position index
for k=1:n            % Sample index
!downrbtn          % execute DOWNRBTN.EXE (Quickbasic)
fprintf('Collecting data from buffer for signal %.0f at position %.0f.\n',k,ps)
disp(' ')
fprintf('Total samples taken %.0f.\n',lb)
disp(' ')
!p2>data.m;        % Store data from buffer in a Matlab File
disp('Moving data into Matlab.')
data;              % Transfer data to Matlab.
disp(' ')
!uprbt             % execute UPRBT.EXE (Quickbasic)
qout=[q,int2str(lb),'.bas']; % Define signal filename
a=1.28-(a*.01);    % Scale data (Original size 0-255)
eval(['save ',qout,' a', '-ascii']) % Save signal
y = fft(a,h);      % Calculate the FFT
x=1:h;             % X axis points
t=x*.03125;        % Scale time axis
Pyy = y.*conj(y)/h; % Compute power spectrum
fname=[q,'P',int2str(lb),'.bas']; % Construct an output filename
power=Pyy(5:uf);  % Group the first 2 MHz worth of points
eval(['save ',fname,' power ', '-ascii']) % Save the grouping to fname
f=s*(0:uf)/h;     % Compute frequency axis
et=sum(Pyy(5:uf)); % Compute total energy
!cls;
subplot(211),plot(t(1:h-1),a(1:h-1)) % Plot signal versus time
xlabel('time microseconds');
title(['Signal ',qout,'.']);
ylabel('volts');
grid;
subplot(212),semilogy(f(5:uf),Pyy(5:uf)); % Plot power spectrum
xlabel('frequency MHz');
title(['Power spectrum ',fname,' has a total energy of ',num2str(et),'.']);
pause(ptime);

```

```

clg;
lb=lb+1;           % Increment file counter
end
!spinbt           % execute SPINBT.EXE (Quickbasic)
end
disp(' Do you wish to calculate energy values or combine spectral values?');
qe=input('Yes=1 No=2 ');
if qe==1
!enrgyda
end
q=input('Do you wish to take more data? Yes=1 No=2 ');
if q==1
rbtbot
end
end
end

```

## 6.9 DOWNRBT.EXE

```

' This program lowers the SCARA robot head after a request.
2 CLS
3 PRINT "PRESS ENTER TO LOWER SENSOR."
4 INPUT Q$
10 OPEN "com2:9600,e,7,2,cs,ds,cd" FOR RANDOM AS #1
20 PRINT #1, "C-1"
30 PRINT #1, "J"; : GOSUB 110
40 GOSUB 140
50 IF I(0) = 1 THEN 90
60 PRINT #1, "C?"; : GOSUB 110
70 IF W > 45 THEN 30
80 GOTO 20
90 PRINT #1, "CX";
100 END
110 IF LOC(1) = 0 THEN 110 ELSE W$ = INPUT$(LOC(1), #1)
120 W = ASC(W$) - 32
130 RETURN
140 IF W AND (2 ^ 0) THEN I(0) = 1 ELSE I(0) = 0
150 RETURN

```

## 6.10 UPRBT.EXE

```

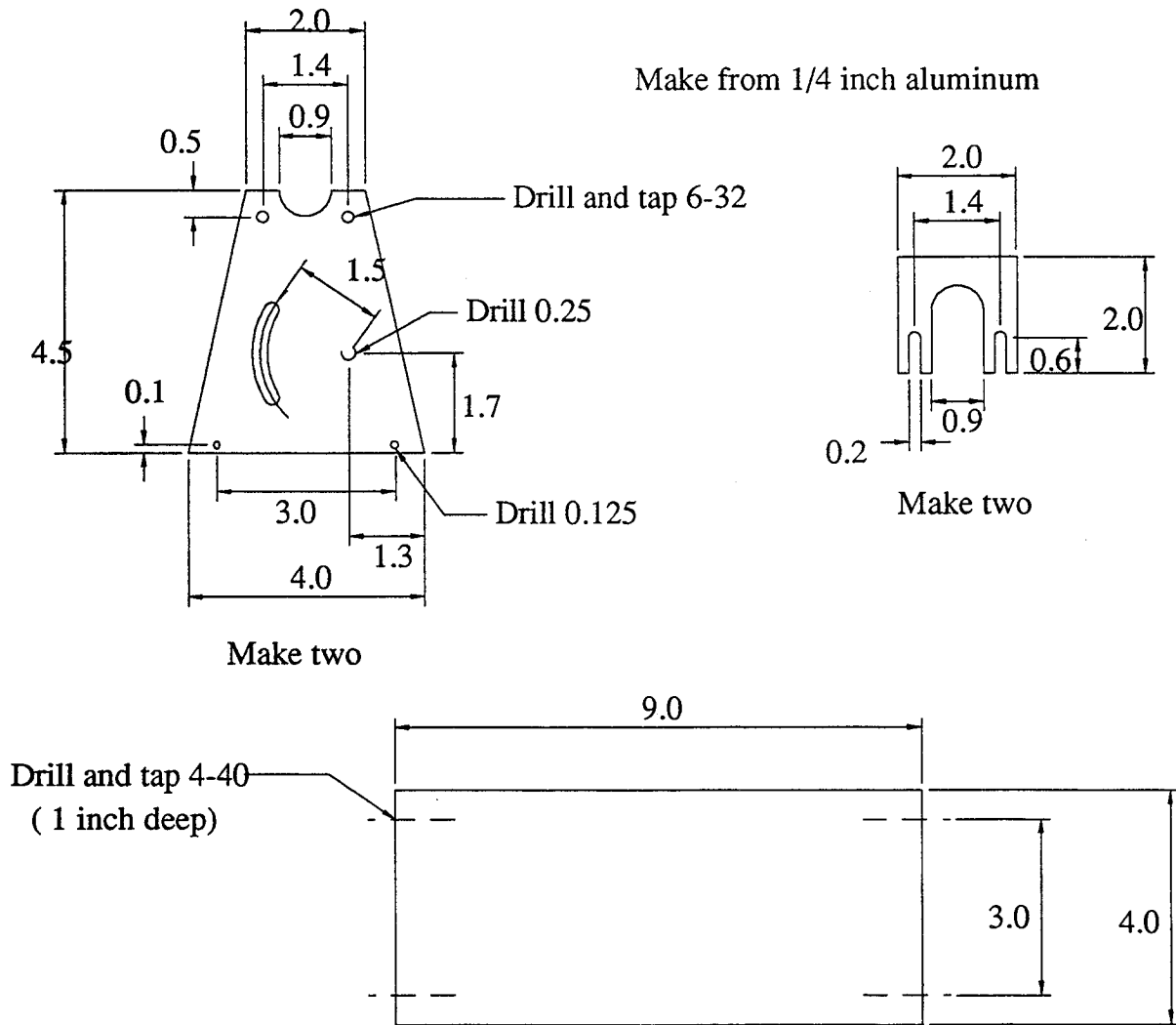
' This program moves the SCARA robot arm up.
1 CLS
10 OPEN "com2:9600,e,7,2,cs,ds,cd" FOR RANDOM AS #1
160 FOR I = 1 TO 5
170 PRINT #1, "C+20"
180 PRINT #1, "C?"; : GOSUB 220
190 IF W > 45 THEN 180
200 NEXT
210 END
220 IF LOC(1) = 0 THEN 220 ELSE W$ = INPUT$(LOC(1), #1)
230 W = ASC(W$) - 32
240 RETURN

```

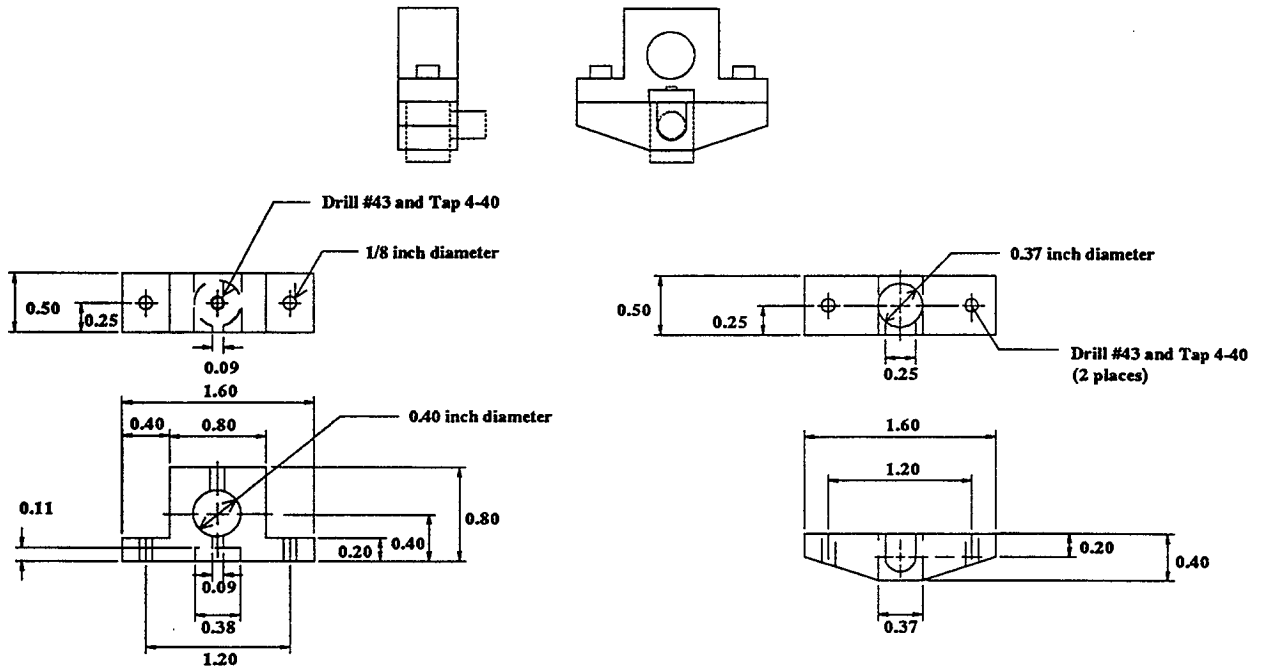
### 6.11 SPINBT.EXE

```
' This program spins the pressure vessels 40/1600 of a turn.
1 CLS
10 OPEN "com2:9600,e,7,2,cs,ds,cd" FOR RANDOM AS #1
170 PRINT #1, "H+40"
180 PRINT #1, "H?"; : GOSUB 220
190 IF W > 45 THEN 180
200 END
220 IF LOC(1) = 0 THEN 220 ELSE W$ = INPUT$(LOC(1), #1)
230 W = ASC(W$) - 32
240 RETURN
```

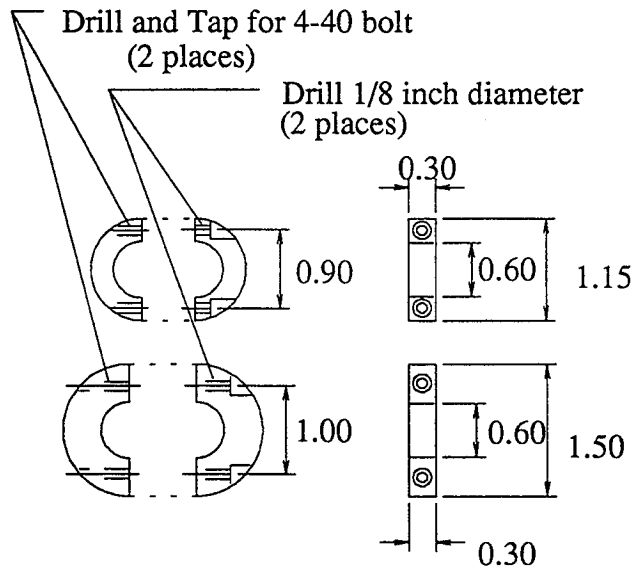
### 6.12 PRESSURE VESSEL CRADLE.



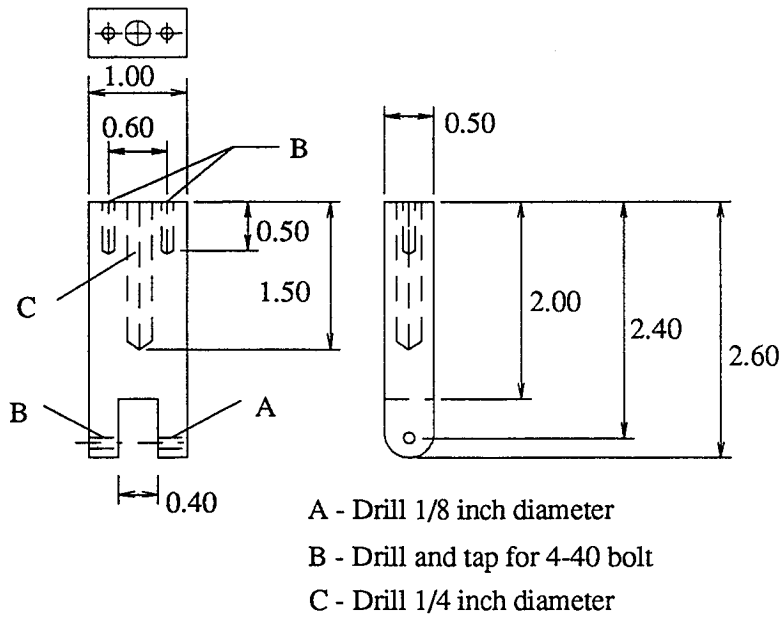
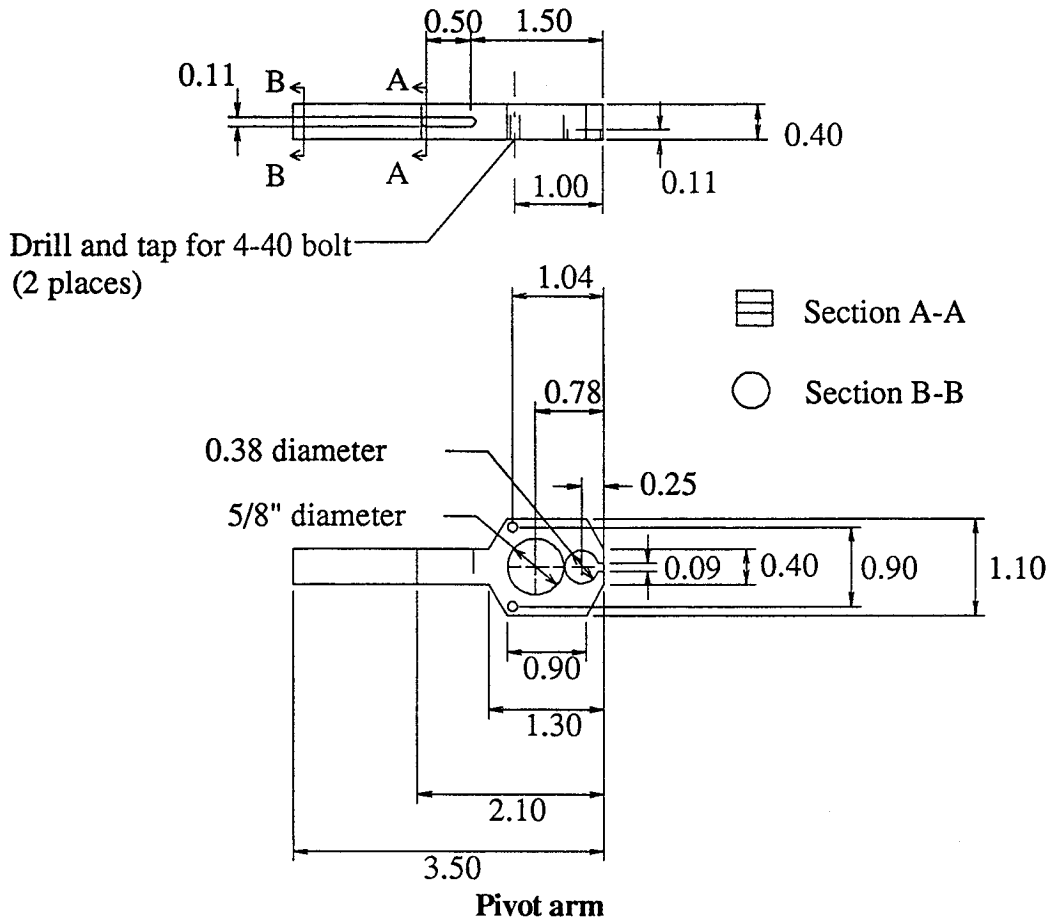
### 6.13 BROADBAND RECEIVER HOLDER

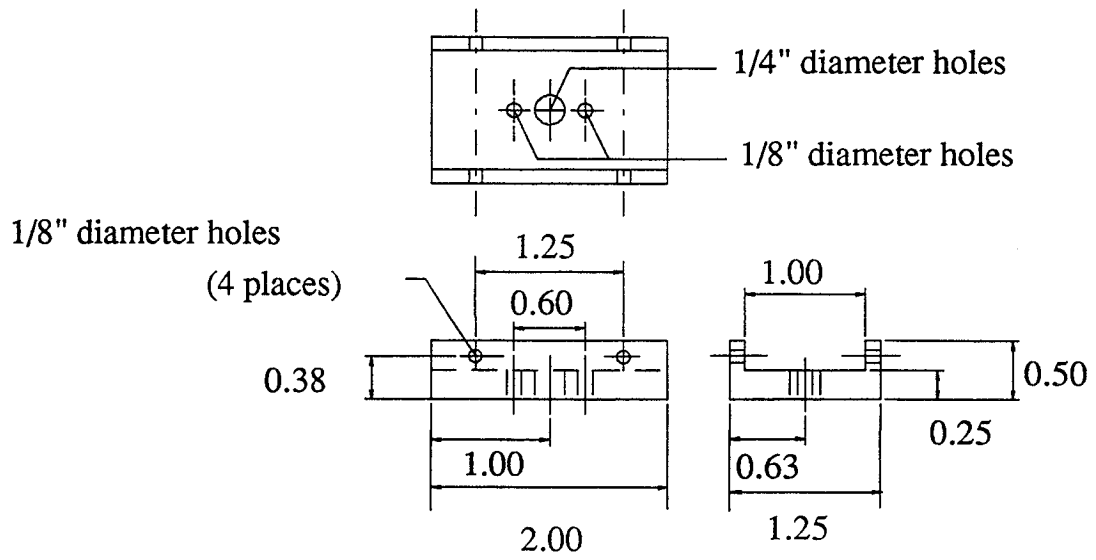


### 6.14 SENSOR ARM FOR AURES



Sensor lock rings





**Pivot support attachment plate**